JAERI-M
91-182

CONCEPTUAL DESIGN OF FUSION EXPERIMENTAL REACTOR (FER/ITER)

—LOWER HYBRID WAVE SYSTEM—

November 1991

Kazuya UEHARA, Takashi NAGASHIMA, Yoshitaka IKEDA
Tsuyoshi IMAI, Haruyuki KIMURA, Sunao MAEBARA
Keigo SANO[*1], Yuichi WATANABE[*1], Masaaki TAKAHASHI[*1]
Keisuke TAKAHASHI[*2], Kazumasa KONISHI[*2], Seiji ASAHARA[*2]
and Keishi OHYA[*3]

日本原子力研究所
Japan Atomic Energy Research Institute

JAERI-Mレポートは，日本原子力研究所が不定期に公刊している研究報告書です。
入手の問合わせは，日本原子力研究所技術情報部情報資料課（〒319-11茨城県那珂郡東海村）あて，お申しこしください。なお，このほかに財団法人原子力弘済会資料センター（〒319-11 茨城県那珂郡東海村日本原子力研究所内）で複写による実費頒布をおこなっております。

JAERI-M reports are issued irregularly.
Inquiries about availability of the reports should be addressed to Information Division Department of Technical Information, Japan Atomic Energy Research Institute, Tokai-mura, Naka-gun, Ibaraki-ken 319-11, Japan.

編集兼発行　日本原子力研究所
印　　刷　いばらき印刷㈱

JAERI-M 91-182

Conceptual Design of Fusion Experimental Reactor(FER/ITER)
- Lower Hybrid Wave System -

Kazuya UEHARA, Takashi NAGASHIMA[+1], Yoshitaka IKEDA
Tsuyoshi IMAI[+2], Haruyuki KIMURA[+3], Sunao MAEBARA[+1]
Keigo SANO[*1], Yuichi WATANABE[*1], Masaaki TAKAHASHI[*1]
Keisuke TAKAHASHI[*2], Kazumasa KONISHI[*2], Seiji ASAHARA[*2]
and Keishi OHYA[*3]

Department of Fusion Facility
Naka Fusion Research Establishment
Japan Atomic Energy Research Institute
Naka-machi, Naka-gun, Ibaraki-ken

(Received October 7, 1991)

This report describes a conceptual design of Lower Hybrid Wave (LH) system for FER and ITER. In JAERI, the conceptual design of LH system for FER has been performed in these 3 years in parallel to that of ITER. There must be a common design part with ITER and FER. The physical requirement of LH system is the saving of volt·sec in the current start-up phase, and the current drive at the boundary region. The frequency of 5GHz is mainly chosen for avoidance of the α particle absorption and for the availability of electron tube development. Seventy-two klystrons (FER) and one hundred klystrons (ITER) are necessary to inject the 30 MW (FER) and 45-50 MW (ITER) rf power into plasma using 0.7-0.8 MW klystron per one tube. The launching system is the multi-junction type and the

---

+1 Department of Fusion Engineering Research
+2 Department of Fusion Plasma Research
+3 Fusion Experimental Reactor Team
*1 Nippon Electric Company
*2 Sumitomo Heavy Industry
*3 Toshiba Corporation

rf spectrum must be as sharp as possible with high directivity to improve the current drive efficiency. One port (FER) and two ports (ITER) are used and the injection direction is in horizontal, in which the analysis of the ray-tracing code and the better coupling of LH wave is considered. The transmission line is over-sized waveguide with low rf loss.

Keywords: Lower Hybrid System, ITER, FER, Launcher, Transmission Line, Klystron

JAERI－M 91－182

核融合実験炉(FER/ITER)の概念設計
－低域混成波システム－

日本原子力研究所那珂研究所核融合装置試験部

上原　和也　・永島　　孝[+1]・池田　佳隆・今井　　剛[+2]
木村　晴行[+3]・前原　　直[+1]・佐野　圭吾[*1]・渡辺　勇一[*1]
高橋　雅明[*1]・高橋　慶函[*2]・小西　一正[*2]・浅原　政治[*2]
大家　圭司[*3]

(1991年10月7日受理)

本報告は，核融合実験炉（FER)と国際熱核融合炉(ITER)の低域混成波(LH)システムの概念設計について述べたものである。原研では，FER のためのLHシステムの概念設計をITERの概念設計と併行してこの3年来やってきた。LHシステムの物理的要請は，電流立上げ時に於けるVolt・sec の節約と周辺電流駆動である。周波数は5GHzを選んでいるが，これは主にα粒子によるパワー吸収を避けることと電子管の汎用性から来ている。プラズマに注入するrfパワーは FERでは，30MW，ITERでは45－50MWを予定しているが，これを達成するためには一本当りの出力が0.7－0.8MWのクライストロンがFERでは72本，ITERでは100本が必要となる。高周波の入射アンテナは，マルチジャンクション型で，rfのスペクトルは，電流駆動の効率を上げるために，方向性が改善されるようにできるだけシャープにしている。FER では1つのポートで，ITERでは2つのポートを用いてランチャーを水平方向に設置するが，これはレイトレーシングコードや波のプラズマへの結合を良くすることが加味されているためである。

那珂研究所：〒311-01　茨城県那珂郡那珂町大字向山801-1
＋1　核融合工学部
＋2　炉心プラズマ研究部
＋3　核融合実験炉特別チーム
＊1　日本電気㈱
＊2　住友重機㈱
＊3　東芝㈱

Contents

目　　次

1. INTRODUCTION

1.1 Concepts of FER and ITER

JAERI has performed a conceptual design of the fusion experimental reactor in both domestic programme and international cooperation programme in these three years. Fusion Experimental Reactor (FER)[1] corresponds to the domestic programme. Basic objectives of FER are to explore a machine that solves reasonable minimum physics and technological issues necessary to proceed to a demonstration power reactor (DEMO) without any further intermediate steps. Achievements of Q (energy multiplication factor) = 20 and steady state at least separately under well controlled condition are considered to be a reasonable minimum step to proceed to DEMO. International Thermonuclear Experimental Reactor (ITER)[2] corresponds to the international cooperation programme, where four parties (EURATOM, Japan, the Soviet Union and the United States) join under the auspices of IAEA. Major objectives of ITER are as follows: [1] to demonstrate controlled ignition and extended burn of D-T plasma, with steady state as an ultimate goal, [2] to demonstrate technologies essential to a reactor in an integrated system and [3] to perform integrated testing of the high-heat-flux and nuclear components required to utilize fusion power.
Major device and plasma parameters for FER and ITER are as follows:

	FER	ITER
Major radius (m)	4.7	6.0
Minor radius (m)	1.6	2.15
Elongation	2.0	2.0
Toroidal field (T)	5.25	4.85
Plasma current (MA)	15	22
Fusion power (GW)	0.6	1

1.2 Heating and Current Drive Scenario of FER and ITER

Roles of heating and current drive system necessary for operations of FER/ITER are considered as follows[2-3]:

[1] Ionization, Preheating, and Current Initiation
[2] Non-inductive Current Ramp-up Assist
[3] Heating to Ignition
[4] Steady-state Current Drive

[5] Local Current Profile Control

[6] Burn Control

As it is difficult to cover these functions by any single heating and current drive system, combination of plural systems is inevitable. Following four heating and current drive systems were thought as the candidate.

[1] Neutral Beam (NB) System

[2] Ion Cyclotron Wave (IC) System

[3] Lower Hybrid Wave (LH) System

[4] Electron Cyclotron Wave (EC) System

Selection was made from the database obtained before and during the conceptual design phase and the modelling calculations.

For FER, 50 MW, 0.5 - 1 MeV NB is selected as main current drive and heating system, since some database exists for the current drive[4-6] and a theoretical current drive efficiency shows the best value among all schemes. 30 MW, 5 GHz LH system is selected for current ramp-up assist and current drive in the outer region. A plenty of database on the current drive by LH waves have established in many tokamaks. A record value of the current drive figure of merit (γ) of 0.34 x $10^{20}Am^{-2}W^{-1}$ was obtained on JT-60.[7] However, in the steady-state scenario of FER/ITER, a flow channel of the driven current will be limited in the outer region because of a high electron temperature (volume-averaged electron temperature $<T_e>$ ~ 20 keV). Current profile control can be thus expected in combination with NB current drive in order to obtain stable plasmas at high-β and to avoid the sawtooth oscillation. In addition, Volt•sec saving by LHCD[8] in the current ramp-up phase is quite useful in order to get higher plasma current or longer pulse discharge in FER, whose magnetic flux of the ohmic coil is relatively small. Thus the combination of NB and LH of a total power of 80 MW is chosen for the heating and current drive system of FER.

In order to supplement a central heating capability, either 20 MW, 50-85 MHz IC system or 20 MW, 140 GHz EC system is added. With IC system, unique central ion heating can be expected. This capability is favorable for getting high Q and for burn control, even at high electron density, where penetration of NB tends to be difficult. With EC system, strong central heating based on the electron heating is possible. In addition, EC system is a powerful tool for the preionization and the current initiation. If IC system will be chosen for a central heating method, a short pulse ($\leq$ 1 sec), several MW EC system will be necessary for the preionization and the current initiation. Stabilization and control of the sawtooth oscillation can be expected with both IC and EC systems.

For ITER, following two options have been determined in the course of the Conceptual Design Activity (CDA).

Reference: 75 MW, 1.3 MeV NB System
50 MW, 5 GHZ LH System
20 MW, 120 GHz EC System

Alternate: 130 MW, 15-80 MHz IC System
50 MW, 5 GHZ LH System
20 MW, 120 GHz EC System

A reason why the combination of NB and LH is adopted for the reference current drive and heating scenario is the same as in FER. EC system is included in the reference scenario. Role of EC system is partly different from the one of FER. Capability of local current profile control near q=2 surface for the purpose of avoidance of disruptions is included instead of the central heating as considered in FER. In the alternative scenario, IC system replaces NB system. A reason why IC system is not chosen as a reference system is its sparse database on the current drive and its lower theoretical current drive efficiency (about two thirds of NBCD efficiency). However, from considering merits of IC system (unrivaled central ion heating, unnecessary of a large scale engineering development and low cost), it is proposed that both NB and IC be part of the reference system. This point will be discussed in the coming Engineering Design Activity (EDA).

1.3 Lower Hybrid Wave System for FER and ITER

This report describes a conceptual design of Lower Hybrid Wave (LH) system for FER and ITER. In JAERI, the conceptual design of LH system for FER has been performed in these 3 years in parallel to that of ITER. There must be a common design part with ITER. In FER, the physical requirement of LH system is the saving of Volt·sec in the the current start-up phase, and the boundary current drive. The specification of LH system for FER/ITER is shown in Table1-1.

Table 1-1 Main specification of LH system for FER/ITER

	FER	ITER
System		
frequency	5 GHz	←
pulse width	1000 sec	CW

RF power	30 MW	45-50 MW
RF port dimension	1.2 m width x 3 m height	1.2 m x 3.4 m
RF power source		
tube type	klystron	←
output power per unit	0.7 MW	←
Efficiency	60 % (objective 70 %)	←
Number of tube	72	about 100
Transmission line	WR-229 or WR-650	←
Coupling system		
Launcher type	Multi-junction	←
N parallel	1.3 - 1.8	1.3 – 2.5

where, the sign of arrows means the same item as the left column. The frequency of 5GHz is mainly chosen for avoidance of the α particle absorption and for the availability of electron tube development.. About seventy two klystrons are necessary to inject the 30 MW rf power into plasma using 0.7-0.8 MW klystron per one tube. The launching system is the multi-junction type and the rf spectrum must be as sharp as possible and high directivity to improve the driving efficiency. One port is used and the injection direction is in horizontal, in which the analysis of the ray-tracing code and the better coupling is considered. The transmission line is over-sized waveguide with low rf loss.

In section 2, physics basis is given concerned with wave coupling including wave spectrum analysis and the ray tracing code analysis due to the quasi-linear theory. System design of LH system for FER is presented in section 3. In section 4, the design study for ITER LH system, which was performed by Japanese design team, is reported. In section 5, the design study of 5 GHz klystron for FER/ITER is given. In last section, R & D needs and conclusions are given.

2. PHYSICS BASIS

2.1 Coupling and Wave Spectrum of the Launcher

The physical requirements of the LHRF launcher on ITER/ FER are to excite wave spectrum $N_{//}$ of 1.3 to 1.8 at the frequency of 5 GHz. To launch this wave spectrum, the

RF power	30 MW	45-50 MW
RF port dimension	1.2 m width x 3 m height	1.2 m x 3.4 m
RF power source		
tube type	klystron	←
output power per unit	0.7 MW	←
Efficiency	60 % (objective 70 %)	←
Number of tube	72	about 100
Transmission line	WR-229 or WR-650	←
Coupling system		
Launcher type	Multi-junction	←
N parallel	1.3 - 1.8	1.3 – 2.5

where, the sign of arrows means the same item as the left column. The frequency of 5GHz is mainly chosen for avoidance of the α particle absorption and for the availability of electron tube development.. About seventy two klystrons are necessary to inject the 30 MW rf power into plasma using 0.7-0.8 MW klystron per one tube. The launching system is the multi-junction type and the rf spectrum must be as sharp as possible and high directivity to improve the driving efficiency. One port is used and the injection direction is in horizontal, in which the analysis of the ray-tracing code and the better coupling is considered. The transmission line is over-sized waveguide with low rf loss.

In section 2, physics basis is given concerned with wave coupling including wave spectrum analysis and the ray tracing code analysis due to the quasi-linear theory. System design of LH system for FER is presented in section 3. In section 4, the design study for ITER LH system, which was performed by Japanese design team, is reported. In section 5, the design study of 5 GHz klystron for FER/ITER is given. In last section, R & D needs and conclusions are given.

2. PHYSICS BASIS

2.1 Coupling and Wave Spectrum of the Launcher

The physical requirements of the LHRF launcher on ITER/ FER are to excite wave spectrum $N_{//}$ of 1.3 to 1.8 at the frequency of 5 GHz. To launch this wave spectrum, the

pitch of the waveguide Δ[cm] and adjacent phase θ[°] in the launcher should be satisfied in following equation

$N_{//}^{peak} \approx \theta/12f\Delta$.

Another requirement is to launch a sharp wave spectrum with a high directivity for a high current drive efficiency. The directivity η_D is given by,

$$\eta_D = \frac{\int_1^{\infty} P(N_{//})\ dN_{//} \quad - \int_{-\infty}^{-1} P(N_{//})\ dN_{//}}{\int_{-\infty}^{\infty} P(N_{//})\ dN_{//}}$$

Moreover, to have a symmetric geometry in the multijunction module, the number of the subsidiary waveguides in a module (m) is given by

$m \times \theta = 180° \times n$ (n = 1,2,..).

On the contrary, the structure of the launcher is constrained by the geometrical arrangement of the ITER torus vacuum vessel. The launcher must be located in a space of 120 cm width.

These conditions require that the launcher is composed of 26 individual multijunction modules in toroidal direction, and that the launcher parameters of (θ, Δ, m) are (60°, 0.6, 6,) or (90°, 0.9, 4). The total waveguide numbers in these launchers are 26×6 for the former case (case I), and 26×4 for the later case (case II).

We estimate RF properties of these two launcher structures by using a multijunction coupling code, which has agreed well with experimental results on JT-60. Since the total waveguide number of the ITER launcher (156 /104) is more than the limitation of the coupling code (60), we can't directly obtain RF properties. Therefore, we modify this coupling code to apply the ITER launcher as follows;

Firstly, we calculate the RF properties of a multijunction launcher composed of 9 (case I) or 11 (case II) multijunction modules, where the total number of waveguides is less than 60.

And then, we extend the calculated RF properties of the central module in this model launcher to that of the ITER launcher as shown in Fig.2- 1, because the module number of ITER launcher is large enough to consider the RF properties of the central modules to be symmetric.

Thus, the total reflection coefficient is given by

$$\rho = \frac{\sum_{i=1}^{4\text{ or }5} \rho_i + \sum_{i=6\text{ or }7}^{9\text{ or }11} \rho_i + (18\times\rho_5 \text{ or } 16\times\rho_6)}{26},$$

where ρ_j is the reflection coefficient of each module calculated by coupling code. And the wave spectrum is given by

$$P(N_{//}) = \frac{1}{2} Y(N_{//}) \left| \sum_{j=1}^{4\text{ or }5} E_j + \sum_{k=5\text{ or }6}^{22\text{ or }21} E_{5\text{ or }6} e^{i(k-5\text{ or }6)\varphi} + \sum_{j=6\text{ or }7}^{9\text{ or }11} E_j e^{i(17\text{ or }15)\varphi} \right|^2,$$ where

$Y(N_{//})$ is plasma surface admittance, E_j the electric field at the module mouth calculated by coupling code, j the phase difference of adjacent modules.

We can estimate RF properties of ITER launcher in these procedures.

Figure 2-2 shows the typical wave spectrum of the case I, where the edge plasma density and density gradient are 5×10^{11} cm^{-3} and 5×10^{11} cm^{-4}, respectively. A very sharp spectrum can be obtained in the range of $1.2 < N_{//} < 2.5$ by changing the phase between adjacent modules.

Figure 2-3 shows the $N_{//}^{peak}$ dependence of the reflection coefficient and η_D for two cases. In view of coupling, there is no significant difference between two cases, and good coupling (r < 10 %) are obtained for both cases. As far as the directivity is concerned, however, the η_D of case I is about 10 - 20 % higher than that of case II. Therefore, the launcher of case I is more attractive to achieve a high current drive efficiency.

2.2 Current Drive Analysis

Main roles of the LHRF system in ITER/FER are to drive current , control current profile and save volt−second consumption through LHCD. Therefore, basic design of the LHRF system is to determine the frequency and $N_{||}$-spectrum to perform these purposes efficiently. Experimental database of the LHCD is the largest. The LHCD has achieved 2MA current drive, the highest efficiency (~3.4×10^{19}m^{-2}A/W) and the largest current drive products (~12.5×10^{19}m^{-2}MA) [9-11].

The key point to choose frequency is to avoid α particle absorption before electron Landau damping. Higher frequency is desirable for this purpose but it increases engineering difficulty, too. The frequency should be as low as possible in the constraint of avoiding significant α particle absorption. The calculation of α particle absorption of the lower hybrid wave was carried out as a function of frequency in Fig.2-4 (a) , using ray tracing with electrostatic and electromagnetic wave approximation of the dispersion relation. Here the damping rate is calculated from linear Landau damping of α particles

12). Plasma parameters are corresponding to those of ITER/FER. It is clear that the α particle absorption is negligible at the frequency more than 5 GHz.

As for the $N_{||}$ spectrum, we have to consider two main usages of LHCD in ITER/FER. One is volt-second saving during current ramping up phase and another is current drive of outer core and current profile control in flat top phase. In the former role, the efficiency of the volt-second saving is proportional to the efficiency of current drive. $N_{||}$ should be as small as possible if the accessibility condition is satisfied. It is clearly demonstrated that the saving of the resistive part is quite efficient during ramp up phase in JT-60[8]. Since the density of the ramping up phase is $2\text{-}3\times10^{19}m^{-3}$ in ITER/FER, $N_{||} > N_{||}^{acc}\sim1.3$ for this purpose.

In the second role, LHCD is expected to drive current in the outer core (r/a=0.6~0.8) of the flat top plasma (T_e~30 keV) while negative NBI drives the center current. Using the same ray tracing code with one dimensional steady state solution of the Fokker Planck equation, current profile was calculated with various $N_{||}^{peak}$ at 5 GHz , as shown in Fig. 2-4 (b). Penetration of the lower $N_{||}$ wave is better but wave of $N_{||0}^{peak}=1.6$ ($N_{||0}$ is the $N_{||}$ at the launching point) can not penetrate because of the accessibility. It is found that outer core current covering r/a=0.6~0.8 is possible through the control of the $N_{||0}^{peak}$ from 1.7 to 1.8. Since sharp $N_{||}$ spectrum improves the efficiency and penetration, $\Delta N_{||}=0.1\sim0.15$ is required. More outer current profile is desirable in the case of m=2 MHD stabilization.

Therefore, it is necessary that controllable range of $N_{||0}^{peak}$ = 1.3~1.8 with $\Delta N_{||}=0.1\sim0.15$ and high directivity to satisfy both requirements of the volt-second saving in ramping up phase and outer core current drive in flat top phase. It is desirable to extend the range of $N_{||0}^{peak}$ up to 2.2 for the stabilization of m=2 mode.

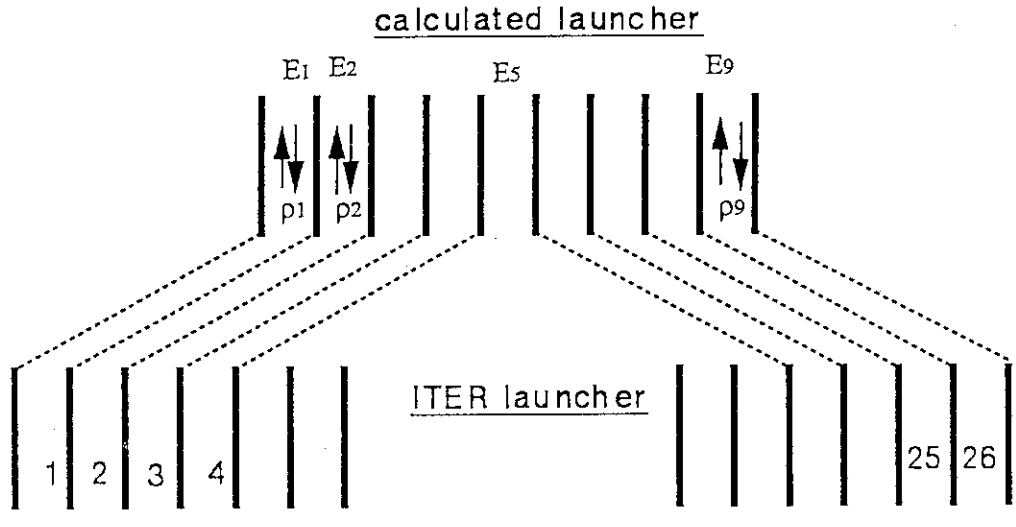

Fig. 2.1 Coupling model for the calculation of multi-junction launcher

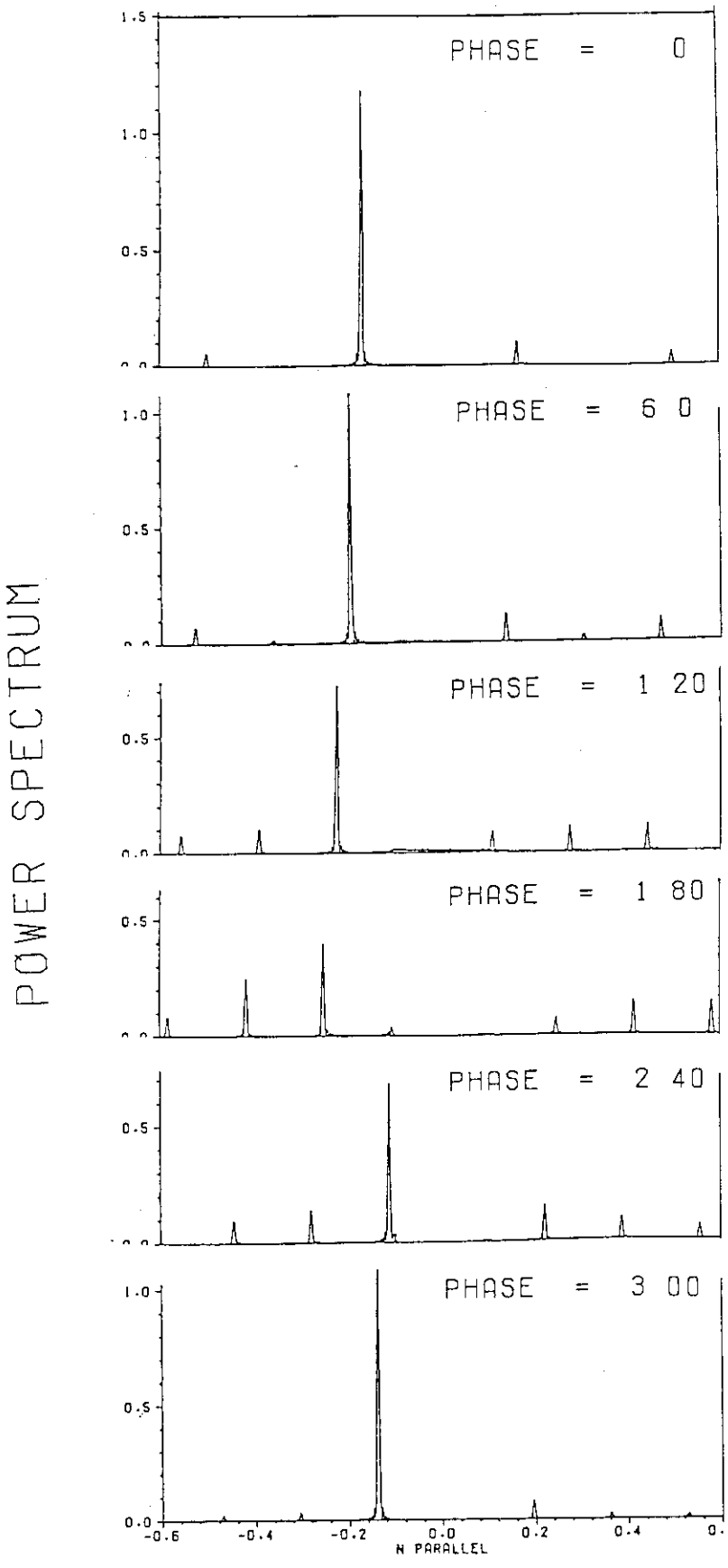

Fig. 2.2 Calculated power spectrum putting the phasing as a parameter

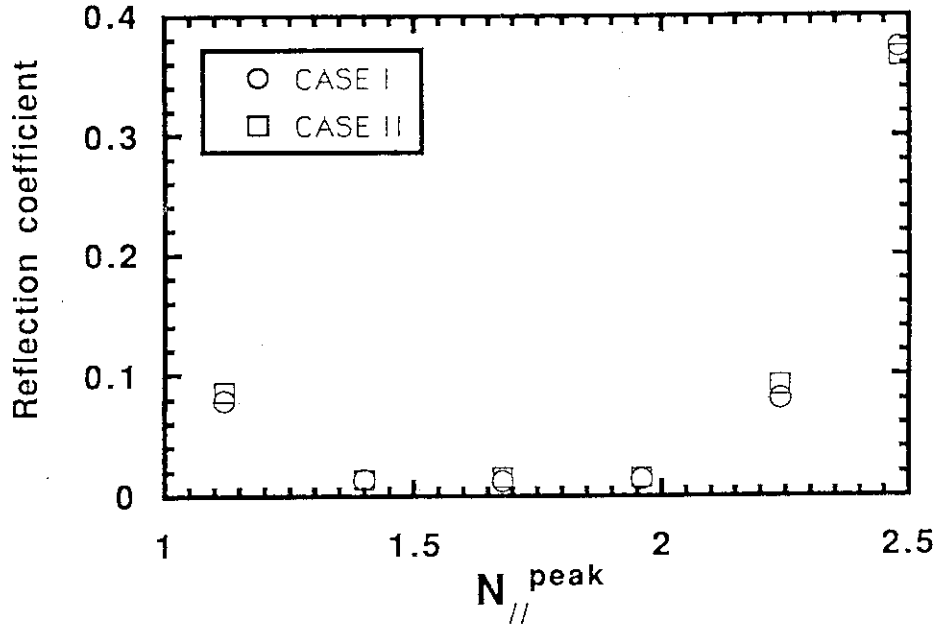

(a) Reflection coefficient against the N parallel

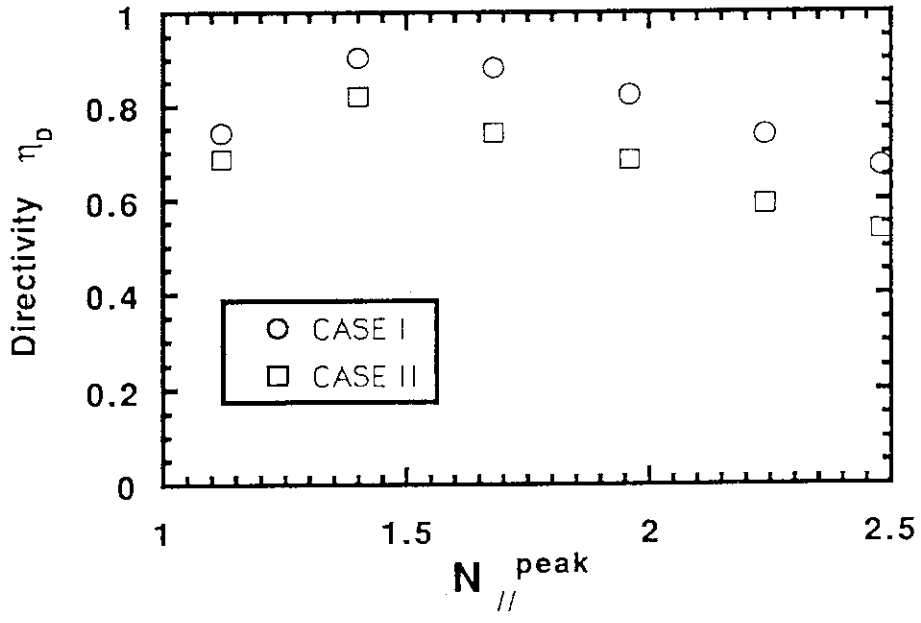

(b) Efficiency against the N parallel

Fig. 2.3 Calculated results for the coupling of LHRF launcher

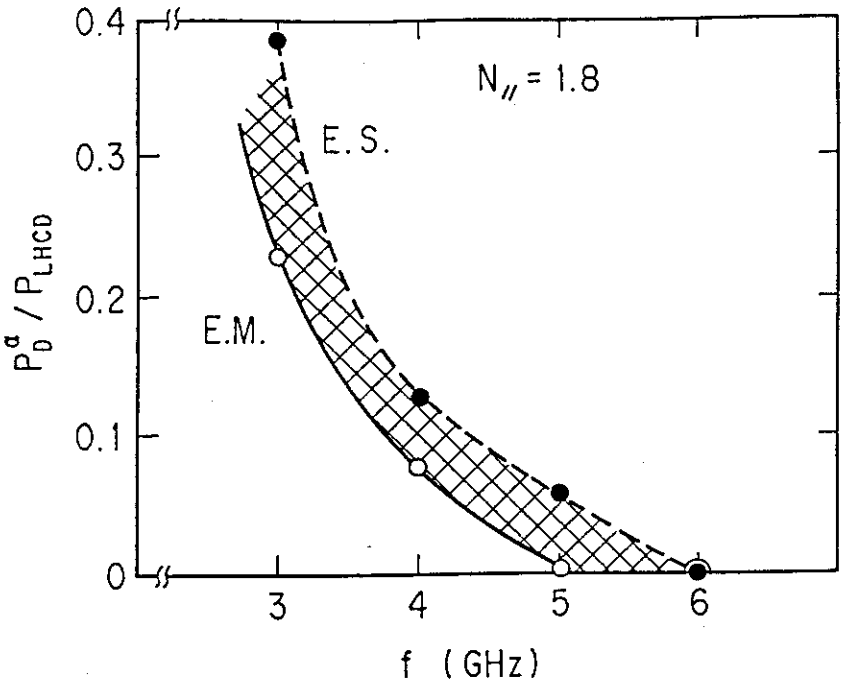

(a) Fraction of a particle absorption against frequency in ITER parameters with electrostatic (ES) and electromagnetic (EM) approximations.

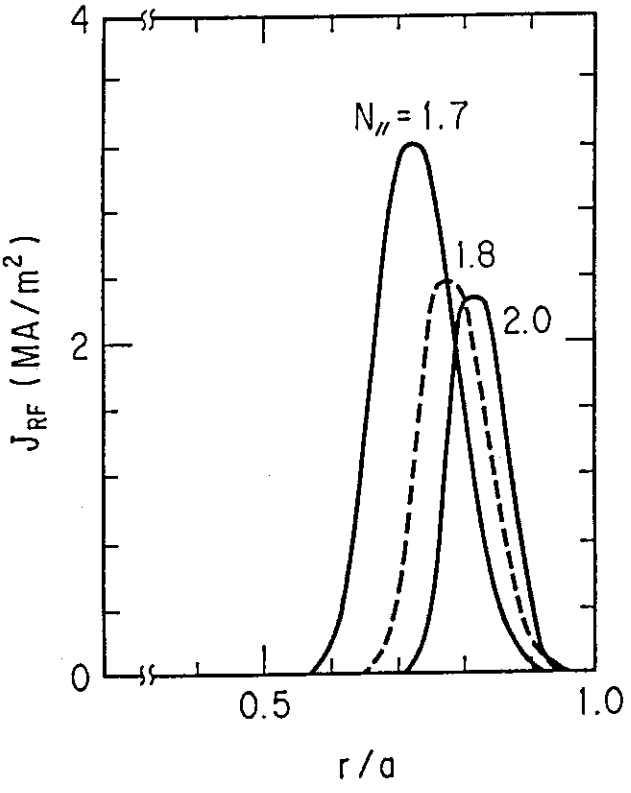

(b) Current profile of LHCD with various $N_{||}$ in ITER parameters.

Fig. 2.4 Calculation results of the current drive due to the quasi-linear theory

3. DESIGN STUDY OF LHRF SYSTEM FOR FER

3.1 Design Study of LH Launcher for FER

The LHRF launcher for FER is composed of launcher itself, the support structure for supporting the launcher itself, the moving structure for moving the launcher, bellows for vacuum seal and an auxiliary equipment. The launcher itself is composed of a main waveguide, a cooling-shield part and a differential pumping part. The auxiliary equipment is composed of differential pumping system, baking system and cooling system. The specification of LH launcher for FER is shown in Table 3-1

Table 3-1 Specification of LH launcher for ITER

Waveguide	
Number of module	24 (toroidal) x 3 (poloidal)
Number of main waveguide (per one module)	6 (toroidal) x 8 (poloidal)
Dimension of main W/G	a=50 mm b=4.5 mm d= 1.5 mm
fixed phase difference	60 degree
Transmission power density	5.0 kW/cm^2
Materials of waveguide	
Main part	S.S.304
Waveguide	S.S.316L + Copper (Glidcop)
Front end	Be
Guard limiter	Carbon Fiber Reinforced Carbon Composite (From now we call this C-C composite)
Temperature	150 (during operation) 350 (during baking)
Pressure	10^{-7}Torr•l/sec•cm^2
Neutron dose	10^{18} n/cm^2

(1) Main Waveguide for LH Launcher

The candidate of the main waveguide in the multi-junction launcher for 5 GHz range are WR-187,WR-159 and WR-229. The power rating of WR-229 at 5 GHz is 2.16 MW with the electric field 1.5 kV/mm and the transmission loss is 0.031 dB/m at 20°C, which is more excellent than other species of waveguides. The allowable height of the mouth waveguide is between 37.5 - 57.0 mm, which is 1.25 - 1.9 times smaller than the cut off wave length in WR-229. The decided dimension of unit waveguide is 50 mm in height, 4.5 mm in width and 1.5 mm in septum as shown in Fig.3-1 (a). The transmission power density at the mouth of the launcher, therefore, 33.8×10^3 /(24x3x6x8x5x0.45)=4.3 kW/cm^2. The division part in the poloidal direction forms a coupler having directivity of rf power. The transmission line for the launcher in the toroidal direction is divided with a tournament like method. The power divider at the entrance of launcher must have a capability of the directivity with a short slot type. The dimension of this point is decided in the following, where the sign of the dimension is shown in Fig.3-1 (b),(c) and (d). The value of W is in the range of $\lambda < W < 1.5\lambda$ to excite TE_{20} mode and not to excite higher modes more than TE_{30}, where λ is the wave length. Since the value of W is usually chosen to be $W=1.3\lambda$, we set W=78 mm, L=52.87 mm, a_1=38.25 mm, a_2=47.17 mm, l_2=19.4 mm and l_1=24.2 mm. The phase shifter is composed of the $\lambda/4$ composer. The width of the waveguide S_1 in Fig.3-1 (d) must be larger than 1.25 times of the cut-off wave length. Each case for S_1=40,42, 44, 45 mm is calculated in the following.

S_1	S_2	λ_2	$\Delta\theta$(degree)	l_1(mm)				
(mm)	(mm)	(mm)	(l_2 x 2),	$\Delta\theta$=60°	120°	180°	240°	300°
40	44.7	20.2	7.1° x 2	55.2	127.4	199.7	272.0	344.2
42	45.8	19.8	5.2° x 2	82.7	182.7	282.7	382.7	482.7
44	46.9	19.5	3.7° x 2	128.1	274.2	420.4	566.5	712.6
45	47.4	19.4	3.0° x 2	164.9	348.1	531.3	714.5	897.7

On the manufactory view point, it is better for (l_1+l_2) to be short, however, it is better for S_1 to be as large as possible from the view point of the low reflective loss and small thermal loss.

The structure of the main waveguide is in the following.

[1] The launcher waveguide is interfaced to the transmission line by the WR-650 X 72 waveguides and is transfered to the WR-229 waveguide to connect to the launcher through a double sealed vacuum window and a RF gate valve.

[2] Seventy two input waveguides in the launcher are divided into two fold ways in the poloidal direction by 3 dB coupler with a short slot type. One hundred forty four waveguides are further divided into two fold ways in the poloidal direction in double and is divided into two fold ways in the toroidal direction by the panel perpendicular to the rf electric field.

[3] The configuration of the waveguide at the top LH launcher is 24 columns in the poloidal direction and is the 6 divider waveguide with 24 unit waveguides in the toroidal direction as shown in Fig.3-2 and Fig.3-3.

[4] The detail of 6 divider waveguide is 6.0 mm pitch in the toroidal direction (4.5 mm in the space and 1.5 mm in septum) and have a phase shifter having phase difference of 60° adjacent waveguides as shown in Fig.3-1 (a).

(2) Structure of LH Launcher

The structure of LH launcher for FER is shown in Figs.3-2, 3-3, 3-4 and 3-5. In Fig.3-2, a cross section in the radial direction is shown. The top of the grill mouth is replaceable if we cut the top parts of launcher by six sections as shown in Fig.3-2. The waveguide transmission line is divided inside launcher and are connected to the launching parts. The waveguide transmission line is divided with 3 dB coupler. The neutron shield is equipped with steel (Fe), which is shown by shadow in the figure. The inside of launcher is evacuated by vacuum pump and is cooled by water, which are shown in Fig.3-2. The sectional view of C-C section in Fig.3-2 is shown in Fig.3-3, in which we can see 24 (toroidal) x 3 (poloidal) modules. One module is composed of 6 (toroidal) x 8 (poloidal) waveguides therefore the total number of waveguide is 144 (toroidal) x 24 (poloidal)=3456. Each module has two passive waveguides in the left side and one in right side as shown in the left side of top corner of the figure. The total length is 1200 mm in the toroidal and 3000 mm in the poloidal direction. The launcher side view of B-B section is shown in Fig.3-4, in which we can see a double seal bellows for moving the launcher, flexible waveguides, a RF gate valve, primary windows, arc detectors and waveguide transfer bend. The section A-A is shown in Fig.3-5, in which we can see the plane view of the launcher. The section D-D in Fig.3-2 is shown in Fig.3-6, in which we can see the cooling water pipes inside the launcher and the detail configuration of waveguides. The section E-E in Fig.3-4 is shown in Fig.3-7, in which we can see the 72 waveguides of WR-650 and the space for the cooling water. Further comments are listed in the following.

[1] The launcher itself is supported by the shielding sleeve fixed by the cryostat. The torsional stress generated at the disruption is cancelled by this shielding sleeve.

[2] Launcher moving during operation is performed by the oil-pressurized fast moving equipment fixed between the shielding sleeve and the launcher. The launcher moving is performed in smoothly by the axi-receiving structure in the straight line. Displacement (830 mm) generated by moving is absorbed by two bellows.

[3] The vacuum seal in the vacuum vessel is maintenanced by the RF port nozzle in the vacuum vessel and bellows between the supporting sleeve and the inner bellows between the launcher itself and the supporting sleeve. The vacuum seal in the cryostat is performed by the lying material of the cryostat and the seal welding in the support sleeve. The bellows between the support sleeve and the launcher is in double in order to form double structure against the outer environment.

(3) Design study of the pumping system

The vacuum pumping system in the launcher is equipped for the aid of enough aging. In order to sustain the vacuum state inside the waveguides the differential pumping part is equipped at the center and at the back side in the launcher itself. The side part of the waveguides in the differential pumping part have many exhausting holes, where being exhausted gas is led from here to the exhausting nozzle at the back of the differential pumping part and is finally pumped out by the vacuum pump. Since the exhausted gas contains tritium and deuterium the gas is sent to a fuel system of the reactor and is finally proceeded. The total conductance at the top of the launcher is calculated by the summation of nine parts of launcher waveguides, which is c_{total}=0.277 m^3/sec for air and c_{total}=1.04 m^3/sec for hydrogen. Since the pumping speed of turbo-molecular pump is 1.6 m^3/sec the pumping speed at the top of the launcher is estimated to be 0.63 m^3/sec for hydrogen. The arrived pressure is estimated to be 1.73 x 10^{-2} Pa before baking and 7.3 x 10^{-6} Pa (=7.3 x10^{-8} Torr) after baking, which is below 1 x10^{-5} Torr. When the gas release rate increases to be 4.23 x 10^{-3} Torr•l/sec by the rf injection, the arrived pressure reduces to 6.7 x 10^{-3} Pa(=5.0 x 10^{-5} Torr). If we use the turbo-molecular pump having better pumping speed of 25 m^3/sec the conductance is improved to be 1.54 m^3/sec for hydrogen and the arrived pressure is 2.1 x 10^{-5} Torr, which is near to the designed value. When we evacuate the wavegude by equipping the duct between the flexible wavegude and the rf gate valve the arrived pressure must be further improved.

(4) Analysis of Cooling Water and Baking System

Since the launcher itself suffers much heat load it is necessary to cool the launcher itself during operation. The detail heat load to the launcher is

[1] Radiation from plasma to the top of the launcher 0.43 MW

[2] Neutron heat load due to neutron to the top of the launcher 2.80 MW
[3] Heat load due to radiation and ripple loss to the guard limiter 0.22 MW
[4] RF loss due to rf current in the waveguide to total waveguide 4.3 MW
[5] Reflection from plasma to the vacuum dummy load 2.80 MW

The summation of this heat load is 10.55 MW per one unit launcher. As shown in Fig.3-3, the cooling water is supplied from the auxiliary cooling system of the reactor and is led into the launcher itself from the entrance of the cooling nozzle at back side. The cooling water inside the launcher travels through the cooling header and cools the top of the launcher and enters to the cooling-shield part. The cooling water can also shield the neutrons and gamma ray. The cooling water in the cooling-shield part is exhausted from the exit of rear cooling nozzle and is returned to the auxiliary cooling system in the reactor. The vacuum dummy load is equipped inside the cooling water and the special cooling line is equipped for this dummy load. This cooling line is divided at the side cooling header and the water in this line cools the dummy load and is sent into the cooling-shield part and is finally jointed with other water. Another cooling line is equipped for the input waveguide and the waveguide in the vacuum box for the differential pumping system, which forms the branch of the main cooling line.

Some explanations on the cooling water analysis is given in this section using the condition in Table 3-4. The rf loss q_R is assumed to be 0.7 MW at the front end of launcher and to be 3.6 MW for other parts. The heat load distribution due to neutrons is $q_N=10\exp(-0.058x)$ (W/cm^3) ,where x is the radial direction. The radiation heat load $q_p=15.4$ W/cm^2 is for the front end launcher. For the guard limiter, the thermal load due to α particle is flooded in addition to above heat loads, which is $q_\alpha=7.0$ (W/cm^2) for the outside of guard limiter and $q_\alpha'=46.34$ W/cm^2 for the front end of the guard limiter. To one of top modules with 6 divisions the cooling water is fed by a pipe having the diameter of 70 mm. The input heat load Q_T is $Q_T=q_R+q_N+q_p+q_\alpha=117+943+77.4+67.1=1204.4$ kW. We assume that the temperature in the inlet of the cooling water is 60°C and that in the outlet is 70°C. The necessary cooling water quantity W is $W=Q_T/4.1868/P\Delta T/1000=0.0288$ m^3/sec and the flow velocity $v=W/A=0.0288/(\pi/4 \times 0.07^2)=7.5$ m/sec. The pressure drop is estimated by the relation $n_e=\lambda(l/d)x(v^2/2g)$, where λ is the pipe friction coefficient $\lambda=0.0032+0.221R^{-0.237}=0.011$, $R(=11.7 \times 10^5)$ is Reynolds number, l(=30 m) is the length of the cooling pipe, d(=0.07 m) is the diameter of the pipe and g is the gravitation acceleration. Thus, the value of n_e becomes 13.5 m. Since the pressure drop at the top module of the launcher must be added to this value, the real pressure drop is estimated to be 15 m (1 kgf/cm^{2}G). The heat load in other part of the launcher except of the top module is $Q_L=q_R+q_N=3600+79.4=3674.4$ kW and the

necessary cooling flow is $W=Q_L/4.1868/P\Delta T/1000=0.0879$ m^3/sec. The flow velocity is $v=W/An=3.2$ m/sec when the cooling water is supplied by three pipes with the diameter of 103 mm

The launcher itself must be baked after the initial installation and after the maintenance operation. The baking is performed using the cooling pipe line in the launcher. After the cooling water is completely drained out the valve for baking is switched on and N_2 gas is heat-exchanged at the reproduction heat exchanger with the return gas sent from the launcher and is heated to the setting temperature and enters to the launcher. The N_2 gas heat the waveguides to the constant temperature and return to the baking system from the cooling nozzle. The return hot N_2 gas is heat-exchanged at the reproduce heat exchanger and is cooled at the entrance of broiler and circulates in the system.

(5) Decomposition and Installment of the LH launcher

The decomposition of the LH launcher is in the following.

[1] The cooling water in the launcher is completely drained out.

[2] The shielding block is removed.

[3] The waveguide in the transmission line and the launcher are resolved.

[4] The pipe for the differential pumping system and the cooling water pipe are resolved with the launcher.

[5] The first and second ceramic window and the arc detector are removed from the RF gate valve in the rear direction.

[6] The launcher is inserted by about 800 mm into the vacuum chamber by using the moving structure and the top of the divider part is removed inside chamber.

[7] The rf port and the launcher are resolved at the double bellows.

[8] The launcher structure ridden on the transport vehicle by using a winch to be removed and is installed in the cask.

The installation sequence is in inverse at the decomposition.

The replacement of top of the launcher is planned in FER design. Since the top of the launcher suffers much heat load and neutron bombardment from plasma its environment is very severe. The top of the launcher is replaced by using the remote controlling vehicle[13] set inside the vacuum chamber. Since the remote vehicle can transport below 1 ton weight the top of the launcher is divided by six components as shown in Fig.3-8. The electrical junction between the grill mouth and the launcher junction is performed by inserting a electric contact as shown in Fig.3-9. When the water pressure is applied to the cylinder the cylinder rod pushes the connector and the electric contact is pressurized. When the top of the launcher is replaced the cooling pipe at the top part of the launcher must be cut by

laser cutter, which is specially developed for the branket pipe environment. Since the laser cutter is travelling inside the cooling pipe the inner diameter of the pipe must be more than 50 mm, which is shown in Fig.3-10. The launcher itself has the same life time as the reactor itself. When the launcher is over the life time the rf gate valve is closed and the transmission line is removed and the cask is connected as shown in Fig.3-11. The concept of the replacement of top of the launcher is applied to the ITER design, which is described in another section.

3.2 Thermal Stress Analysis of Guard Limiter with Carbon

The thermal stress analysis model for the guard limiter made of C/C composite as shown in Fig.3-12 is performed using the analysis code of TRUMP3-JR and SAPV2. The front of the waveguide is made of molybdenum coated by carbon. Inside waveguide water flow is for cooling. Material constant of C/C composite (CC-312) and molybdenum are shown in Table 3-2

Table 3-2 Material constant of CC-312 and molybdenum

	CC-312	Mo
density (kg/mm^3)	$> 1.65 \times 10^{-6}$	10.22×10^{-6}
specific heat (kcal/kg.°C)	0.18	66.2×10^{-3}.
thermal conductivity (kcal/mm.s°C)	$>47.8 \times 10^{-6}$(parallel) $> 23.9 \times 10^{-6}$(perpendicular)	34.18×10^{-6}
thermal expansion rate (kg/mm^2)	<1.5(parallel) < 12 (perpendicular)	4.9
Young modules (kg/mm^2)	2550(parallel) 820(perpendicular)	42857.1
Poisson ratio	0.2	0.3

The heat load due to α particle is assumed as q_α=7.0 W/cm^2 for the out side of guard limiter and $q_\alpha'=(I_F/I_g+1)q_\alpha$ for the top of the guard limiter, where I_F is the length of the waveguide bundle in the toroidal direction and I_G is the length of guard limiter side as shown in Fig.3-13 (a). The cooling condition is shown in the Table 3-3.

Table 3-3 Analysis condition for thermal analysis for LH launcher

Heat conditions	
radiation from the plasma	q_p=15.4 W/cm^2
α particle	q_α=0.0 W/cm^3
neutron	$q_n=q_{n0}\exp(-0.058x)$ W/cm^2 , where q_{n0}=10.0 W/cm^3 and x is the radial direction
RF loss	q_{RF}=0.48 W/cm^2 (for copper) q_{RF}=0.96 W/cm^2 (for beryllium)
Cooling condition	
Flow quantity	W= 1000 m^3/hr.unit
Flow velocity	u= 0.5 m/sec
Temperature	T= 60.0°C
Heat transfer coefficient	h=0.218 W/cm^2 °C
Analysis code	
Thermal analysis	TRUMP3-JR
Stress analysis	SAPV2

The thermal conductivity in the parallel and perpendicular direction is both same 47.8 x 10-6 kcal/mm•s°C When we calculate the thermal analysis of the guard limiter we perform the following four cases.

	width of molybdenum cooling duct	the width of CC-312
case-1	5 mm	10 mm
case-2	5 mm	7 mm
case-3	5 mm	5 mm
case-4	3 mm	5 mm

The direction of fiber in the CC-312 faced at the plasma and the constraint condition are shown in Fig.3-13 (b) and (c), respectively. The result of the thermal analysis is listed in Table 3-4 The allowable shear stress is 4.5 kgf/mm^2 for CC-312 and 12.04 kgf/mm^2 for molybdenum and the analysis results are both tolerable for the shear stress. The maximum stress excited at the CC-312 has the maximum value at the contact surface with molybdenum and this stress is caused by the difference of thermal expansion rate between molybdenum and CC-312. Since this thermal expansion difference is also caused by the temperature difference between the room temperature (say 20°C) and the hot temperature

of guard limiter (say about 400°C) during operation the thermal stress is not caused by the effect of temperature profile in this analysis model. In order to reduce the stress it is necessary to insert the material having the intermediate thermal expansion rate between the molybdenum and CC-312. In Fig.3-14 (a), (b) and (c), the example of the temperature profile, thermal stress and the displacement due to the thermal stress are shown for case 4, respectively.

Table 3-4 Thermal stress of guard limiter

	thermal stress σ_{max}(kgf/mm^2)		Max temp.	Min temp.
	CC-312	Mo	(°C)	(°C)
case-1	≤ 6.0	12.1	428.4	88.0
case-2	< 5.0	10.3	408.4	88.0
case-3	≤ 4.0	8.24	395.7	88.0
case-4	≤ 4.0	9.06	380.6	88.0

3.3 Design Study of Transmission Line for FER

The system line-up of LHRF system for FER is shown in Fig.3-15 The output of the original signal generator is fed to the level controller, where the on/off and the level controlling of rf output power are performed. The rf power is amplified up to the necessary power by using the low power amplifier and then is divided to 72 fold ways by the power divider. This signal is further adjusted by the phase controller and the amplitude compensator and is again amplified to the power level so as to drive the high power klystron. The technological problem at this power level has no problem if we use the conventional amplifier and the solid state amplifier is available for the low power amplifier without using TWT. The higher power klystron has necessities of special R & D, which is described in detail in another section. In the case of two output window of the high power klystron some power combiner and absorption resistance is necessary after the arc detector as shown in Fig.3-15.

The candidate of transmission line at 5 GHz range is WR-159,WR-187 and WR-229. It is desirable to use oversized WR-229 to reduce the transmission loss, however, it is afraid to excite the higher mode such as TE_{20}. In order to avoid these higher modes this waveguide is usually used at the frequency range of 3.22 - 4.9 GHz By the exact calculation the higher mode of TE_{20} is excited at the frequency of 5.157 GHz. The scale of the optimized waveguide using WR-229 is 57.0 mm in height and 28.5 mm in width,

which is available for the frequency range of 3.29 - 5.0 GHz and the attenuation rate is 32.5 dB/km. If we compose the whole length of the transmission line (about 92 m) with only WR-229 the loss is estimated to be 2.9 dB, which may lead the larger output power of klystron with about 944 kW per one tube since we must consider the further loss of rf window and other part. In order to reduce the transmission loss it is considered that the material of the waveguide is changed from phosphorus deoxidized copper to genuine copper (oxygen free electrolytic copper) and/or that the oversized waveguide is used. In the former case we can reduce the transmission loss to 21.36 dB/km. The latter candidate is to use the WR-284,WR-340,WR-430,WR-510, WR-650 and WR-770, however, the transmission line loss saturates for WR-770 and it is afraid to excite the higher mode. The transmission loss using the mode convertor (from WR-229 to WR-650) is about 0.16% for taper tube and below 0.1 % for 90° bend

3.4 System Layout and Overall System Efficiency

The main part of LHRF system is placed at the heating facility room of second floor in the underground floor, whose plane view is shown in Fig.3-16. In this room, high power amplifier, capacity flame for dummy load, rf transmission components, high voltage processor for power supply, power supply panel for magnetic coil, transformer, and power panel, and controller panel and other attachment. The room has a capability having pits for cooling water pipe, power cables and controller cables. It is necessary to design so that the system can produce the fundamental capabilities. Especially, the length of the transmission line is as short as possible to reduce the rf loss. The layout of the system must satisfy the following points.

[1] the maintenance space for the instruments must be occupied
[2] the installation space for machine transportation must be occupied
[3] the moving space for crane must be occupied
[4] the maintenance root for safety must be occupied
[5] the operation room free from the radio-activity and the rf leakage
[6] electrically leakage free due to water invaders
[7] the earth line must be simplified

Figure 3-17 is a simplified transmission line route for FER. From this figure the layout the averaged transmission loss is shown in Table 3-5

Table 3-5 Transmission line loss at the waveguide temperature of 75 °C

root No.	length (m)	waveguide (loss dB/m)	loss (dB)
1	1.5	WR-229 (0.031)	0.046
2	18.5	WR-650 (0.008)	0.148
3	12.3	WR-650 (0.008)	0.096
4	5.0	WR-650 (0.008)	0.040
5	17.3	WR-650 (0.008)	0.142
6	19.5	WR-650 (0.008)	0.156
Total	74.5		0.628
Reactor room		Launcher	0.542
Others		Window, Taper rubes	0.090
Total loss			1.200

As seen in Table 3-5, the general rf loss including klystrons is about 1.32 dB and 45 MW of high power amplifier is necessary, which is 625 kW per one klystron. The rf loss of 1.315 dB is estimated to be 73.9 % of the efficiency. Since the efficiency of klystron is 60 % with matched condition (55.6 % with VSWR=1.5) and the transition efficiency of the power supply is 1- 2 % and cooling facility is 5 % then the overall efficiency is 0.739 x 0.556 x 0.95= 0.39. The necessary power supply capability is 45 MW/(0.39x 0.75) =154 MVA ,where the power factor of the power supply is 0.75 - 0.8.

3.5 Shield for Neutron

(1) Shield for neutron

The neutron dose must be below 2.5 mrem/hr outside of the reactor room and the maintenance area of reactor room one week after after the shut-down of FER. Without any shielding the neutron dose at each area can be estimated in the following value from the calculation of NBI duct for ITER[14)]

	First wall (mrem/hr)	outside of cryostat (mrem/hr)	outside of reactor room (mrem/hr)
during operation	4×10^{13}	5×10^{11}	1.3×10^{10}
one week after shut-down	8×10^{9}	1×10^{8}	3.0×10^{6}

In order to reduce the dose rate we perform the bending of waveguides and setting the shielding material inside the waveguides. Thus, we can estimate the real dose rate at each

the operation. In this estimation, we assume that one order reduction of the dose rate is achieved by each bend and the appropriate shield is performed around the waveguide bend using absorbing materials. As shown in Fig.3-2, the waveguide bends four times inside the launcher and further shielding must be performed at the multi-junction parts, which is confirmed by the estimation using Monte-carno method[14] The value of 10^8 mrem/hr at the RF gate valve is so optimistic because there exists a straight component part beside the bending part in the rf gate valve If we cannot reduce the dose rate it may be necessary to set further bending waveguide in the rf gate valve or setting the shielding material behind the rf gate valve, however, it is afraid that the cask becomes large.

(2) Maintenance for Tritium

A counterplot for tritium yield is planned during operation and when the vacuum window is destroyed. During operation, the following counterplot for tritium is planned.

[1] The launcher itself is double shielded by the bellows for the vacuum environment.

[2] The launcher waveguide is double shielded by two fold vacuum windows against the gas in the transmission line waveguides.

[3] Tritium gas following from the vacuum vessel into waveguide is evacuated at the differential pumping system and is sent to the equipment for the fuel gas producing system

When the vacuum window is destroyed, the counterplot for the tritium shielding is changed. The flow chart around the vacuum window is shown in Fig.3-19. During normal operation, the part 1 and 2 are in full vacuum condition, the part 3 would be in 400 torr and part 4 is in 1000 torr. The counterplot for tritium shield in this case is in the following.

[1] When the arcing phenomena occurs at the vacuum window, the arcing signal is detected by the arc detector and the rf signal is immediately cut-off to protect the window.

[2] When the primary vacuum window is destroyed the vacuum at the point 3 decreases to 0 torr. This pressure drop is detected by the lower setting pressure (say 200 torr) of the pressure inspector detector (PIS) and the fast valve is closed and the tritium flowing into the transmission line side and the pressurized gas flowing in the waveguide into the vacuum vessel are protected by stopping the rf source.

[3] When the secondary vacuum window is destroyed the pressure at the point 3 increases up to 100 torr. This pressure increase is detected by the upper setting pressure (say 600 torr) of PIS and the valve is closed and the gas flowing of tritium and pressurized gas are protected.

By above counterplot it is not afraid that the tritium gas is flowing at the RF amplifier room as long as the secondary vacuum window is placed at the reactor room.

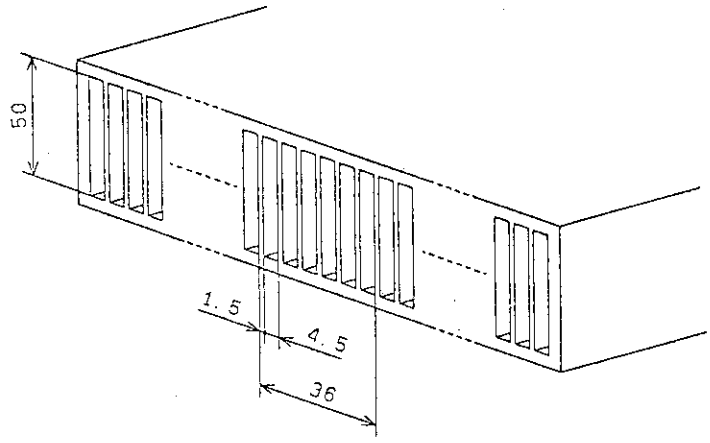

(a) Scale of top part of main waveguide

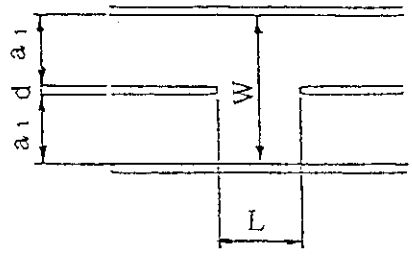

(b) Scale of power divider in the short slot type waveguide

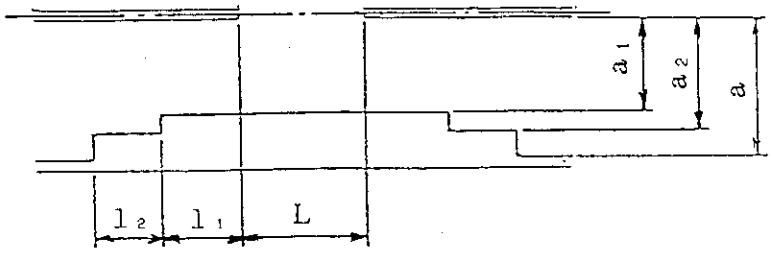

(c) Scale of λ/4 power divider

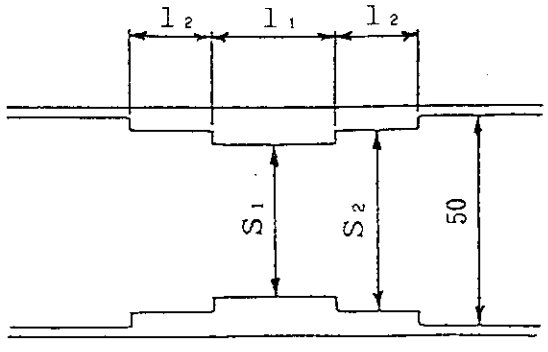

(d) Scale of phase shifter

Fig. 3.1 Scale of the main waveguide

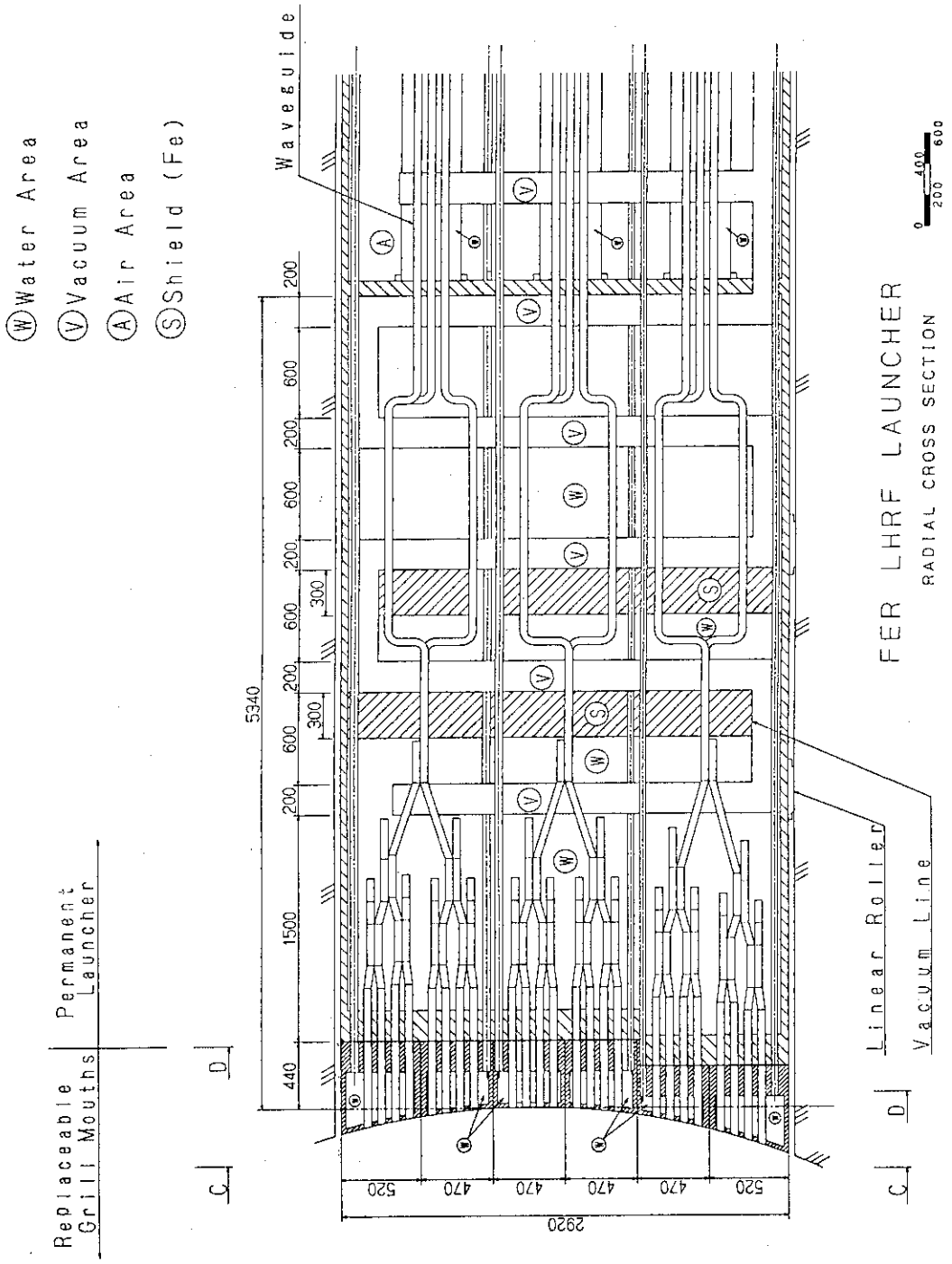

Fig. 3.2 Radial cross section of FER LHRF launcher

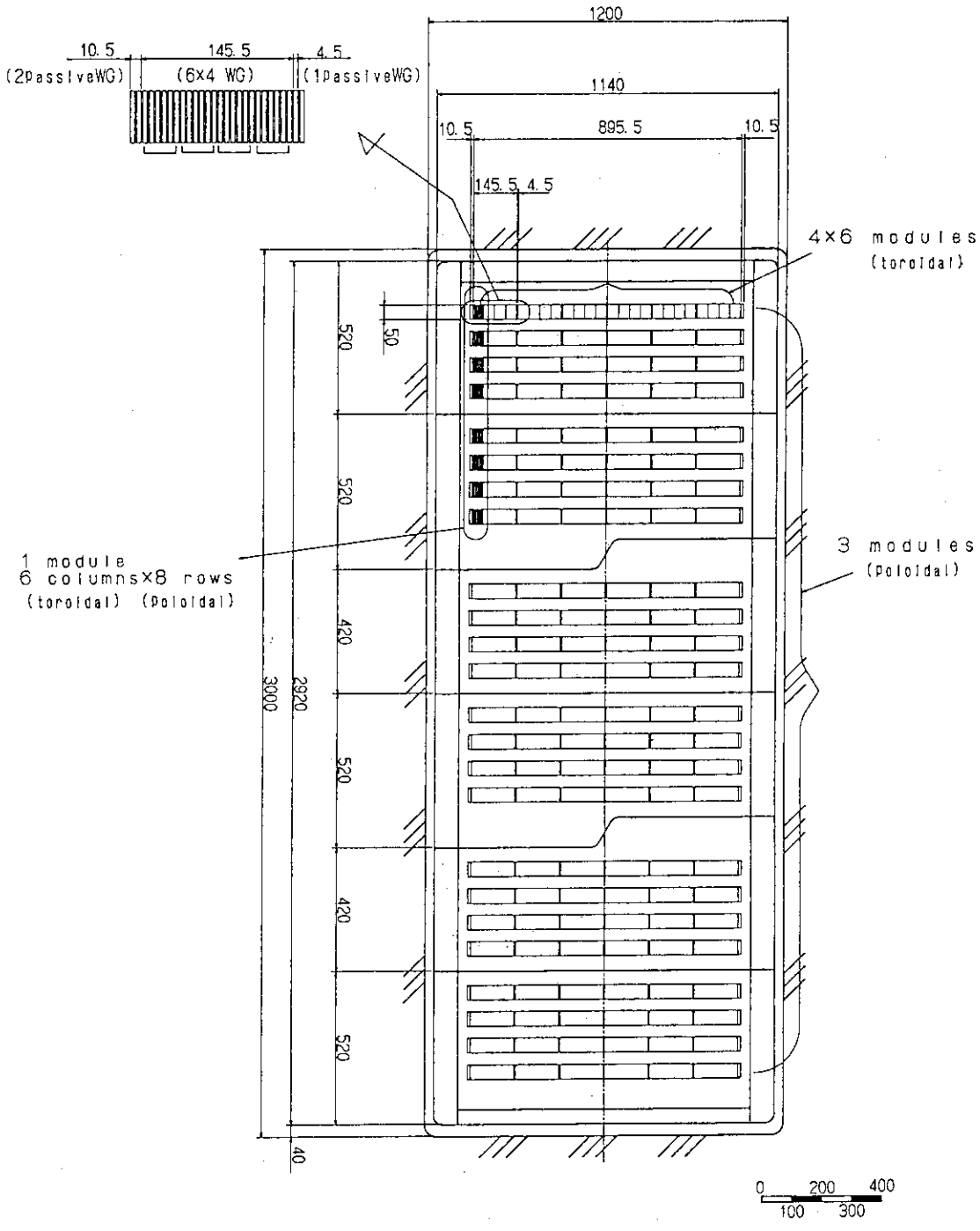

	toroidal	poloidal	total
module	24	3	72
WG/module	6	8	48
total WG	144	24	3456

SECTION C-C

Fig. 3.3 Sectional view of section C-C in Fig. 3.2

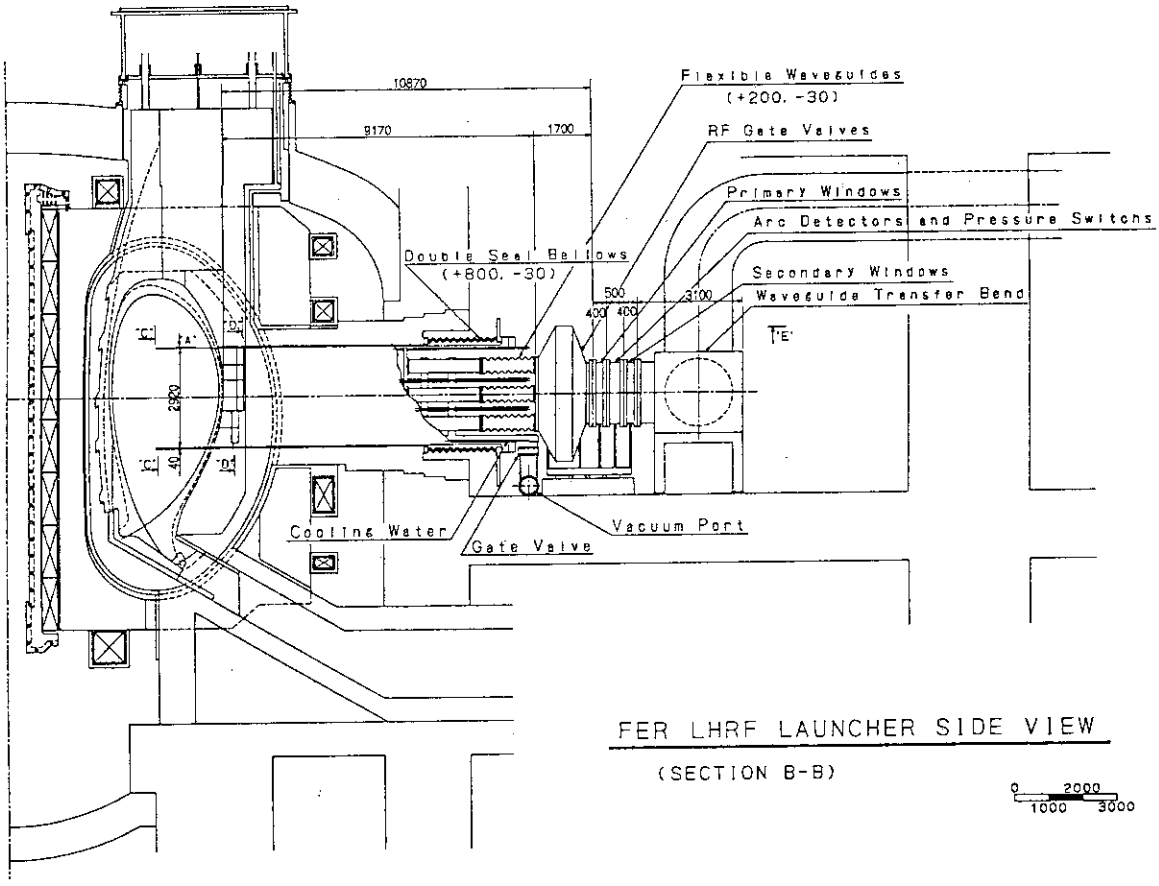

Fig. 3.4 Plane view of FER LHRF launcher (Section B-B in Fig. 3.5)

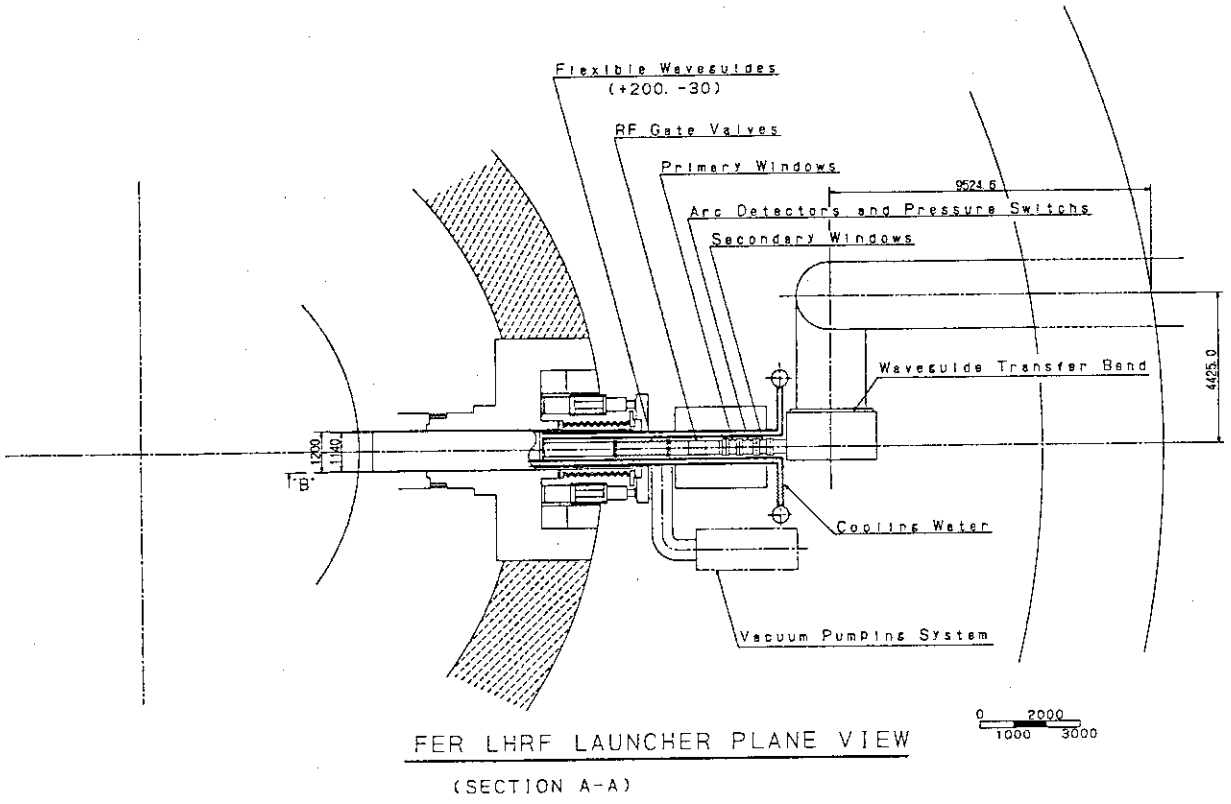

Fig. 3.5 Plane view of FER LHRF launcher (Section A-A in Fig. 3.4)

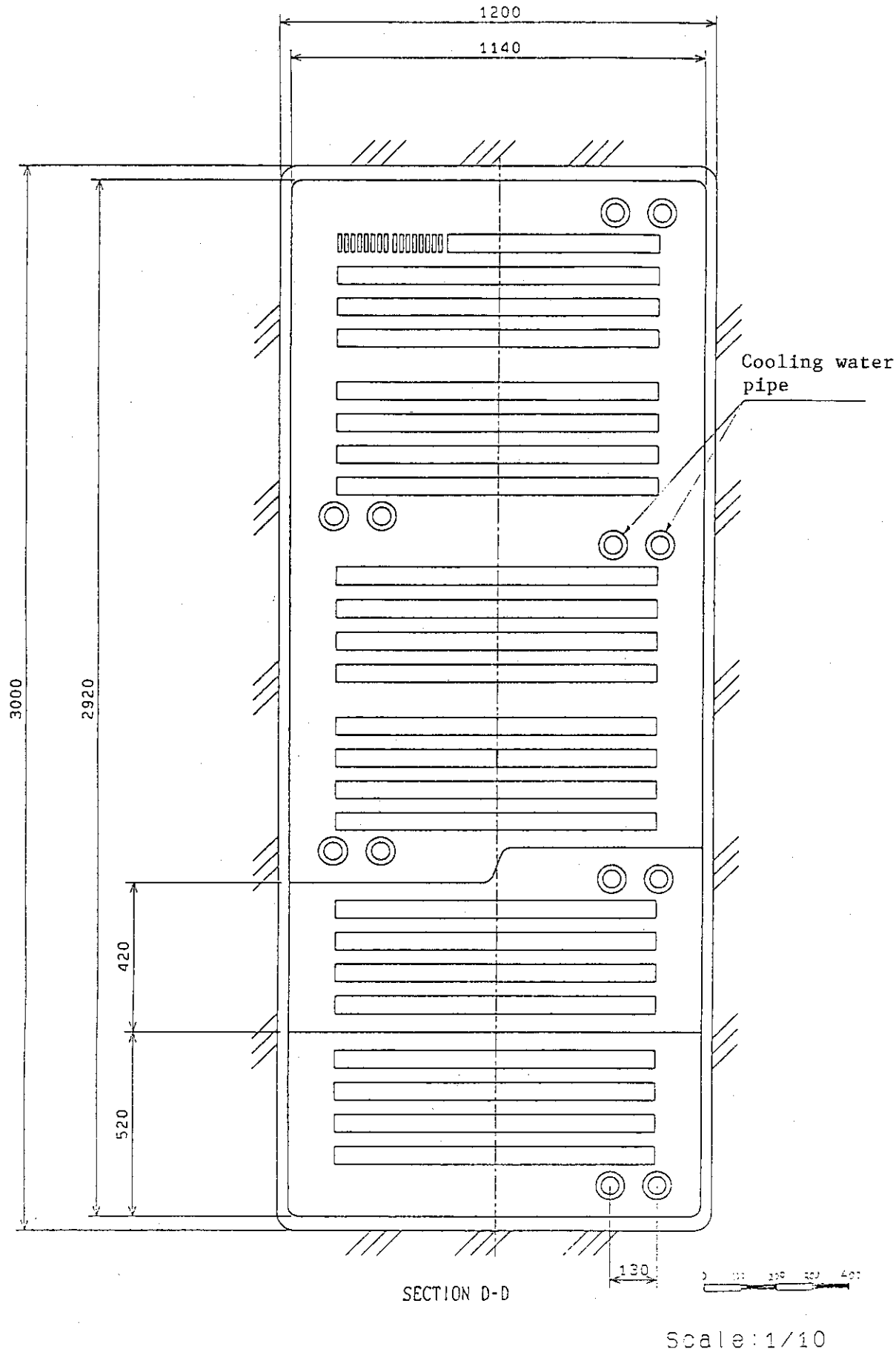

Fig. 3.6 Sectional view of section D-D in Fig. 3.4

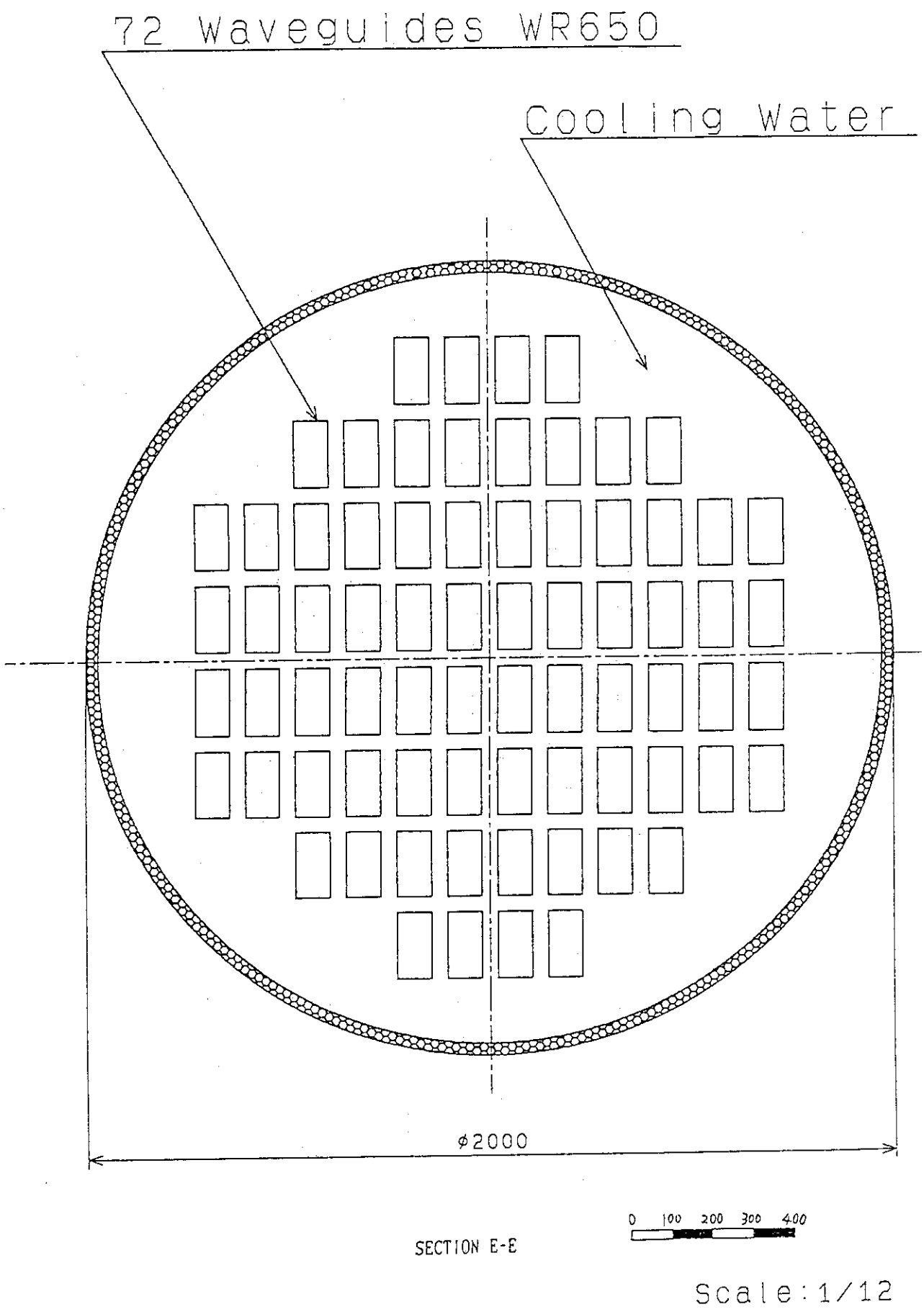

Fig. 3.7 Sectional view of section E-E in Fig. 3.4

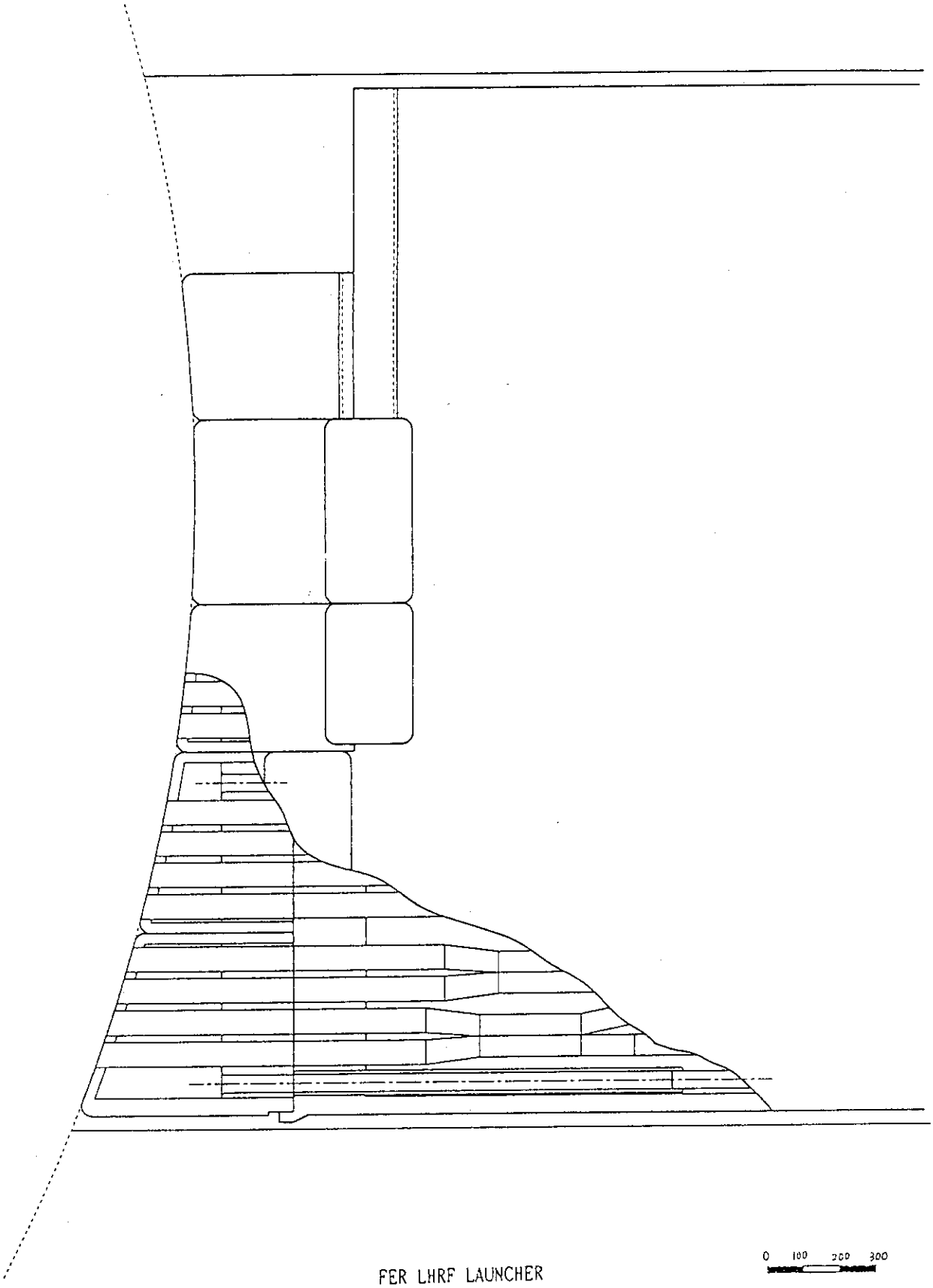

Fig. 3.8 Grill mouth for replacement

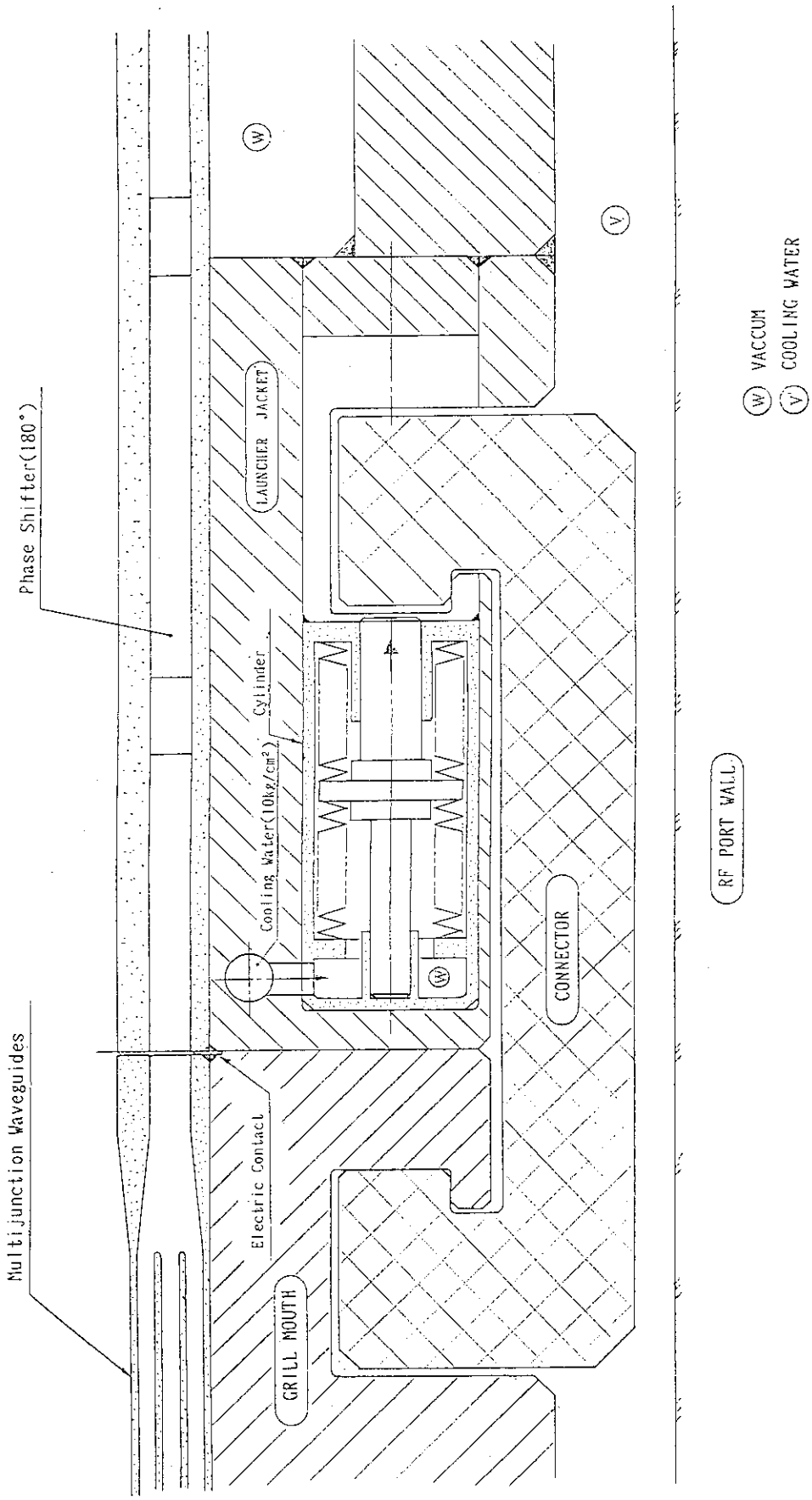

Fig. 3.9 Electrically contact between grill mouth and the launcher jacket

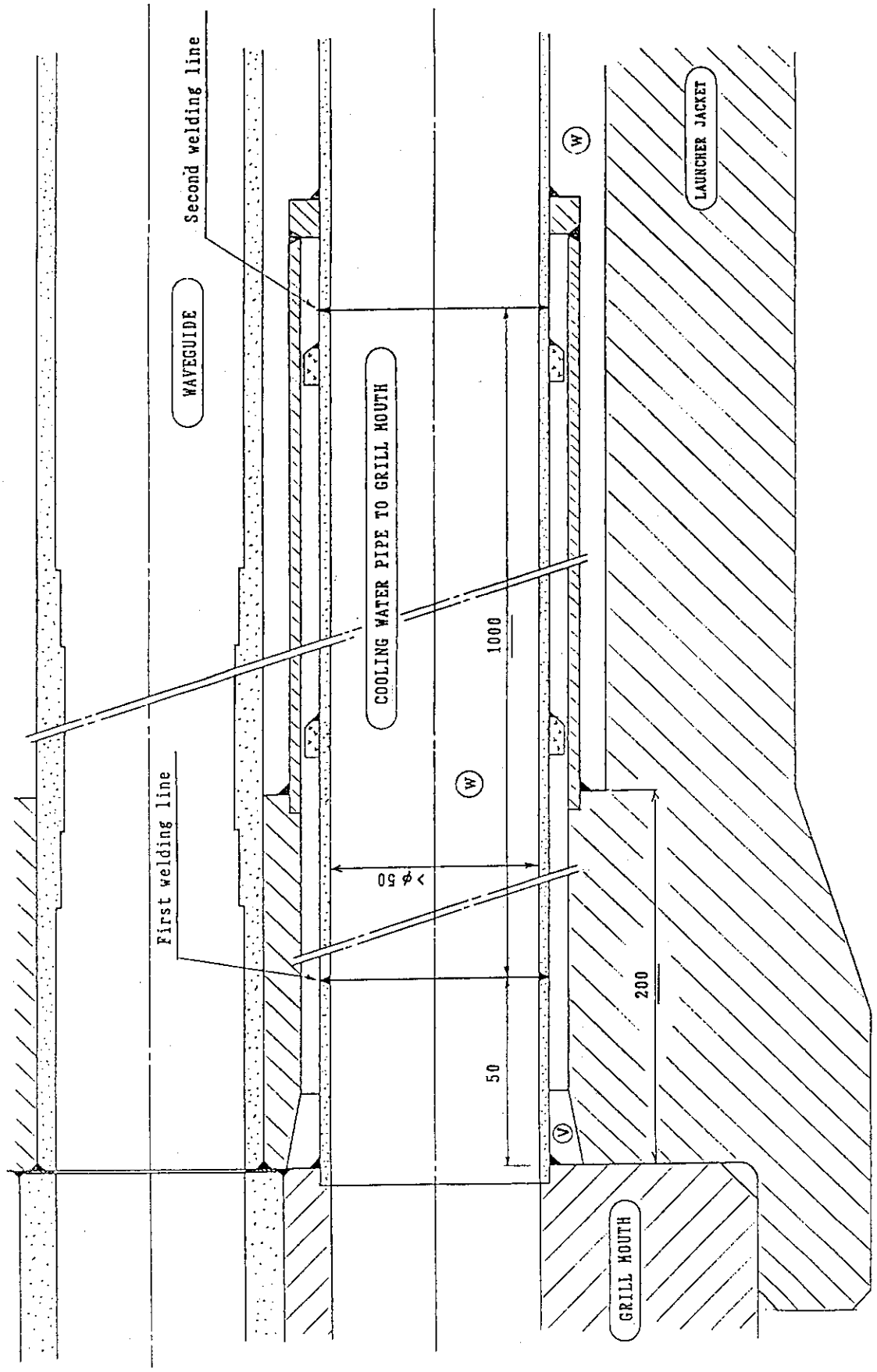

Fig. 3.10 Inside the cooling water ridding the laser cutter

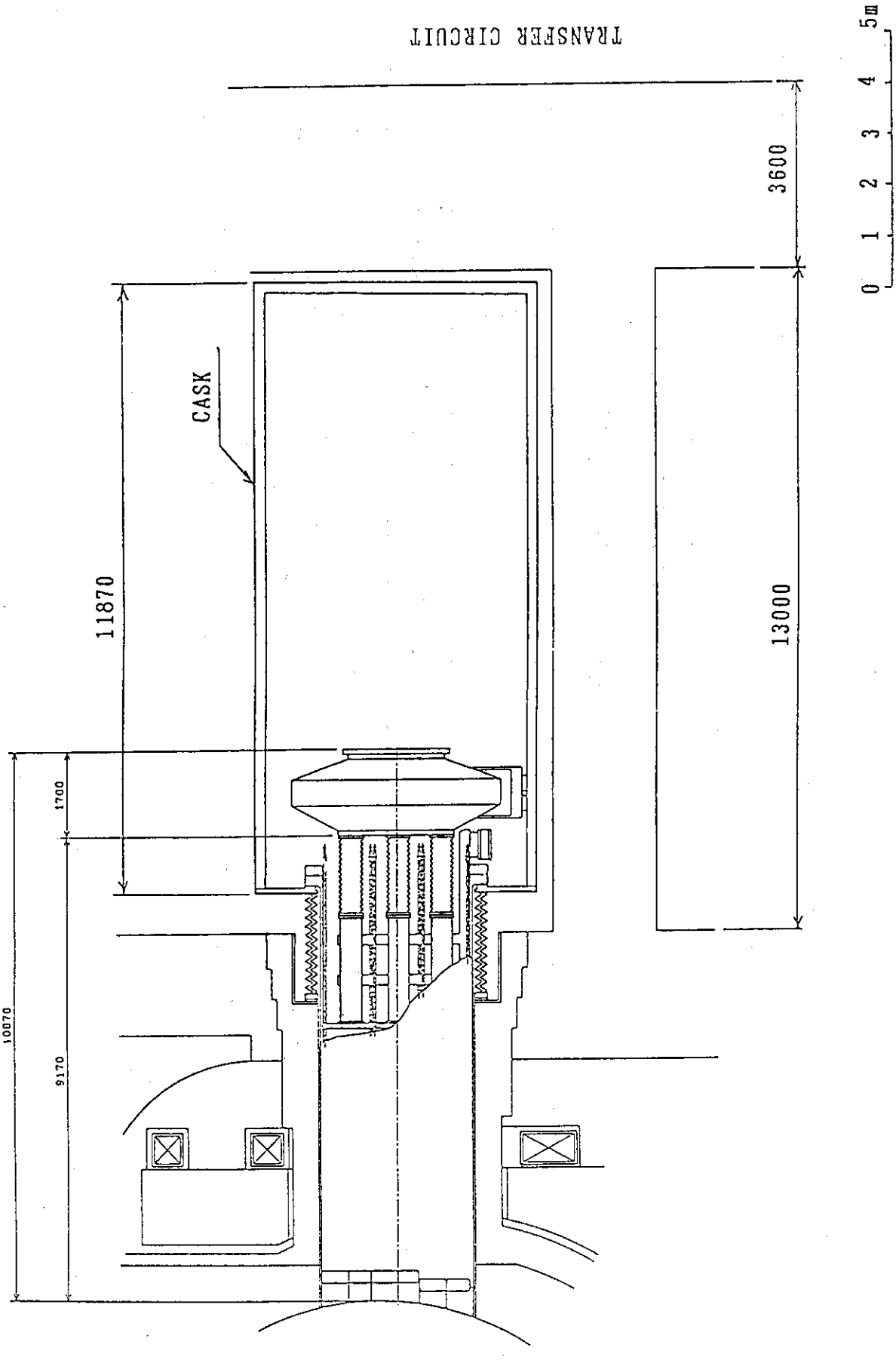

Fig. 3.11 Cask for the replacement of the launcher

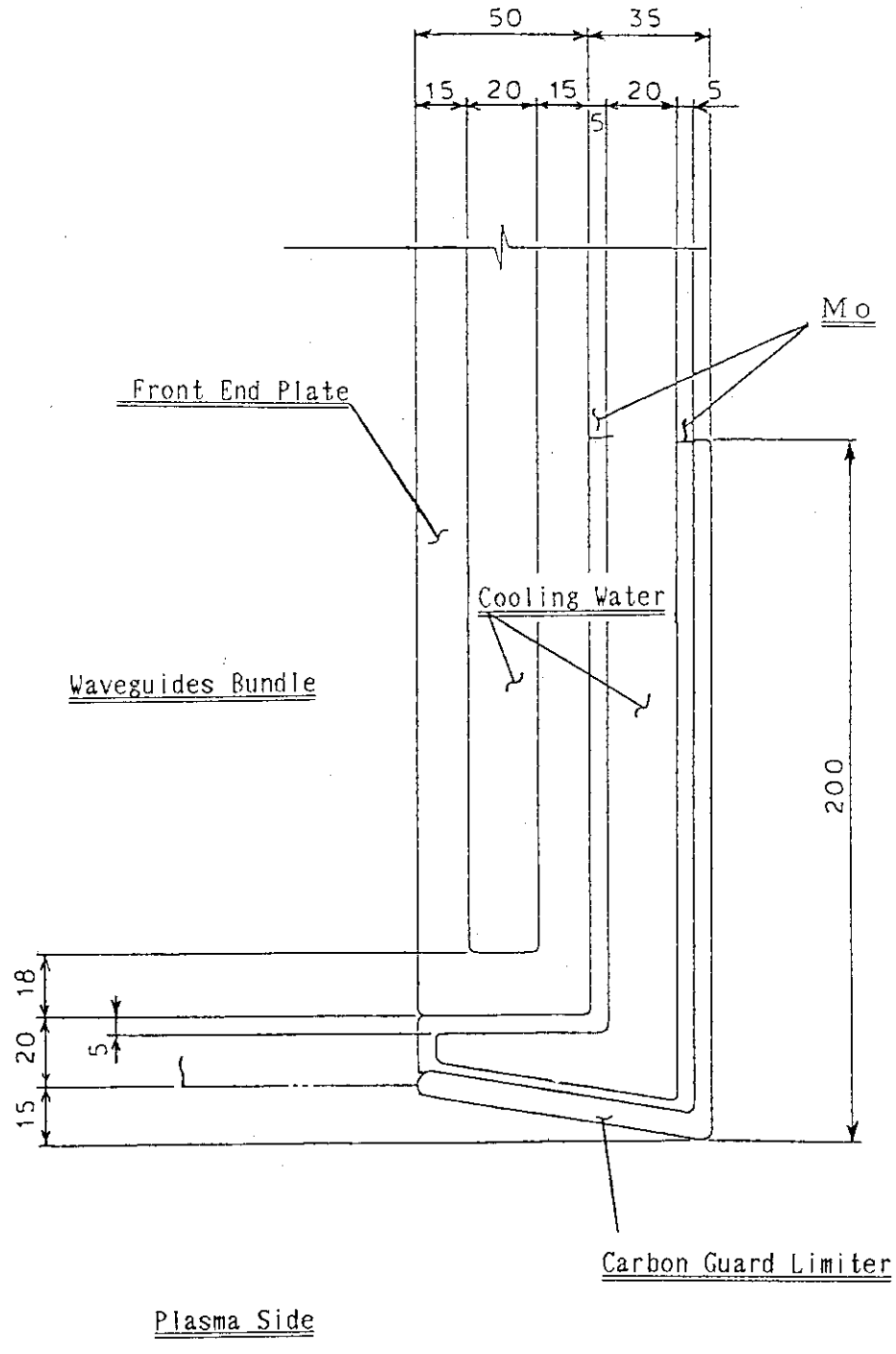

Fig. 3.12 Configuration of the heat analysis of guard limiter

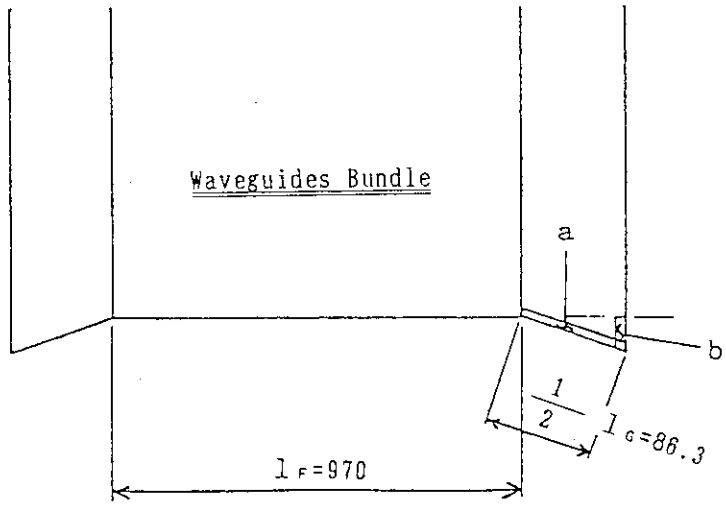

(a) Thermal analysis model for α particle radiation

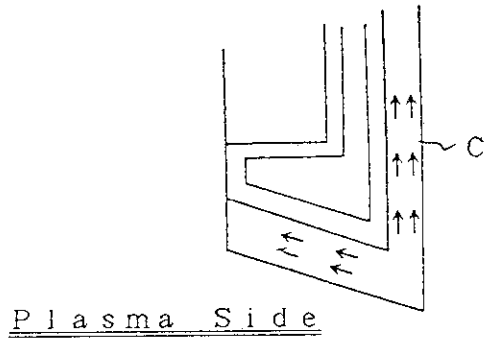

(b) Direction of the fiber in the C-C components

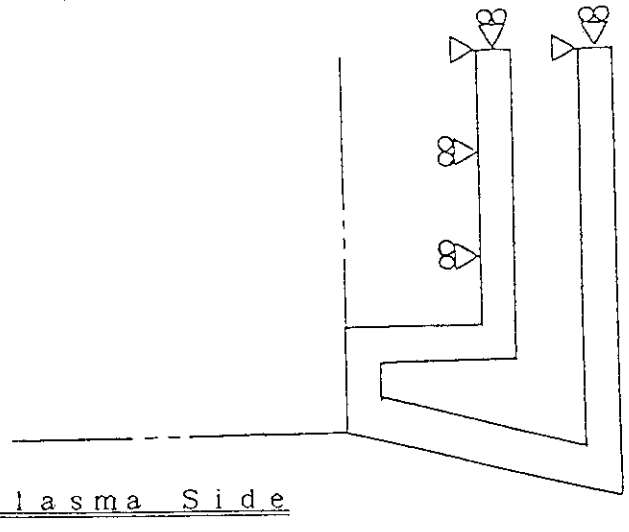

(c) Constraint condition for the analysis of the guard limiter

Fig. 3.13 Analysis model for the calculation

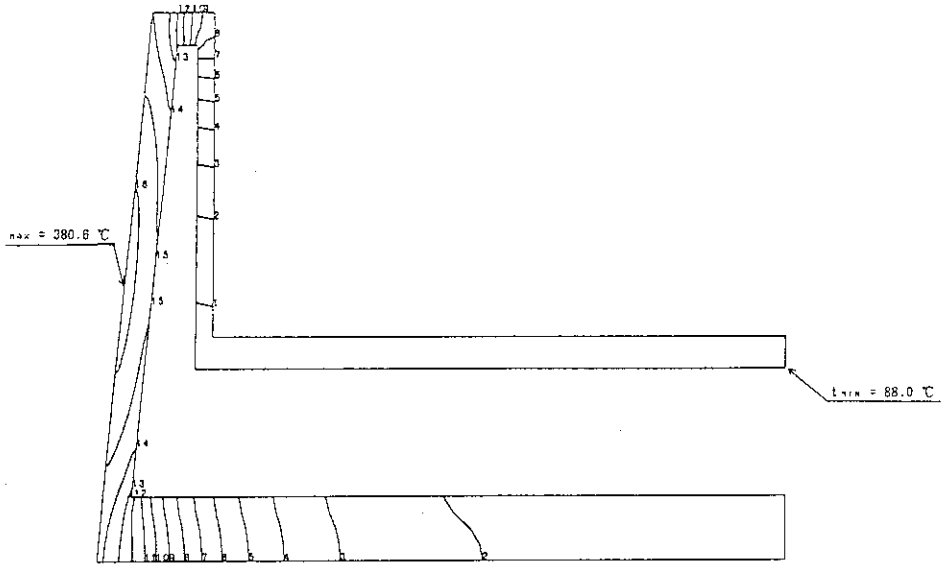

(a) Temperature contour of the guard limiter

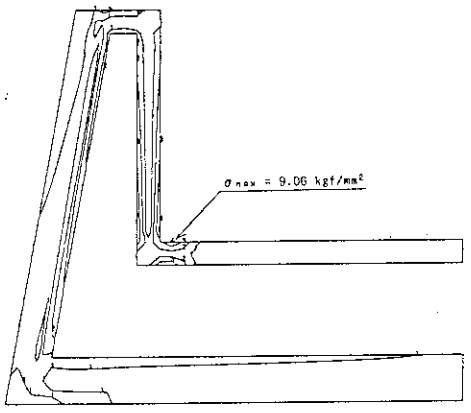

(b) Thermal stress of the guard limiter

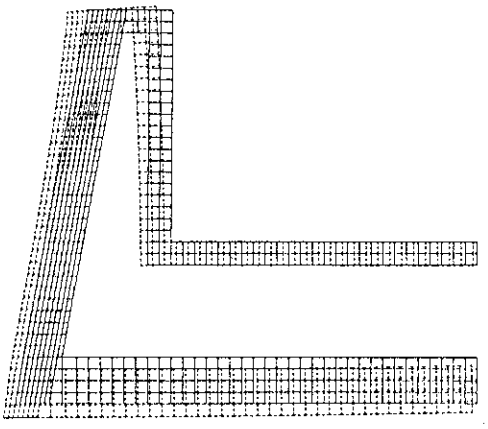

(c) Displacement due to the thermal stress

Fig. 3.14 Analysis results of guard limiter coated by carbon

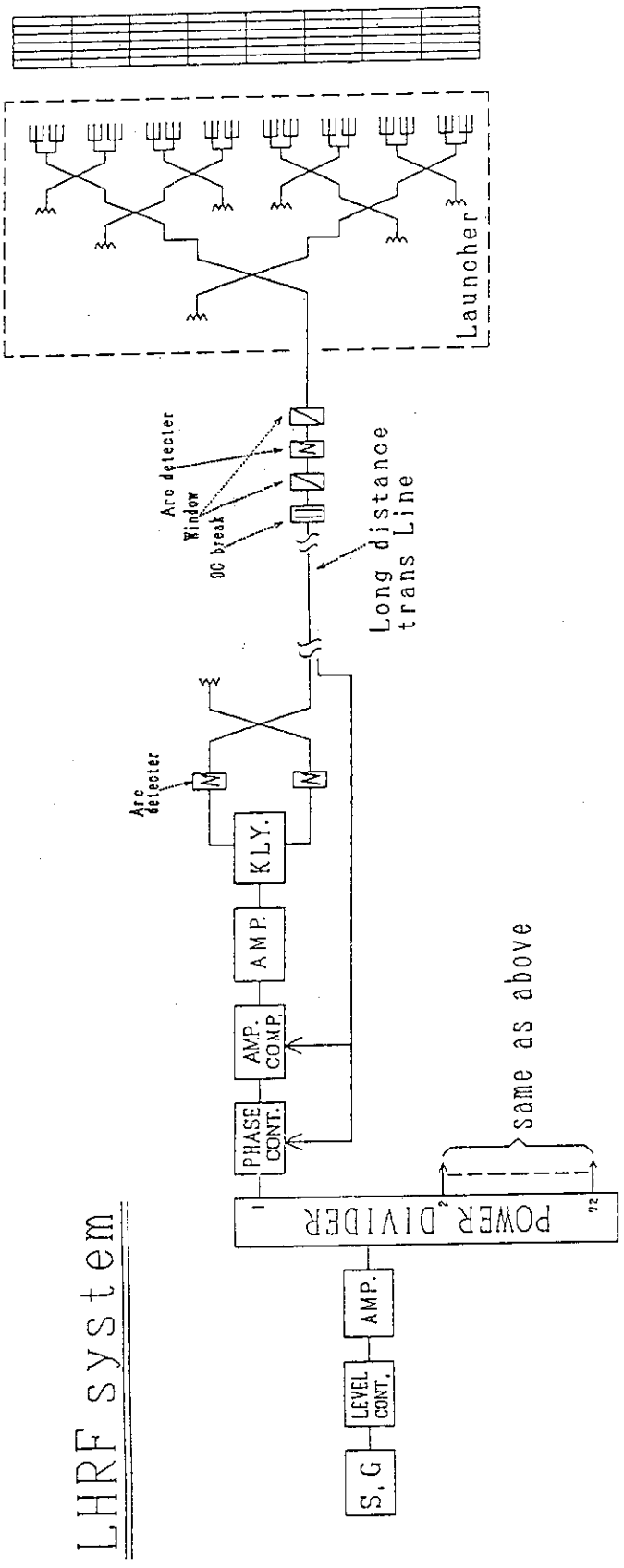

Fig. 3.15 LHRF line-up of LHRF system for FER

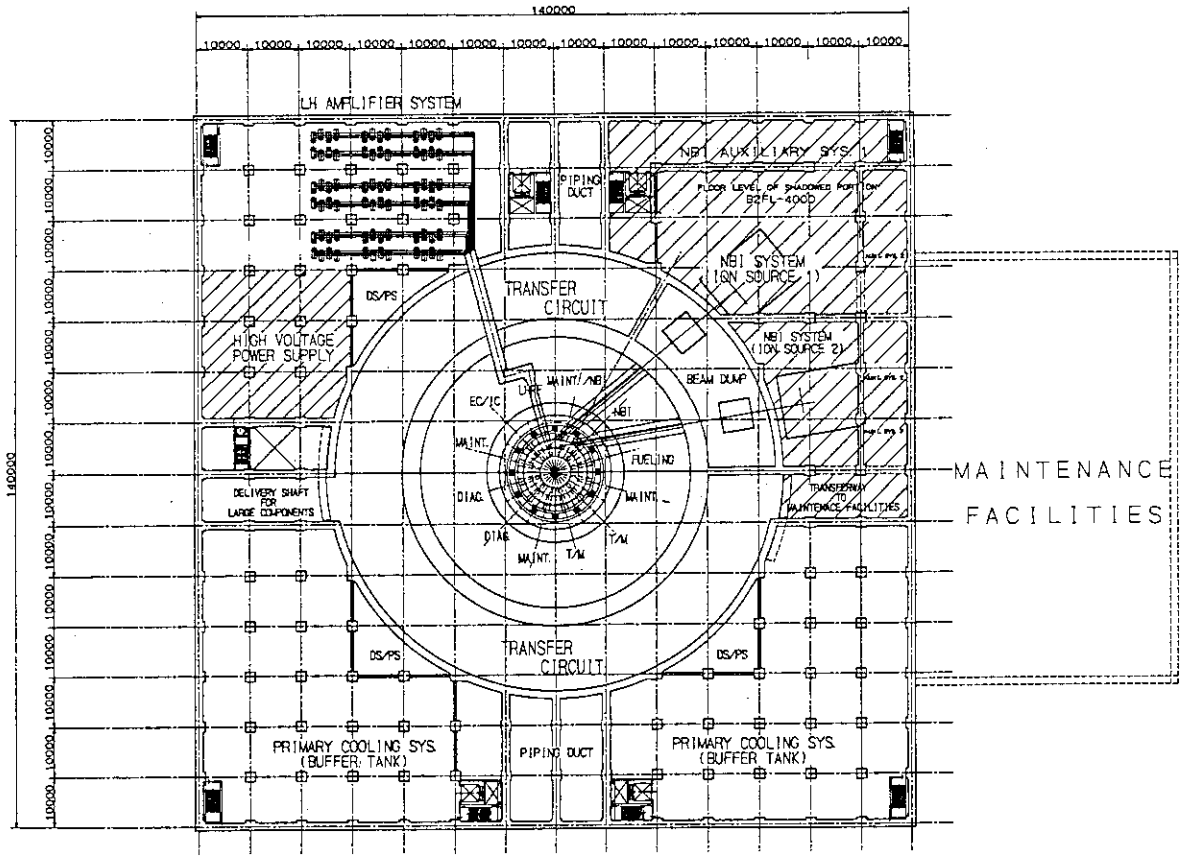

Fig. 3.16 Layout of LHRF system for FER

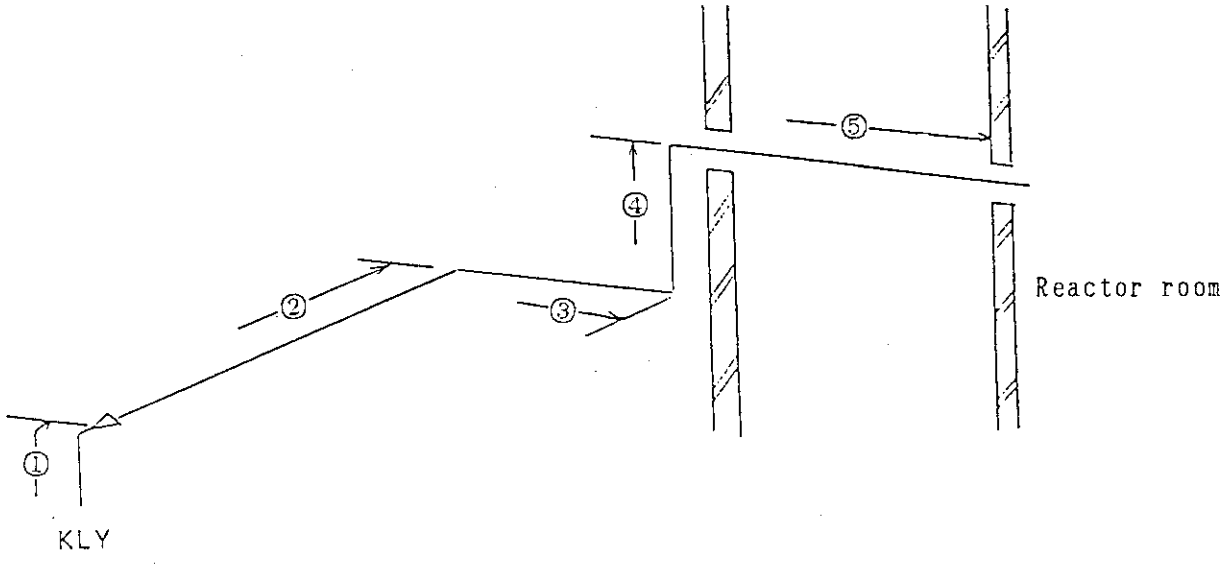

Fig. 3.17 Transmission root for the calculation of rf loss

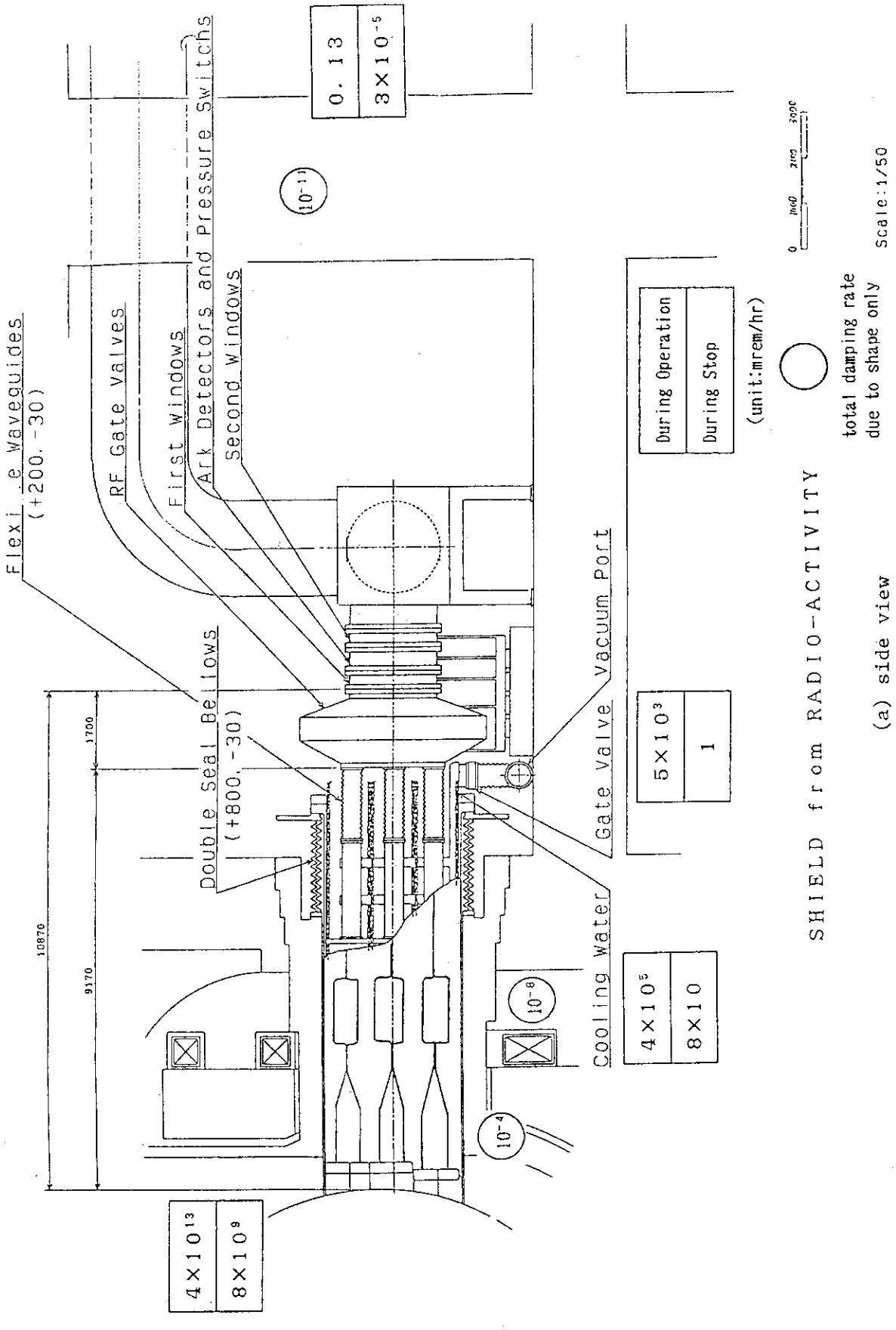

Fig. 3.18 Shiedling effect in the reactor room

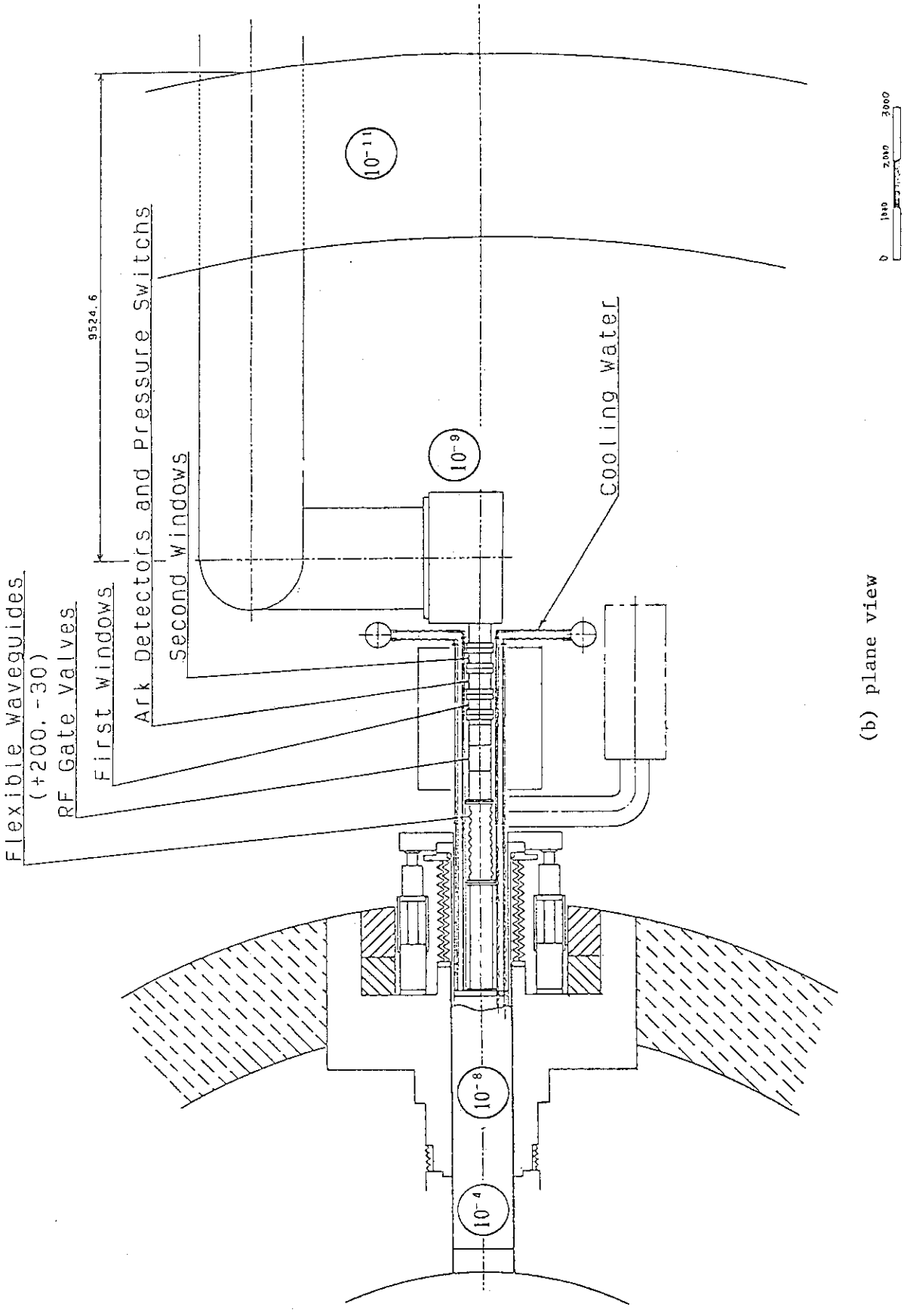

(b) plane view

Fig. 3.16 Shiedling effect in the reactor room

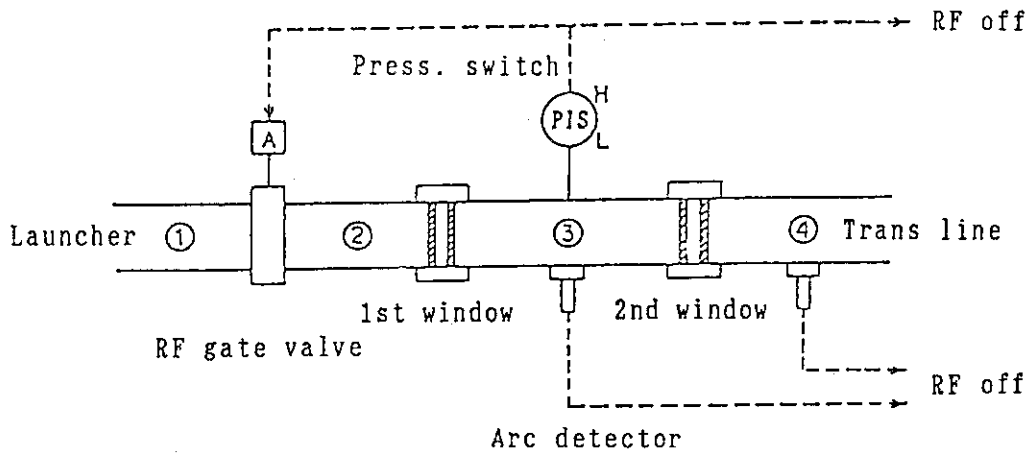

	①&②	③	④
Pressure in Normal Operation	Full Vácuum	~400 torr	~1000 torr

Fig. 3.19 Flow chart around the vacuum window for the counterplot of tritium flowing

4. JAPANESE CONTRIBUTION TO THE LH SYSTEM FOR ITER[15)]

4.1 Launcher Design

(1) Basic Structure of the LH Launcher

The basic specification of the ITER/LH launcher is shown in Table 4-1. The

Table 4-1 Specification of LH launcher for ITER

Waveguide	
Number of module	N (toroidal) x M (poloidal)
Number of main waveguide (per one module)	n (toroidal) x m (poloidal)
Scale of main W/G	a=50 mm
	b=4.5 mm
	d= 1.5 mm
fixed phase difference	60 degree
Transmission power density	4.0 kW/cm^2
Materials of waveguide	
main part	Glidcop
Front end	Be
Guard limiter	C
Temperature	
	150 (operation)
	250 (Baking)
Pressure	10^{-6}Torr•l/sec•cm2
Neutron dose	10^{18} n/cm^2

launcher is the multi-junction type and the number of module is N raws and M columns per one module. One module is consisted by n x m waveguides. The reference values for ITER; n=4 or 6, m=4 or 2 and nN≈100. The fixed phase difference in the unit of waveguide in the multi-junction launcher is 90 ° or 60 °, whose angle has the higher directivity in the wave spectrum. The power density of 4.0 - 4.5 kW/cm^2 is confirmed in the recent LHCD experiment in large tokamaks. The material of the waveguide are beryllium for the front protection of the launcher, carbon for guard limiter and Glidcop for

the waveguide materials, which must bear for the disruption and the thermal stress. The necessity of the insulation between modules must depend on the design study of the disruption analysis, which is seen in later. The temperature of the waveguide and the gas release rate does not coincide between EC design and the Japan design, which is coming from the difference of the estimation of the gas release rate. In Japanese design, the gas release rate is 10^{-8}Torr•l/sec•cm^2, which is estimated from the experiment in JT-60. On the other hand, in EC design two order larger value for the gas release rate is insisted from the data base in Tore-supra Cadarasche experiments. In such a design as EC, it is necessary to use the larger pumping system to evacuate the inside of the waveguides. The dose rate of neutron shield is assumed that the maintenance of the wave guide window is performed at the cryostat, however, if this dose rate cannot be reduced below this value, the waveguides must be bended before the window as shown in Fig.4-1. The bird eye view of the LHRF launcher for ITER is shown in Fig.4-2. The plane view of ITER LHRF launcher is shown in Fig.4-3. This figure is the A-A cross section of the next figure (Fig.4-4). The side view of the launcher is shown in Fig.4-4. The detail of the waveguide cross section in C-C section in Fig.4-3 is shown in Fig.4-5. The fine structure at the top of the waveguide is shown in the top of this figure, in which we can see two passive wave guide in both side. The section D-D in Fig.4-4 is shown in Fig.4-6, in which we can see the cooling water pipe at the right side of the waveguide. The section E-E, G-G and H-H are shown in Fig.4-7,4-8 and 4-9, respectively.

(2) Disruption Induced Stress

Electro-magnetic force during disruption acting on the ITER lower-hybrid launcher was calculated using a simple model with a equivalent circuit. The launcher is composed of upper jacket plate, intermediate jacket rectangular coil and lower copper plate as shown in Fig.4-10 (a). When the plasma current I_p decays suddenly,the eddy currents (i_T,i_{TC} and i_{cu}) are induced around the each part of launcher as indicated in this figure. The equivalent circuit is shown in Fig.4-10 (b). Each component has a finite resistance R and inductance L. The equation of the circuit is

$$Ri + Ldi/dt + d\Phi/dt = 0 \qquad (1)$$

where the magnetic flux $\Phi = \int BdS$ and the poloidal field B_θ changes with the decay time t_D as $B_\theta = (\mu_0/2\pi r) I_p \exp(-t/t_D)$. The toroidal field B_t changes as $B_t = R_0 B_{to}/(R_0+r)$, where

R_0 is the major radius in tokamaks and B_{t0} is the toroidal magnetic field at the center. Equation (1) can be solved using the initial condition i=0 at t=0 and the maximum current i_{max} is obtained when the derivative of the summation of each current becomes zero, di/dt=0 as indicated in Fig.4-10 (c). The value of R and L are obtained using the material constant:; $R=rl/A, L=(\mu_0/\pi)[-aln\{a+(a^2+b^{2)1/2}\}bln\{b+(a^2+b^2)^{1/2}\}$ $+(a+b)ln(2ab/d)+2(a^2+b^2)^{1/2}-7(a+b)/4]$, where μ_0 is the permeability of vacuum and r is the resistivity, A is the cross section of the component, a is the length in the x direction b is in the y direction and d is the width of the plate as shown in Fig.4-11. The maximum force F_T acting on the launcher is $F_T=i_{max}$ x B_T x a and the maximum moment M_T is $M_T=F_T$ x (b/2) x 2. Each part of the component is simplified for the sake of the calculation in the following. The plane plate is considered to be the summation of the N division parts (N=11) and the rectangular coil is simplified by the solid type box as shown in Fig.4-12 (a) and (b), respectively. The copper plate is insulated at the septum with stainless steel (s.s.) and the component is covered with s.s. as shown in Fig.4-12(c). The eddy current, the moment force and the total moment force are calculated in Table 4-2, where the torsional shear stress t_d is calculated

$$t_d=M/\{2d(b-d)(h-d)\} \qquad (2)$$

and the moment on the each component is acting as shown in Fig.4-13, where

Table 4-2 Summary of eddy current and moment force

	Eddy current	Moment force (unit)	Moment force (total)
	(kA)	x 10^3 [kg.m]	x 10^3 [kgf.m]
Jacket plate	I_T = 429.6	M_T = 279.1	$2M_T$ = 558.2
Jacket rectangular coil	I_{TC} = 495.1	M_{TC}= 544.9	M_{TC} = 554.9
Copper plate	I_s =73.0	M_s =9.7	$6M_s$ = 58.2
waveguide block		M_{GL}=4.0	$32M_{GL}$ =128.0
Total moment			M = 1289.3

equivalent length b,h and d in this figure are b=1140 mm,h=2080 mm and d=50 mm. The moment is acting on each component. The torsional shear stress is estimated 5.8 kgf/mm^2, which is smaller than the allowable value of 11.36 kgf/mm^2, which is the tensile strength of the stainless steel.

(3) Thermo-mechanical Analysis

Spatial thermal and stress analysis of ITER lower-hybrid launcher was performed at the stationary state when beryllium is brazed with the width of 10 mm at the top of the launcher. The waveguide grill of launcher is composed of the front end plate with SUS 316 , block spacer of dispersion strengthened copper (DS copper or Glidcop), and the septum of DS copper, whose plane and sectional section are shown in Fig.4-14 (a) and (b), respectively. The grill end is brazed with beryllium (Be) of 10 mm. The analyzed area is shown in shadow hatch in the figure. In Table 4-3, the analysis conditions are shown.

Table 4-3 Analysis condition for thermal analysis for LH launcher

Heat conditions	
radiation from the plasma	q_p=15.4 W/cm^2
α particle	q_α=0.0 W/cm^3
neutron	$q_n=q_{n0}\exp(-0.058x)$ W/cm^2
	,where q_{n0}=10.0 W/cm^3 and x is the radial direction
RF loss	q_{RF}=0.48 W/cm^2 (for copper)
	q_{RF}=0.96 W/vm^2 (for beryllium)
Cooling condition	
Flow quantity	W= 1000 m^3/hr.unit
Flow velocity	u= 0.5 m/sec
Temperature	T= 60.0°C
Heat transfer coefficient	h=0.218 W/cm^2 °C
Analysis code	
Thermal analysis	TRUMP3-JR
Stress analysis	SAPV2

TRUMP3-JR is a finite difference computer program for multi-dimensional nonlinear heat conduction problems, which was first developed at Oak Ridge National Laboratory and was used in the thermal analysis of the cask in LWR. SAPV2 is a stress analysis program using finite element method, which was first developed UCLA and was improved in North California University. Constraint condition are in the following. Neutral point of top

front is kept in horizontal and the weight is given at the neutral point of top launcher, which are shown in Fig.4-14 (c).

Results of the thermal analysis is summarized in Table 4-4 and the equatorial temperature and stress contour in the waveguide grill and the front end plate are shown in Fig.4-15 (a), (b) and Fig.4-16 (a),(b),(c), respectively. Conclusion is in the following. For the front end plate, the thermal stress is tolerable since the maximum value of stress is 24.3 kgf/mm^2, which is smaller than the allowable stress $\sigma_{0.2\,\%}$(=32.8 kgf/mm^2). Stress of waveguide in the stainless steel is strong for the thermal stress, because maximum stress in ss, DS copper and Be are 15.0 kgf/mm^2,13.0 kgf/mm^2 and 13.0 kgf/mm^2, respectively, which are all smaller than the allowable values.

Table 4-4 Results of the thermal analysis

	thermal stress σ_{max} [kgf/mm^2]			displacement (mm)	Max.Temp (°C)	Min. Temp. (°C)
	SUS	G-C	Be	0.144	277.8	143.7
front end plate	24.8					
waveguide						
without weight	13.8	12.0	13.0	0.143	291.1	118.9
with weight	15.0	13.0	13.0	0.144	291.1	118.1
allowable value						
$\sigma_{0.2\,\%}$	32.8	14.8	21.6			

(4) Launcher Maintenance - Replacement of top of the launcher

Inside removal of front part of the launchers has been proposed (ref.15). Front part is divided into four sections in the poloidal direction as seen in Fig.4-17. Size is about 52 cm (in poloidal) x 114 cm (in toroidal) x 35 cm (in axial directions). Connecting part which is about 35 cm from the front mouth is selected as where the thickness of the waveguide septum is thick around 10 mm enough to keep the electric contact good from the experience of JT-60. Weight of each section is limited to less than 1 ton so that remote disassembly and assembly from inside the torus of the front sections is capable using the same remote maintenance vehicle for plates of the first wall.

To realize this concept, a engineering development is necessary as for welding and cutting of water pipes for cooling of the front section of the launcher and electric contact

between the waveguides of the multi-junction. R & D activity of laser welding and cutting was made in Japan related with the maintenance of the diverter in 1989. This technique can be applicable to relatively small diameter pipe (about 5 cm in diameter) in this design. Good electric contact was also realized in the LHRF launchers of JT-60 in the vacuum and where the thickness of the septum is 9 mm and the pre-baking temperature was up to 400°C. In principle, this concept is realized but we need some improvement to confirm this. The LH grill mouth replacement in the torus is shown schematically in Figs.4-18~4-21. In first, the launcher itself and the transmission line are resolved and the launcher itself is pushed in the radial direction by 800mm as shown in Figs.4-18 and 4-19. Then, the cooling pipe is cut by the laser cutter, which is inserted in the cooling pipe. The next, the top of the launcher module are resolved step by step from the upper part as shown in Figs.4-20 and 4-21. The top of modules is easily separated by pulling the connector toward upper side. When the launcher will be removed forever, the launcher is inserted into the cask after removing the ceramic window. These are shown in Figs.4-22~4-24. In Fig.4-22, the procedure of the removement of the ceramic window is shown schematically.

4.2 Transmission line design and Overall Efficiency

The transmission line in the ITER/LH system is shown in Fig.4-25, in which one can see that the common signal generator drive the 52 klystrons and the rf power is divided by 52 fold ways. One klystron feed the rf power in 4 waveguide in the poloidal direction and 8 in the toroidal direction. The klystron is located at the klystron room, which is located at the same level of the ITER torus. The length of the transmission line is about 50 m, which is estimated about 43- 52 % for the total system efficiency including the power source,klystrons, launcher, reflection and the transmission line. The plane view of the klystron room and torus hall is shown in Fig.4-26.

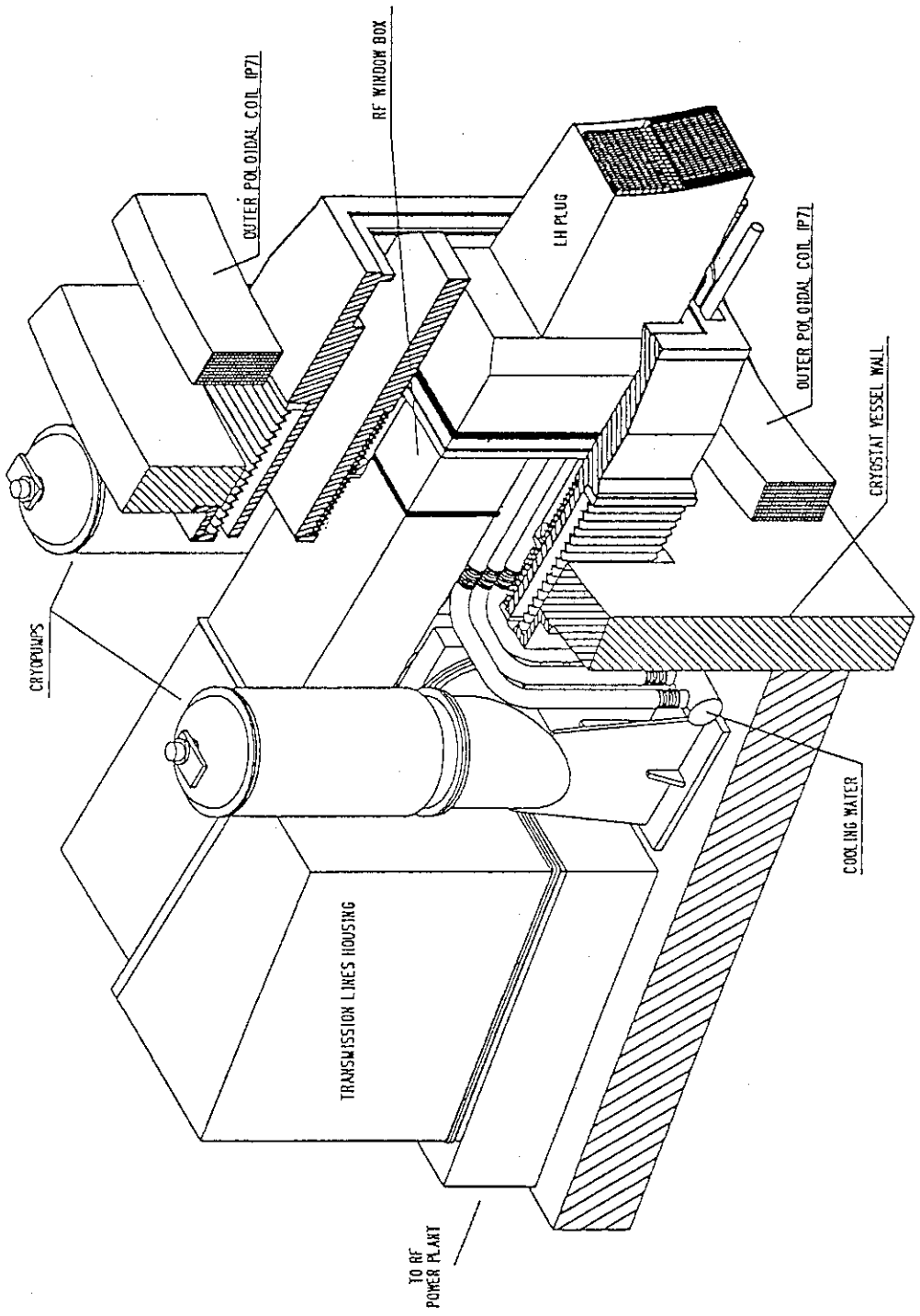

Fig. 4.1 Bird eye view of the LHRF launcher for ITER

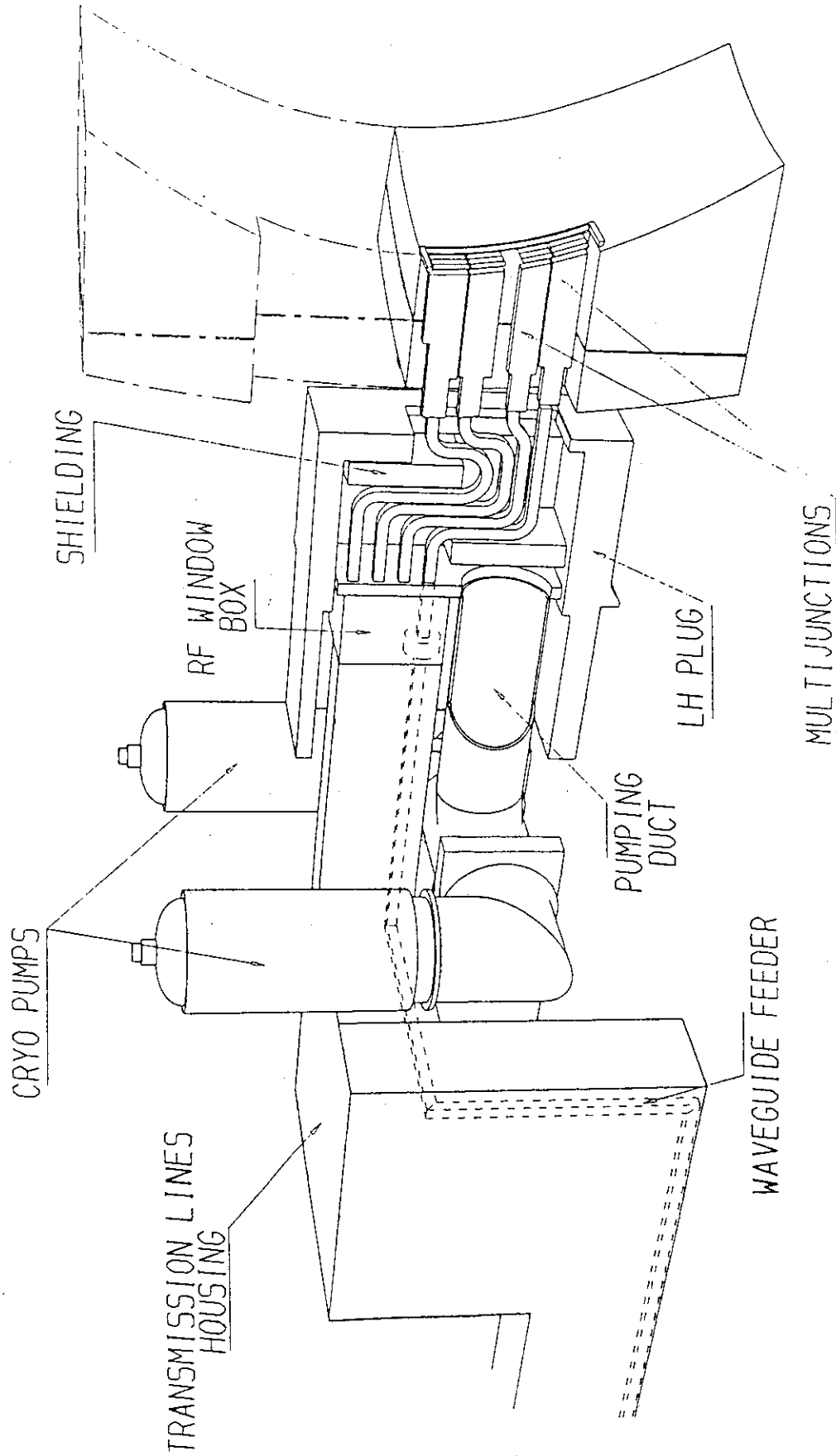

Fig. 4.2 Components of the ITER LHRF launcher

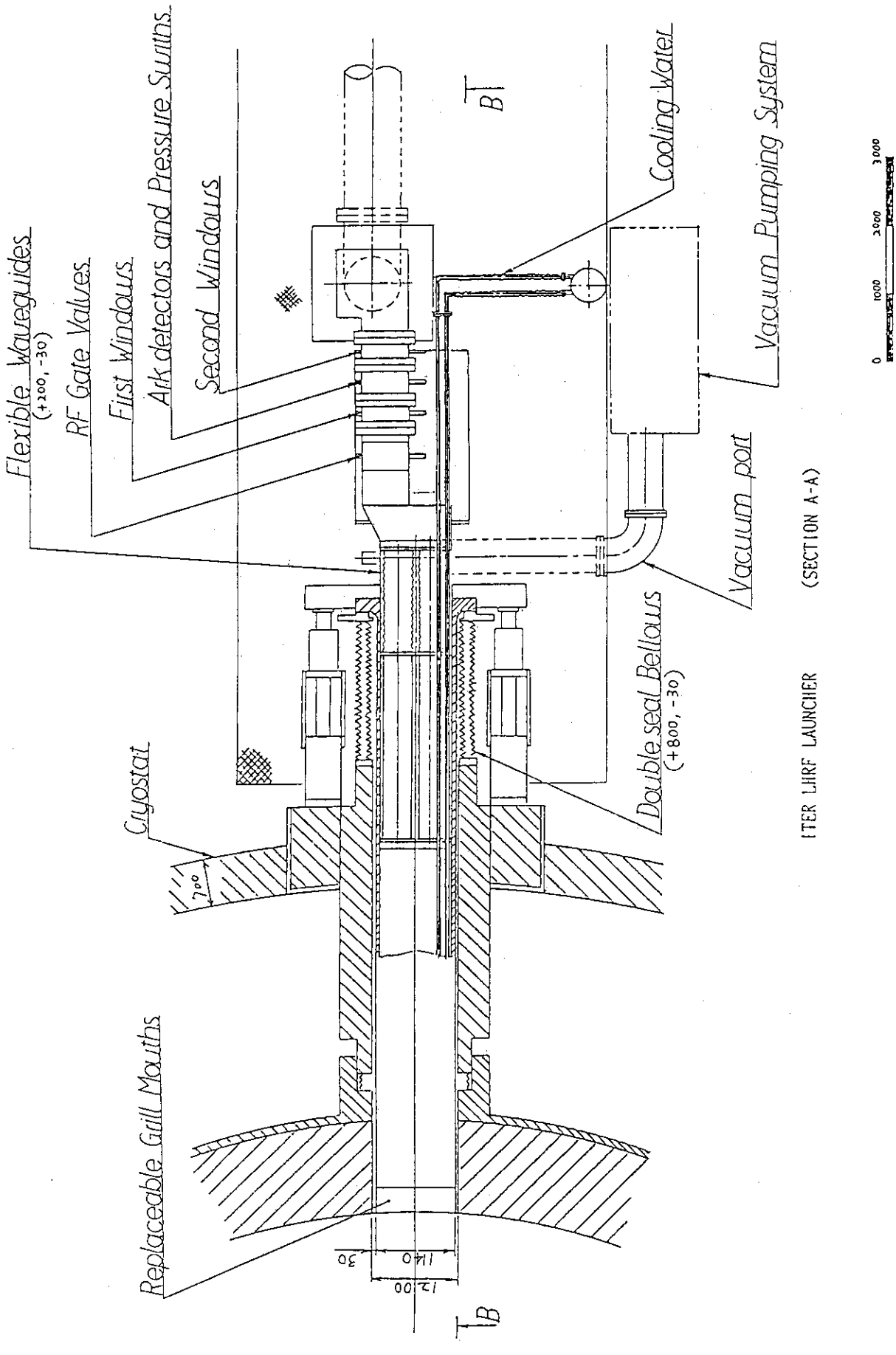

Fig. 4.3 The plane view of ITER LHRF launcher (section A-A)

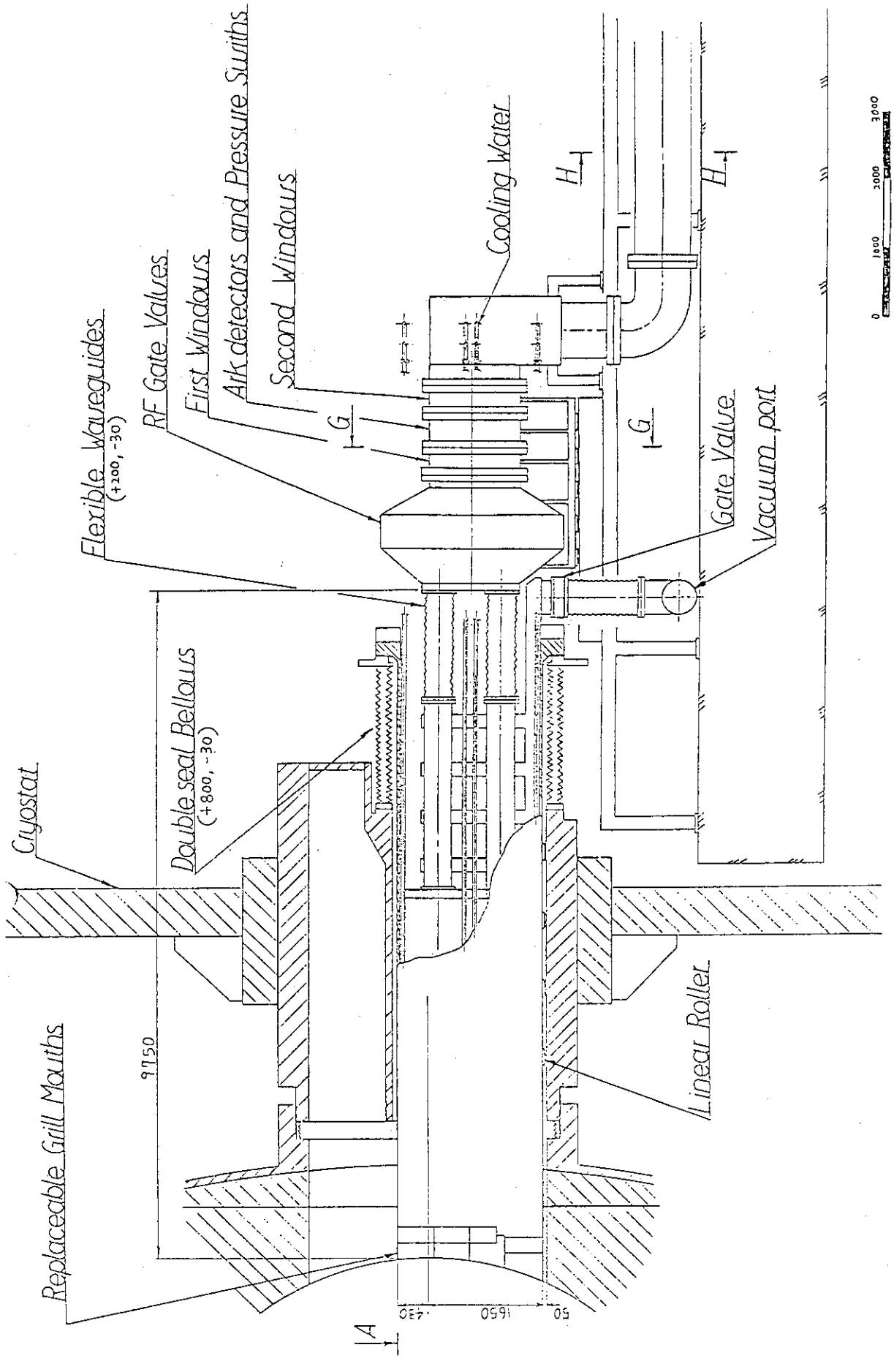

Fig. 4.4 The side view of ITER LHRF launcher (section B-B)

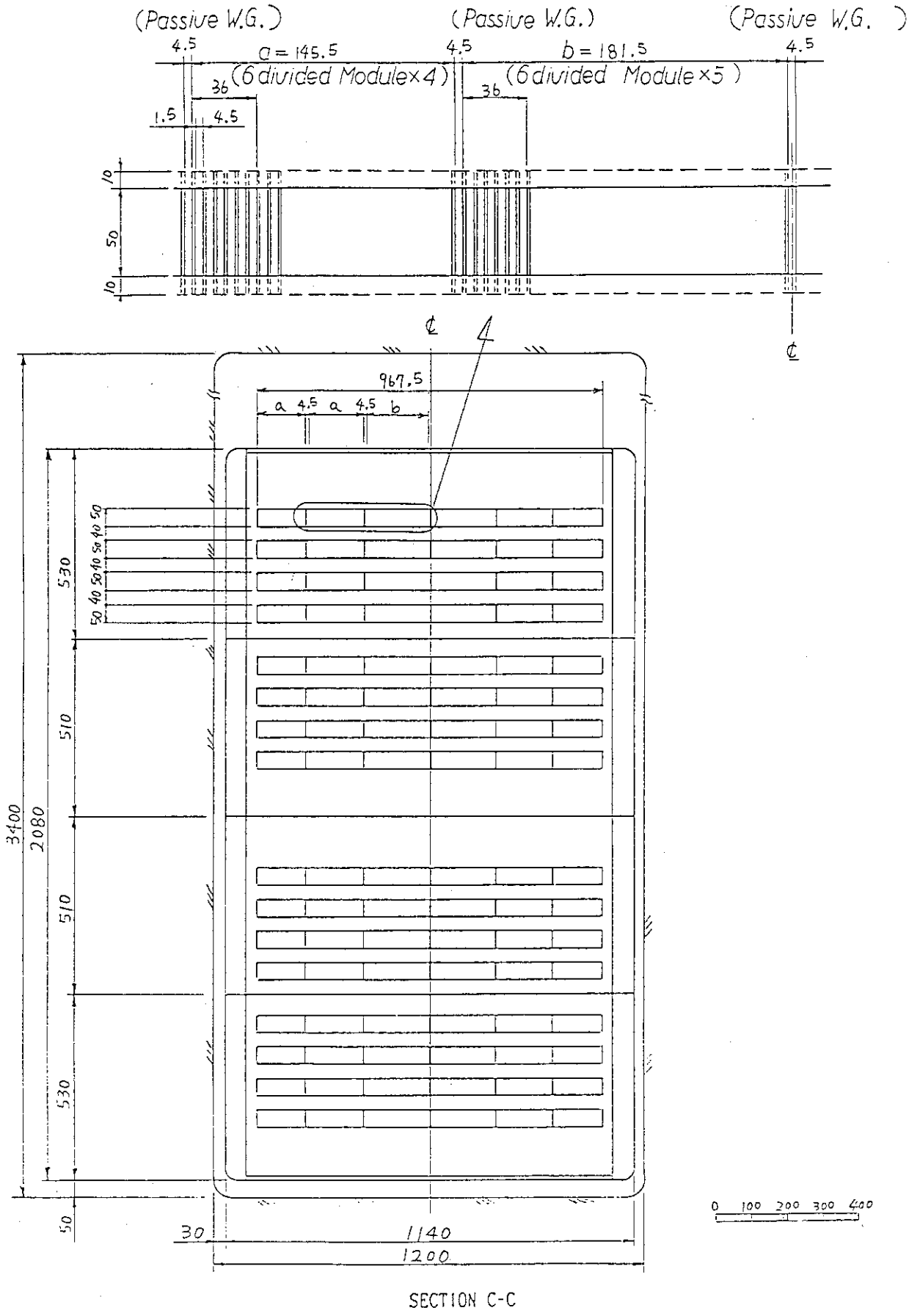

Fig. 4.5 The side view of ITER LHRF waveguide (section C-C)

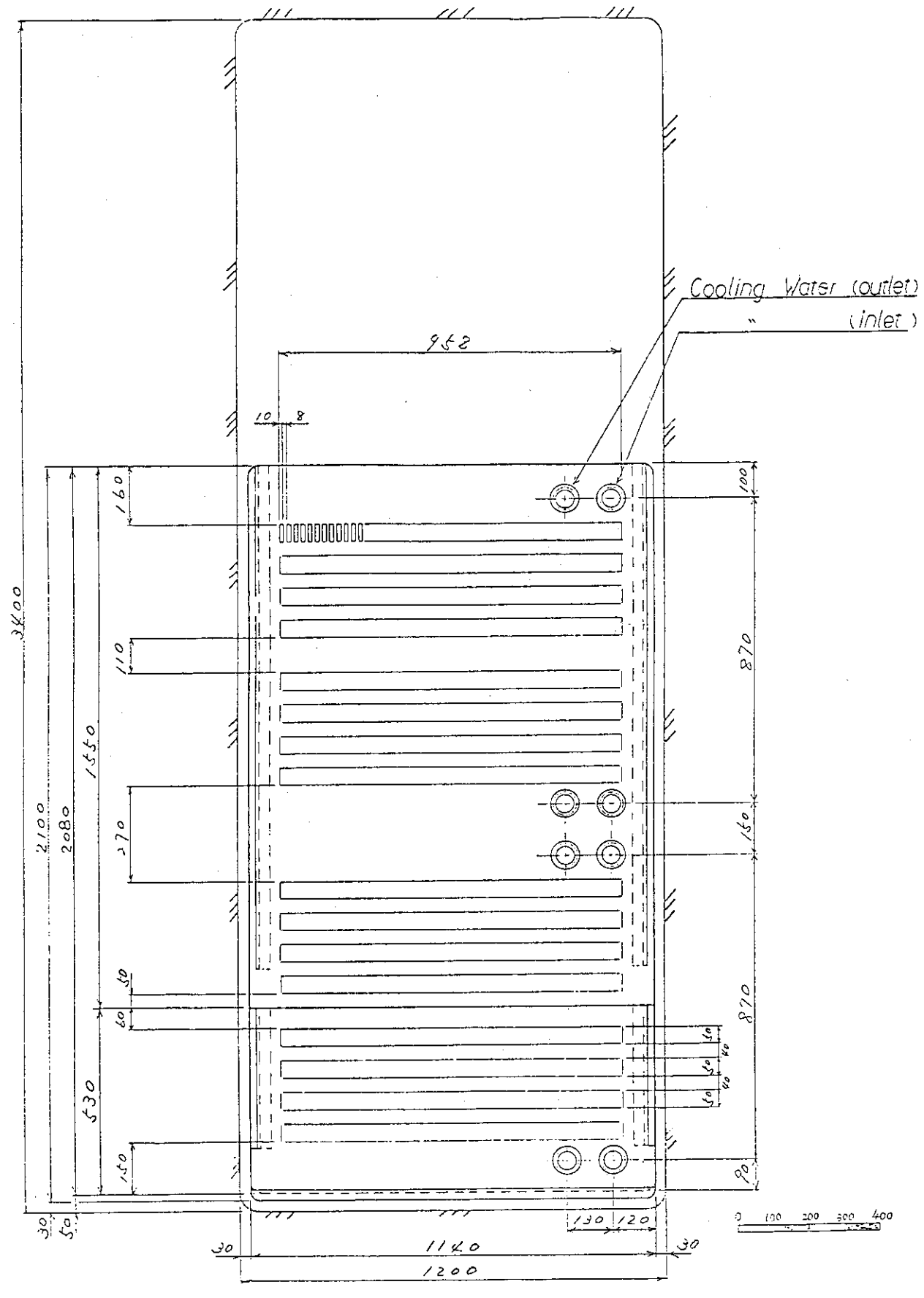

SECTION D-D

Fig. 4.6 The side view of ITER LHRF waveguide (section D-D)

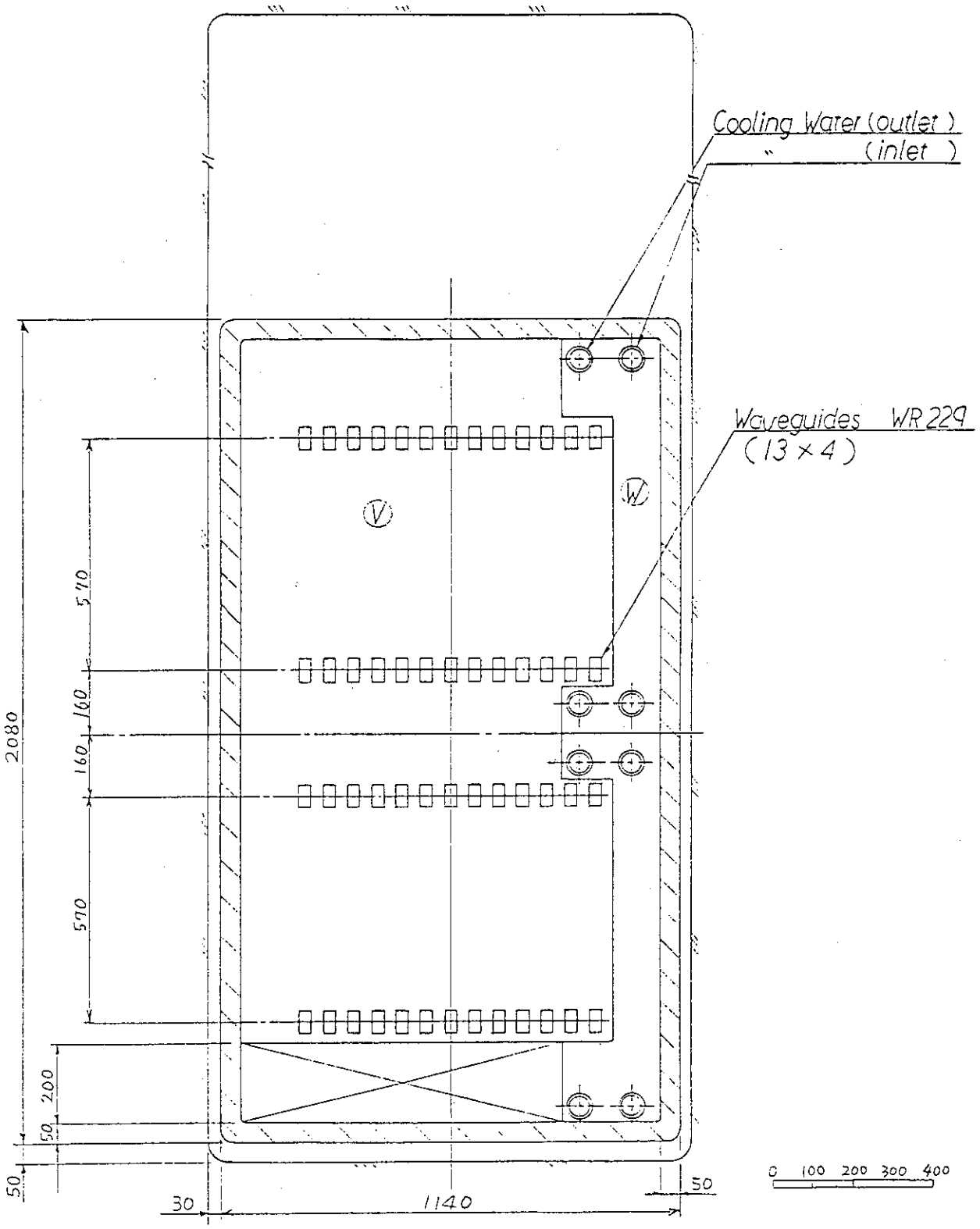

SECTION E-E

Fig. 4.7 The side view of ITER LHRF waveguide (section E-E)

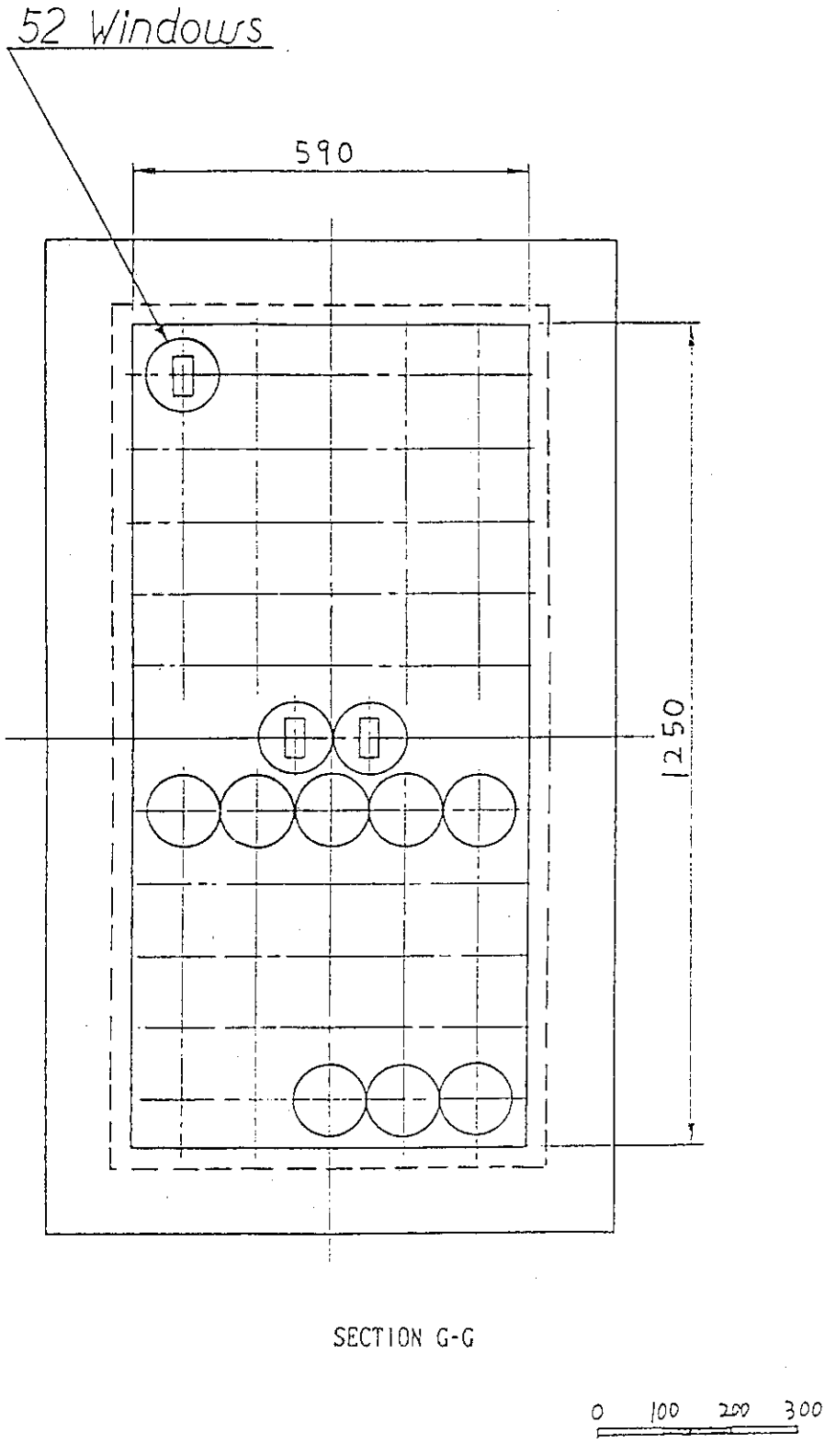

Fig. 4.8 The side view of ITER LHRF waveguide (section G-G)

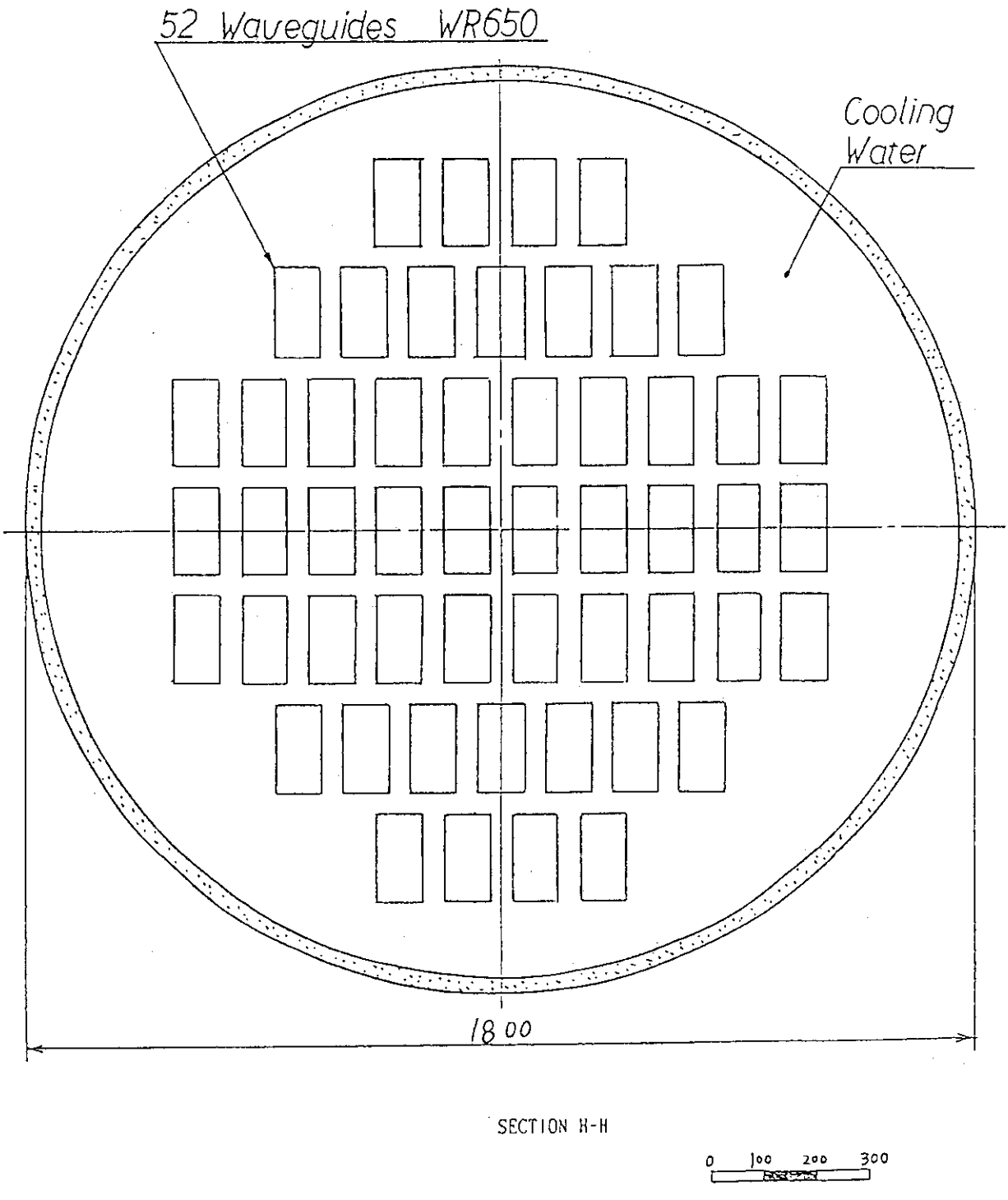

Fig. 4.9 The side view of ITER LHRF waveguide (section H-H)

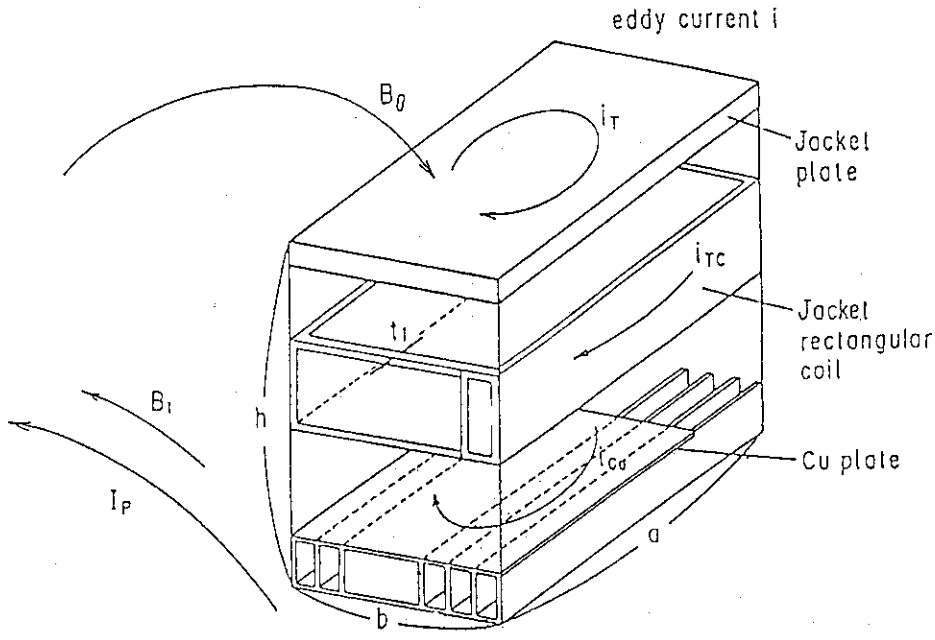

(a) Eddy current induced during disruption on each component of jacket plate, jacket rectangular coil and copper plate

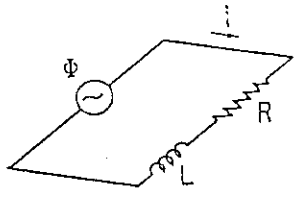

(b) Equivalent circuit analyzing disruption

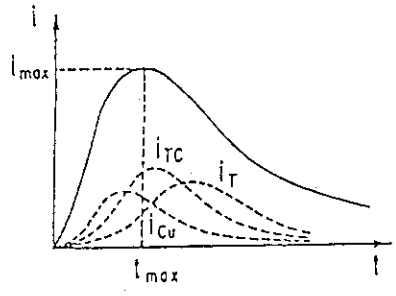

(c) Time behavior of the eddy current. The maximum current i_{max} is the summation of each component.

Fig. 4.10 Analysis model of disruption

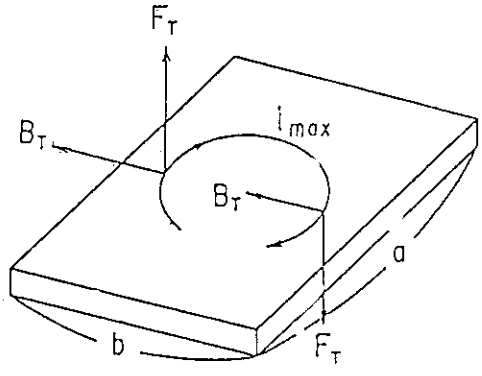

Fig. 4.11 Torque acting on the plane plate

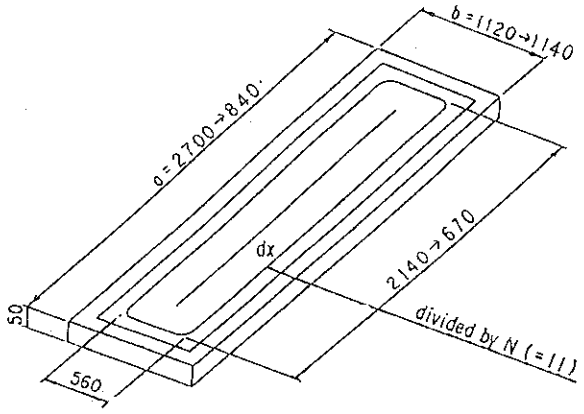

(a) Plane plate is approximated by the plane plated divided by 11 components

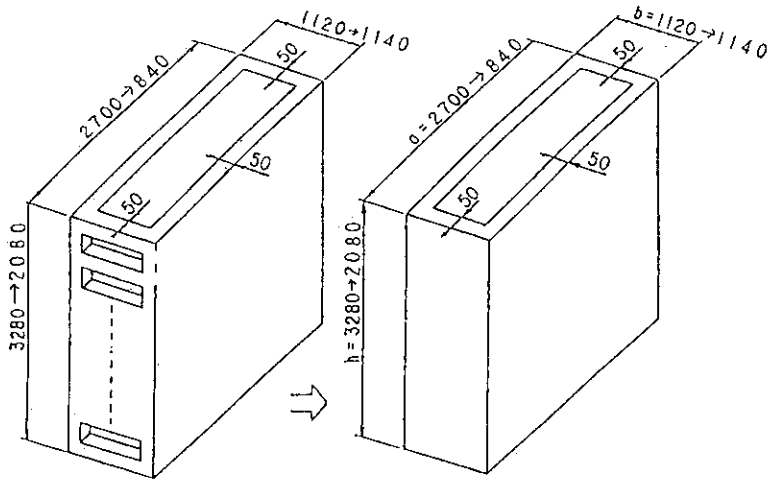

(b) Rectangular coil is approximated by the equivalent rectangular coil

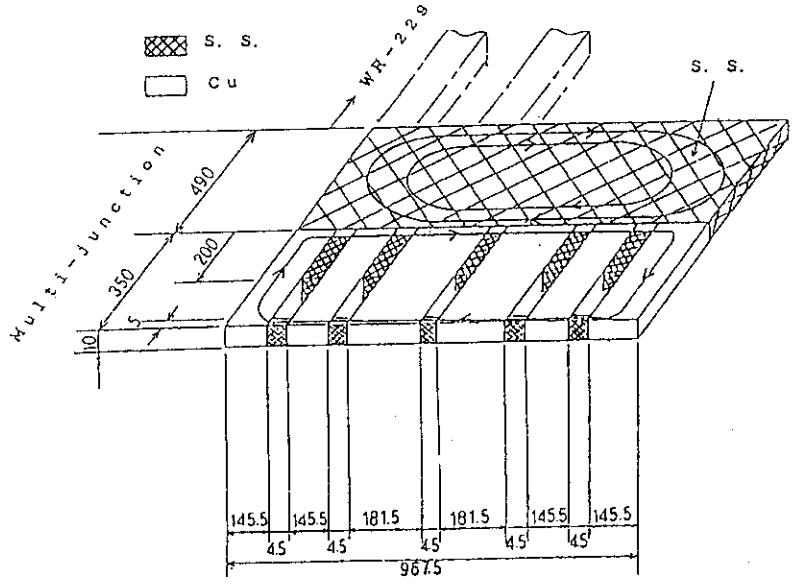

(c) Equivalent insulator model to reduce the eddy current with the low resistive materials. The stainless steel (s.s.) is a low resistive one in this case.

Fig. 4.12 Simplified analysis model of each component

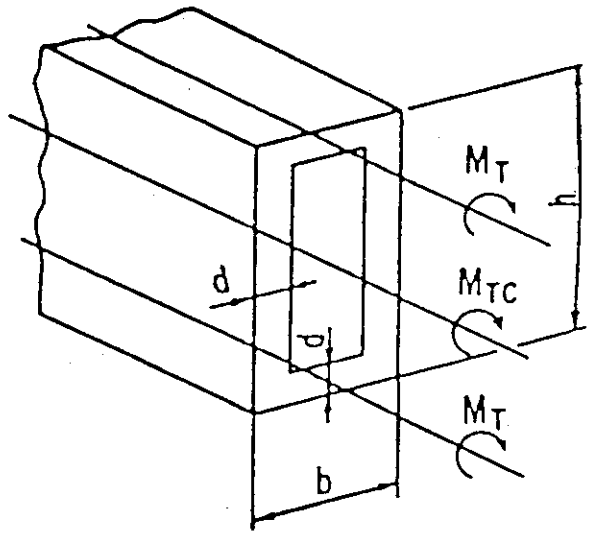

Fig. 4.13 Torque acting on the whole launcher

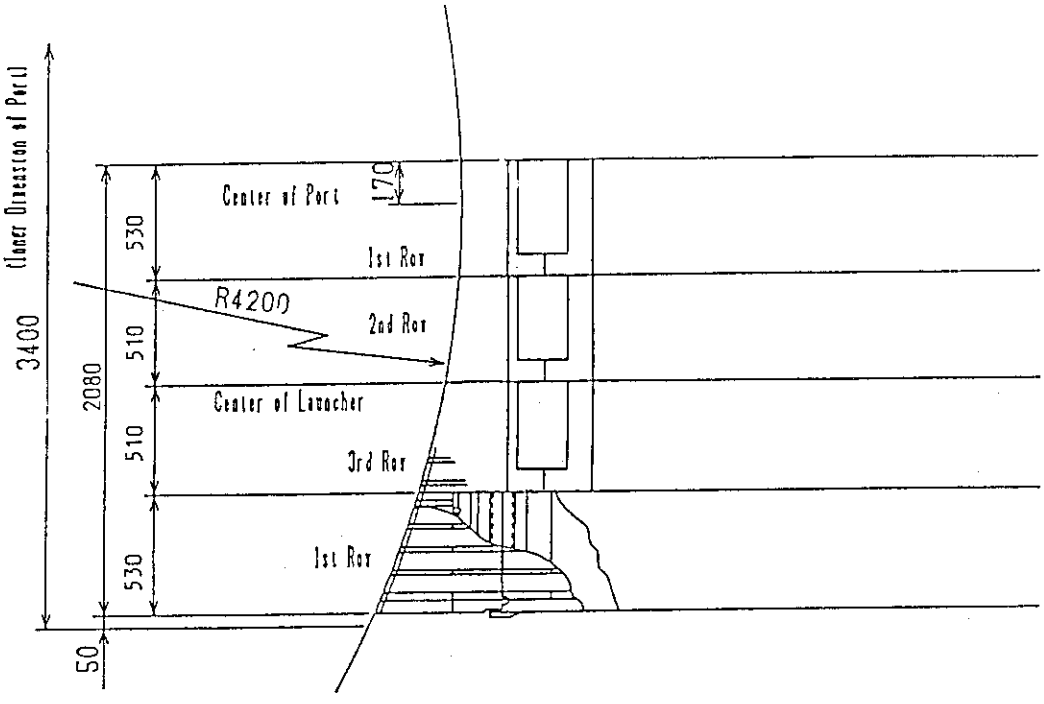

FRONT PART OF ITER LHRF LAUNCHER (SIDE VIEW)

Fig. 4.17 Top of the grill for replacement

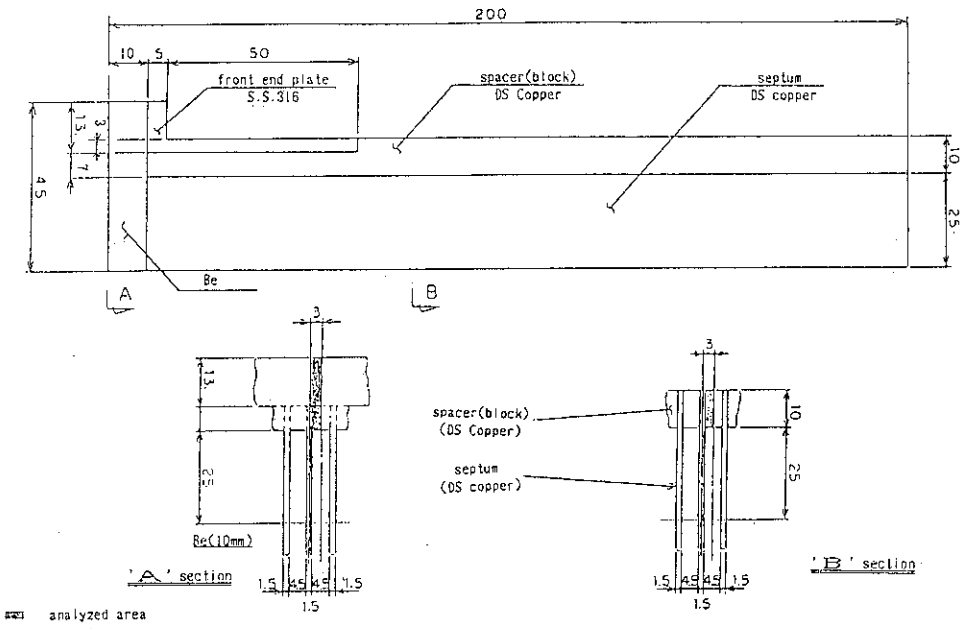

(a) Waveguide grill is composed of the front end plate (s.s.316), spacer (DC copper) and septum (DS copper). Two sectional views are shown in the bottom side and the analyzed area is shown by hatch

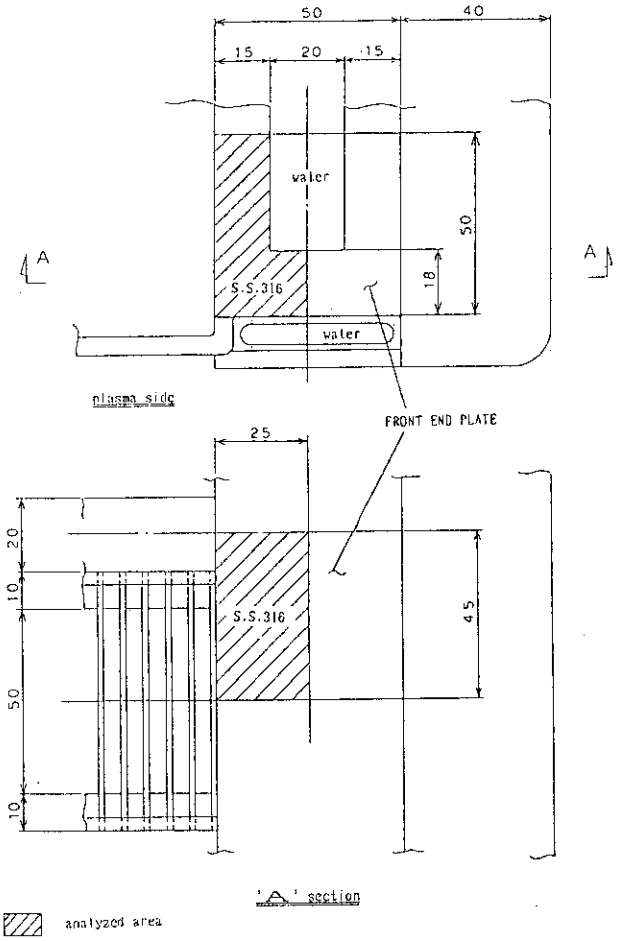

(b) Front end plate (s.s.316) for the analysis and the bottom figure is the A section

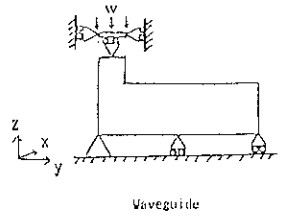

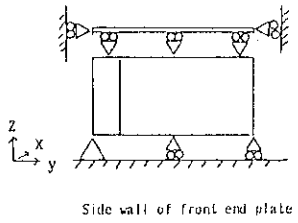

(c) Constraint condition for the thermal analysis of the launcher

Fig. 4.14 Thermal analysis model of the top of the launcher

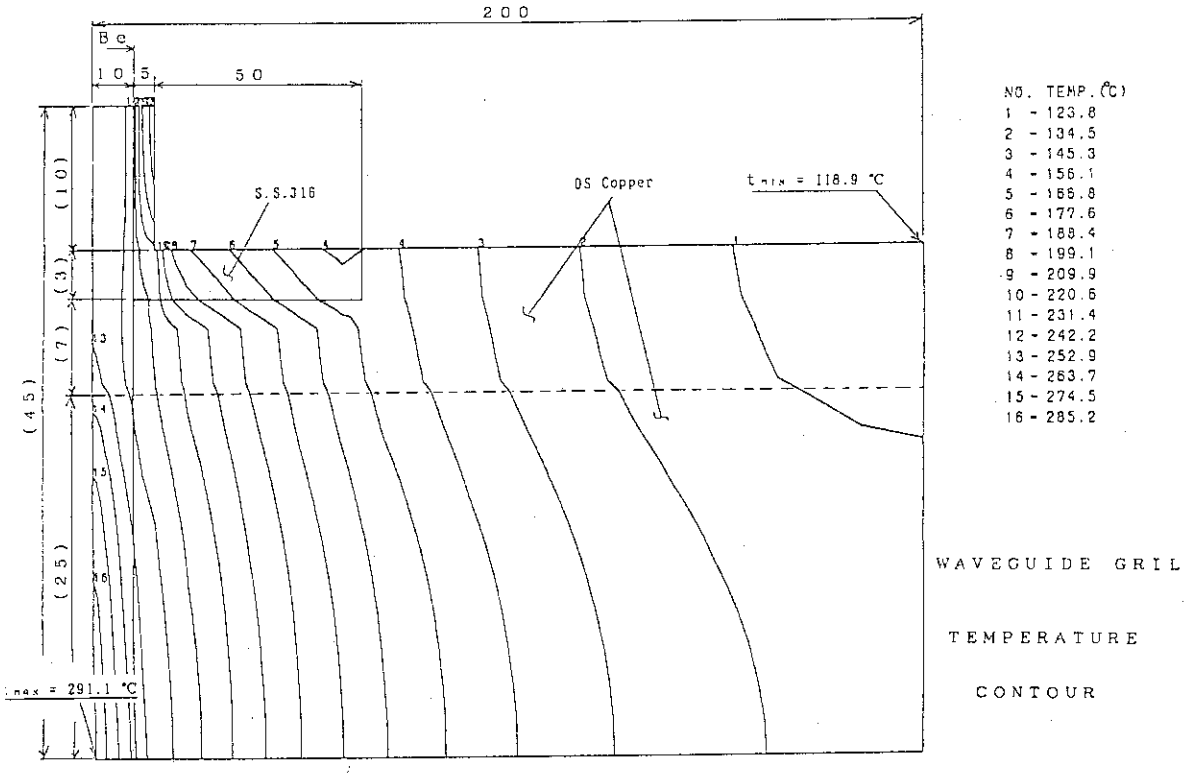

(a) Waveguide grill

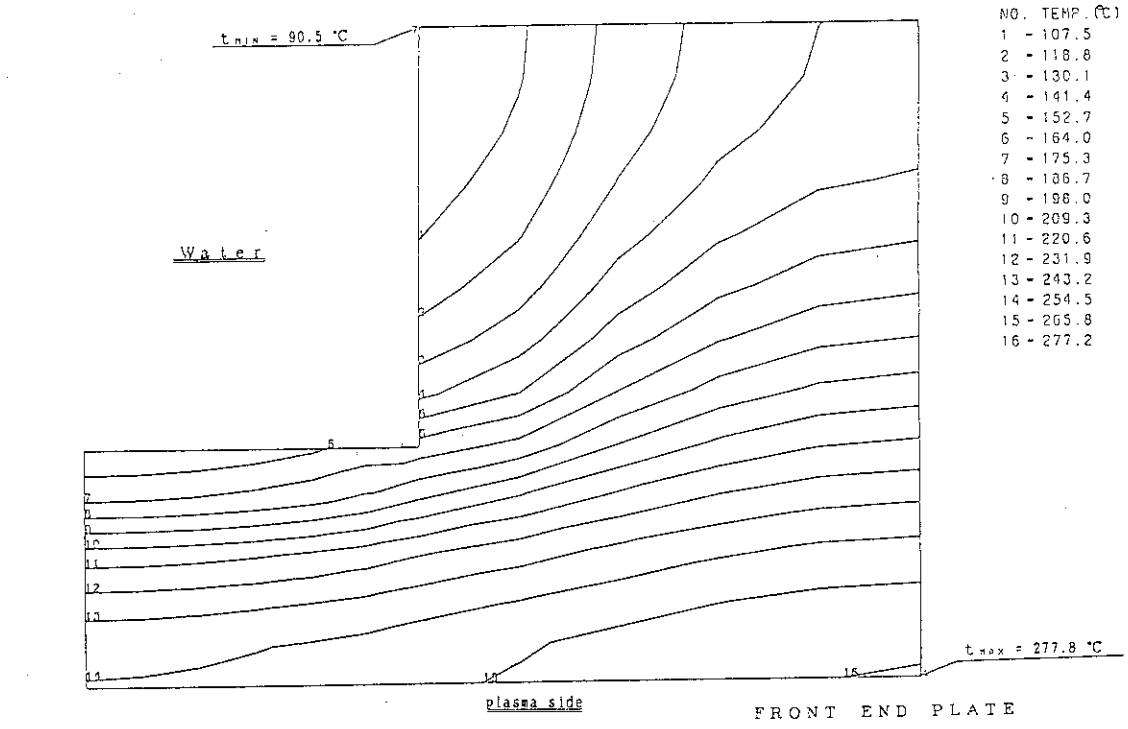

(b) Front end plate

Fig. 4.15 Calculated results of temperature contour

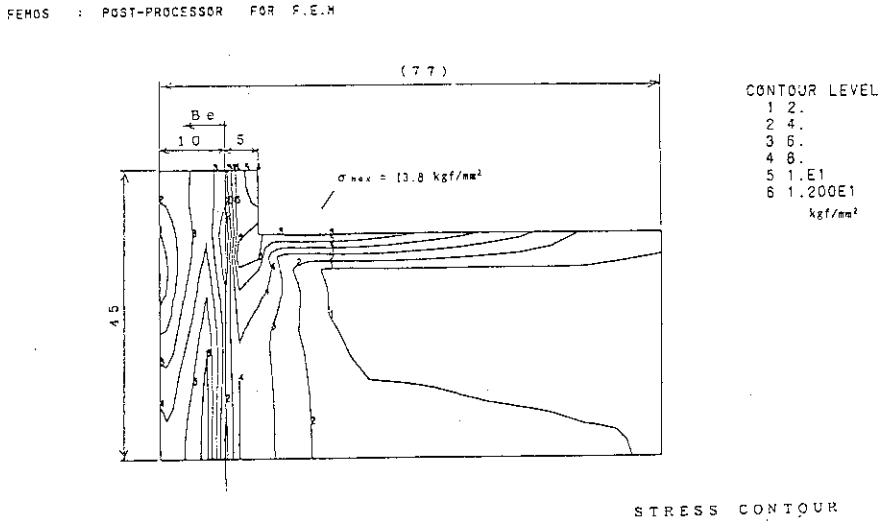

(a) waveguide grill

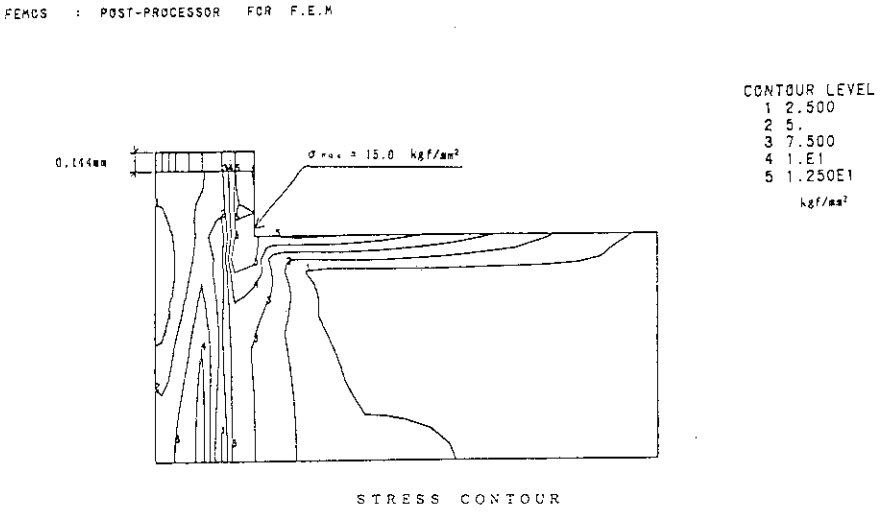

(b) Displacement by thermal stress

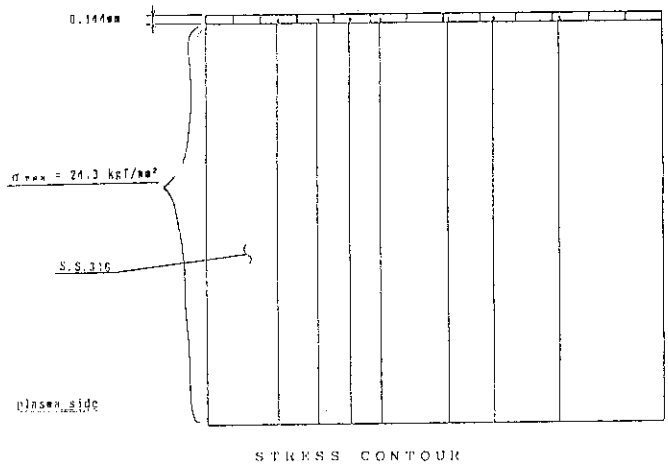

(c) Thermal stress contour of front end plate

Fig. 4.16 Calculated results of thermal stress contour

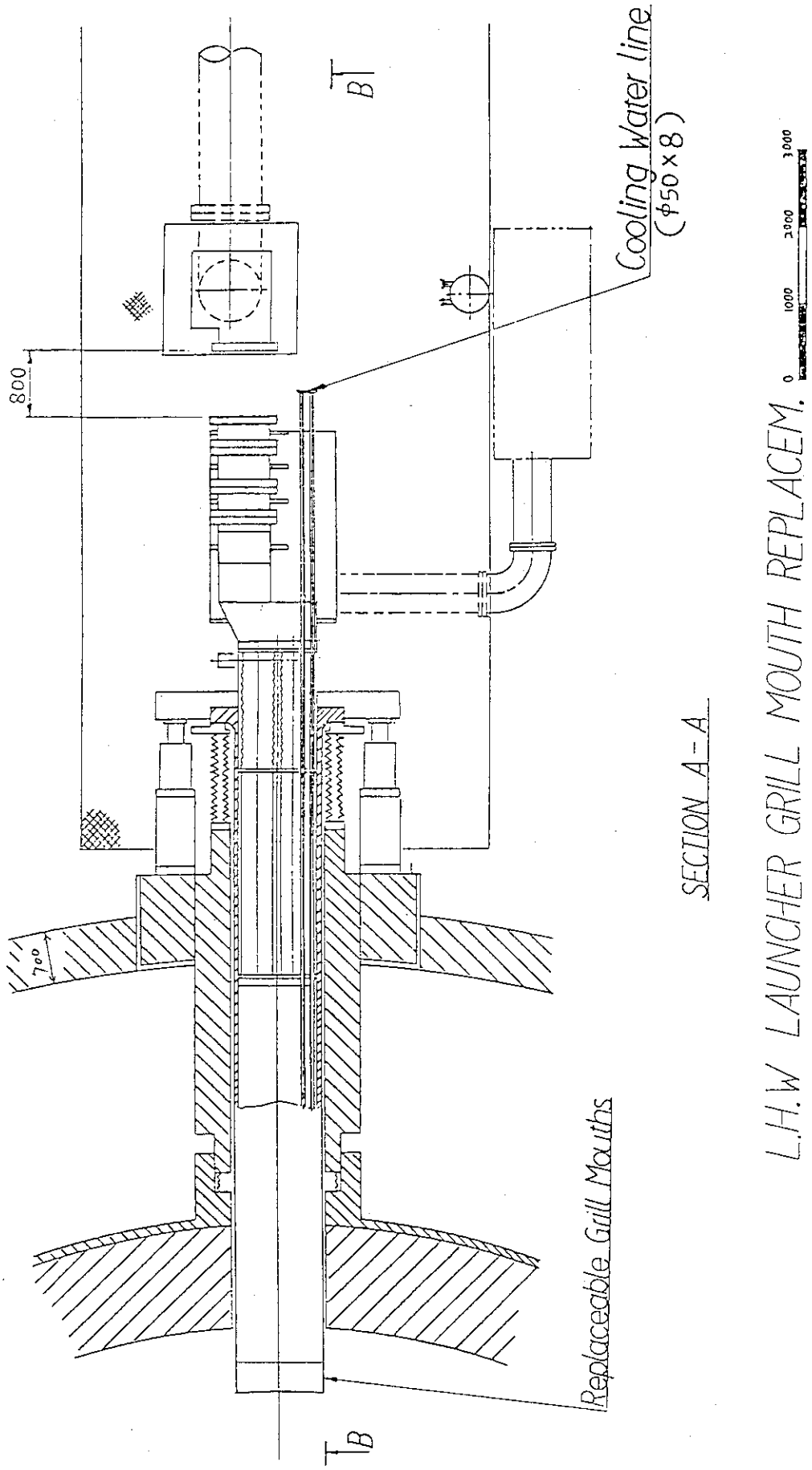

Fig. 4.18 Front part of the launcher (plane view) in case of inside removal maintenance

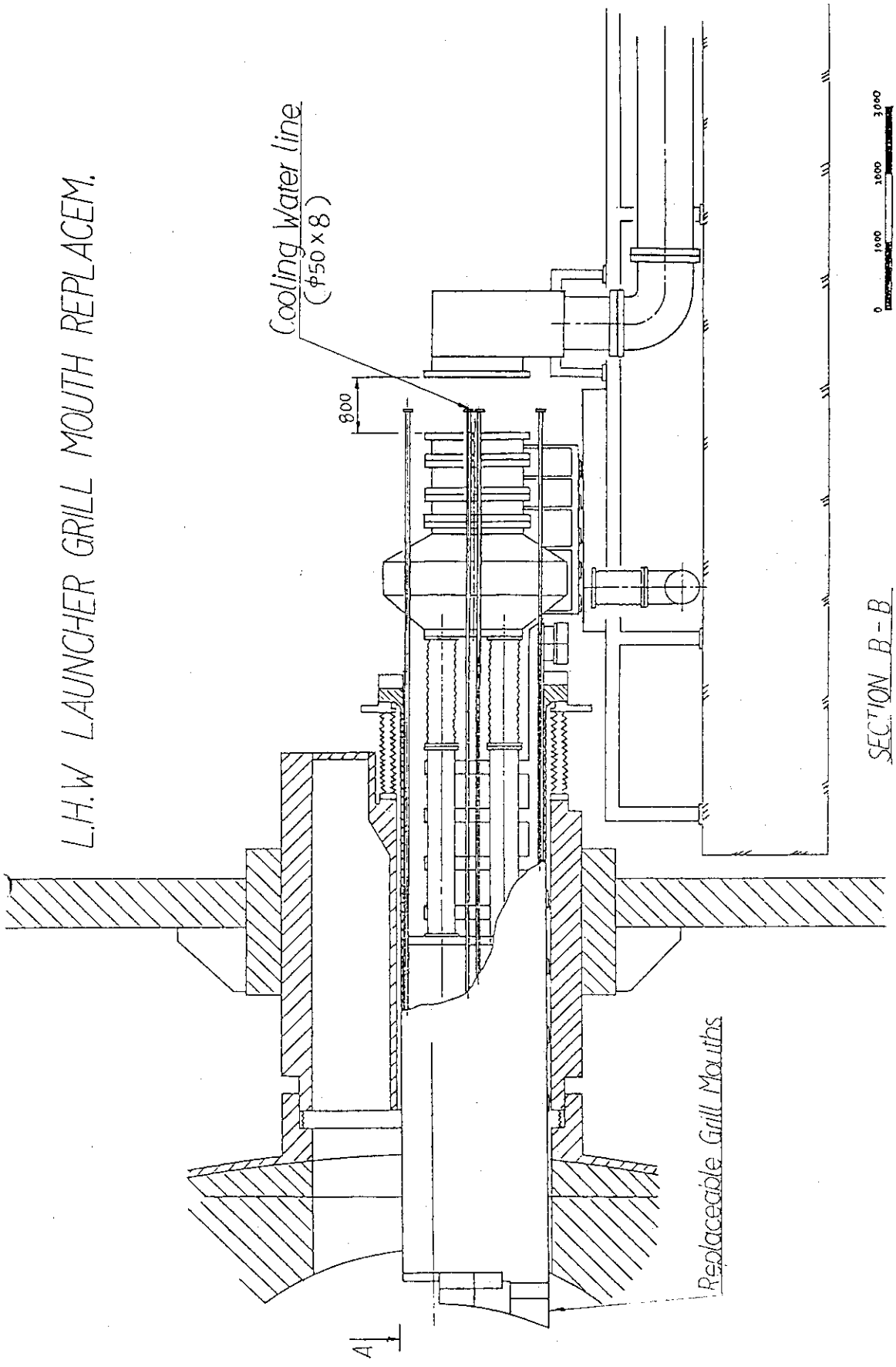

Fig. 4.19 Front part of the launcher (side view) in case of inside removal maintenance

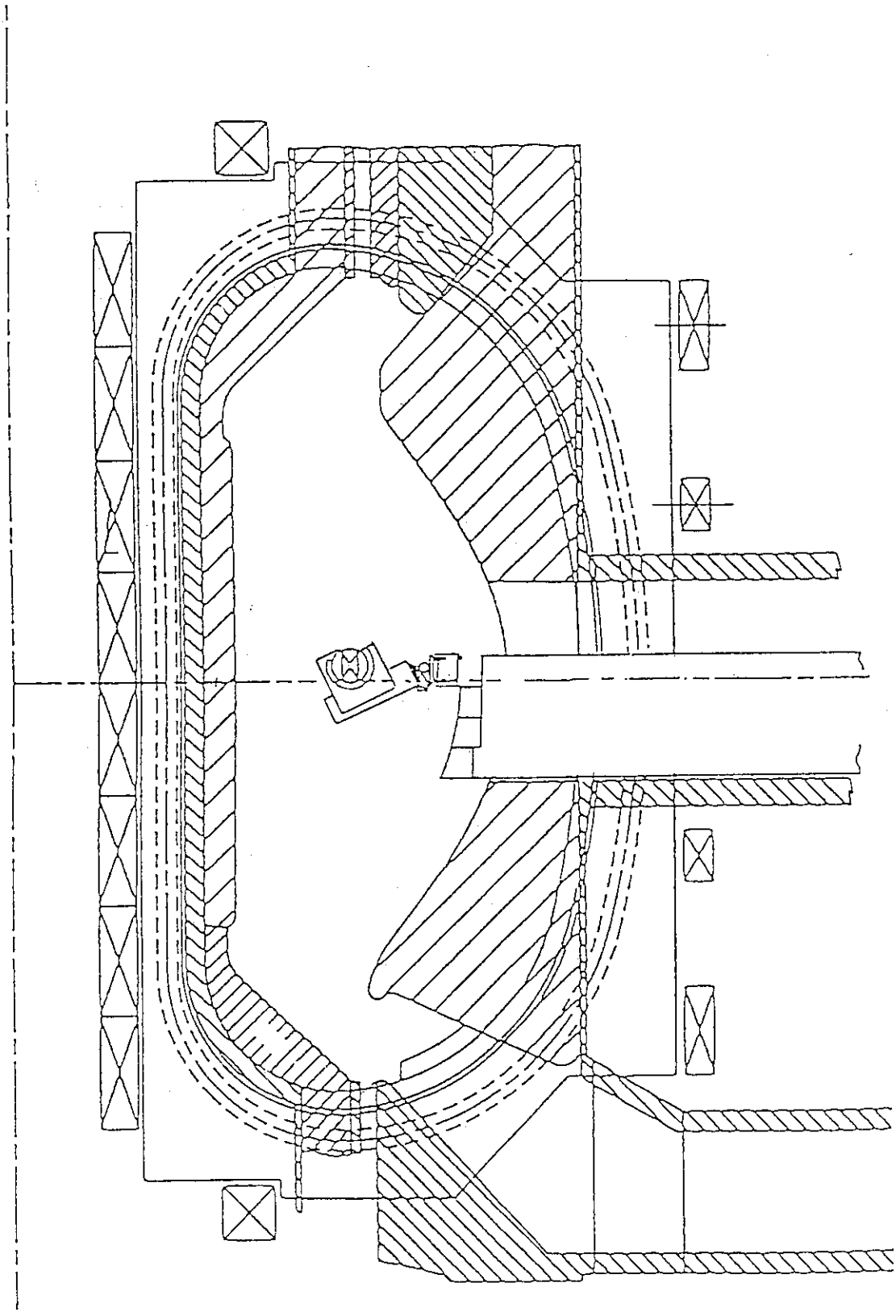

Fig. 4.20 Procedure of the top grill mouth for replacement (part I)

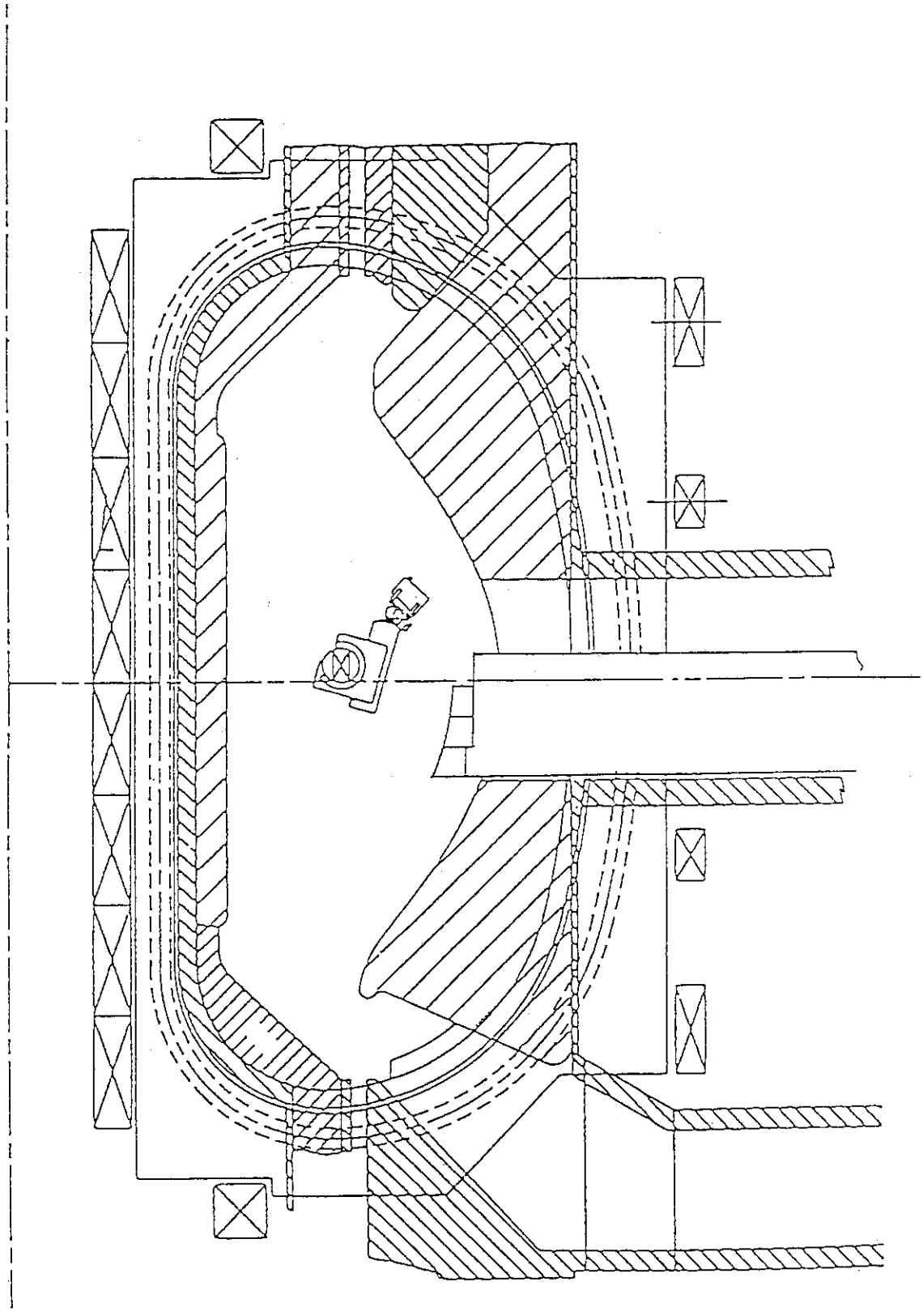

Fig. 4.21 Procedure of the top grill mouth for replacement (part II)

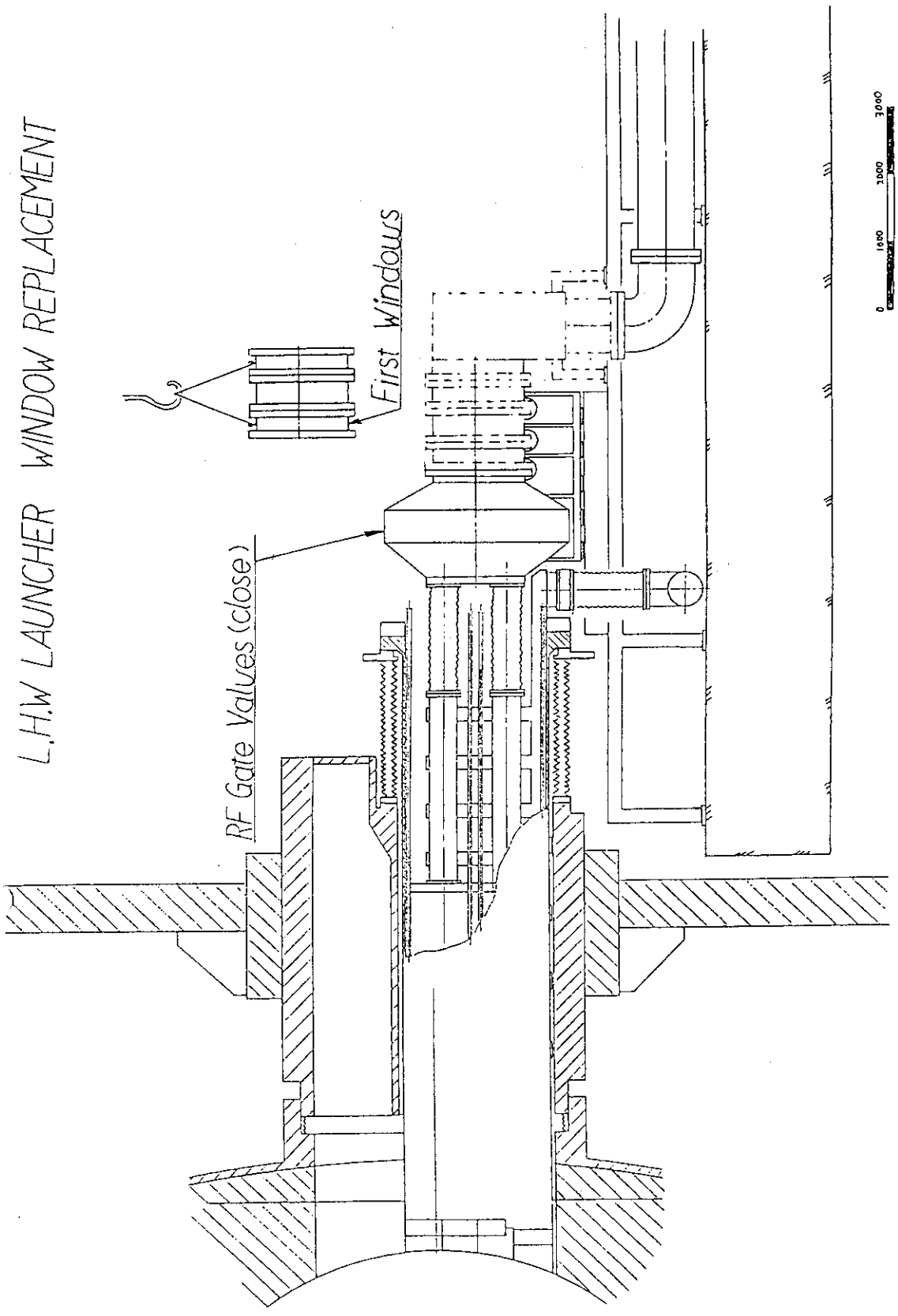

Fig. 4.22 Schematic view of the removement of window

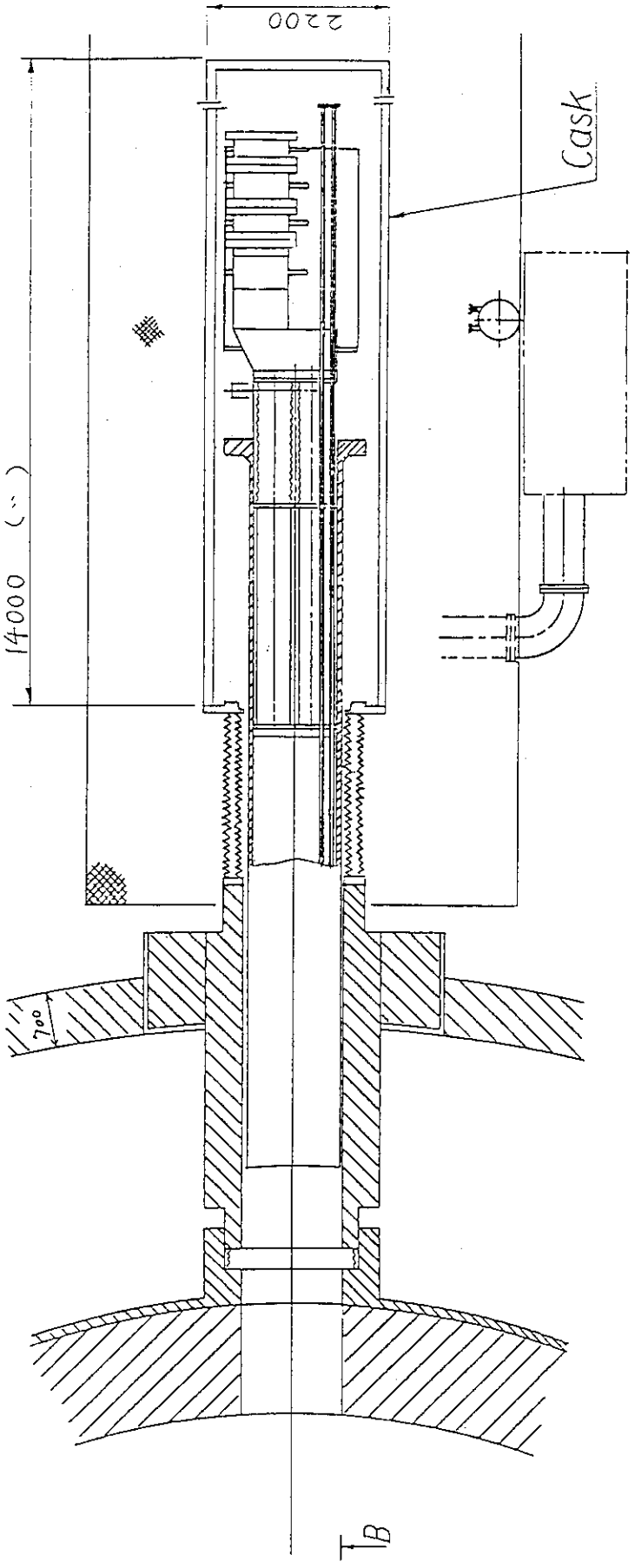

Fig. 4.23 Schematic view of launcher removement (plane view)

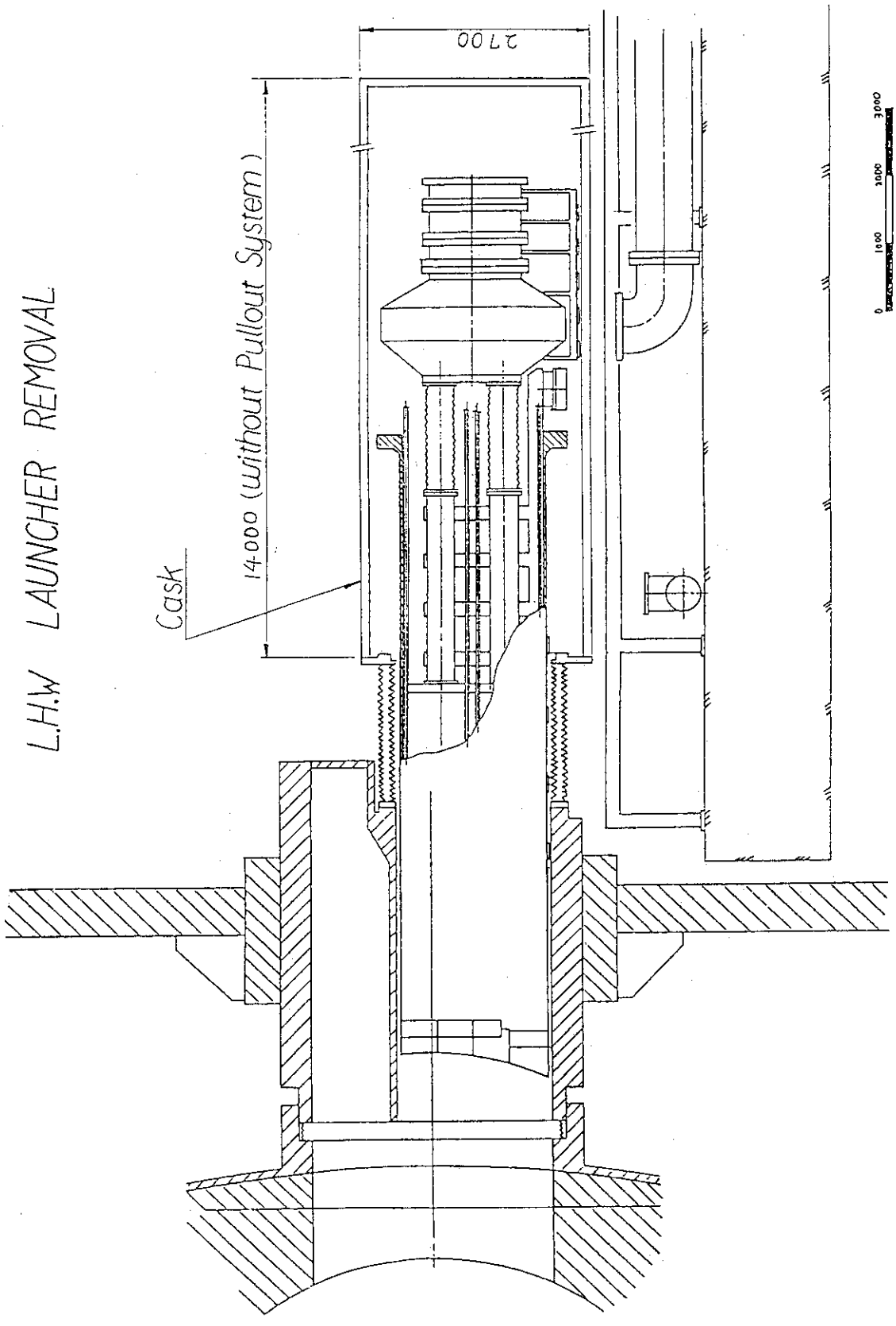

Fig. 4.24 Schematic view of launcher removement (side view)

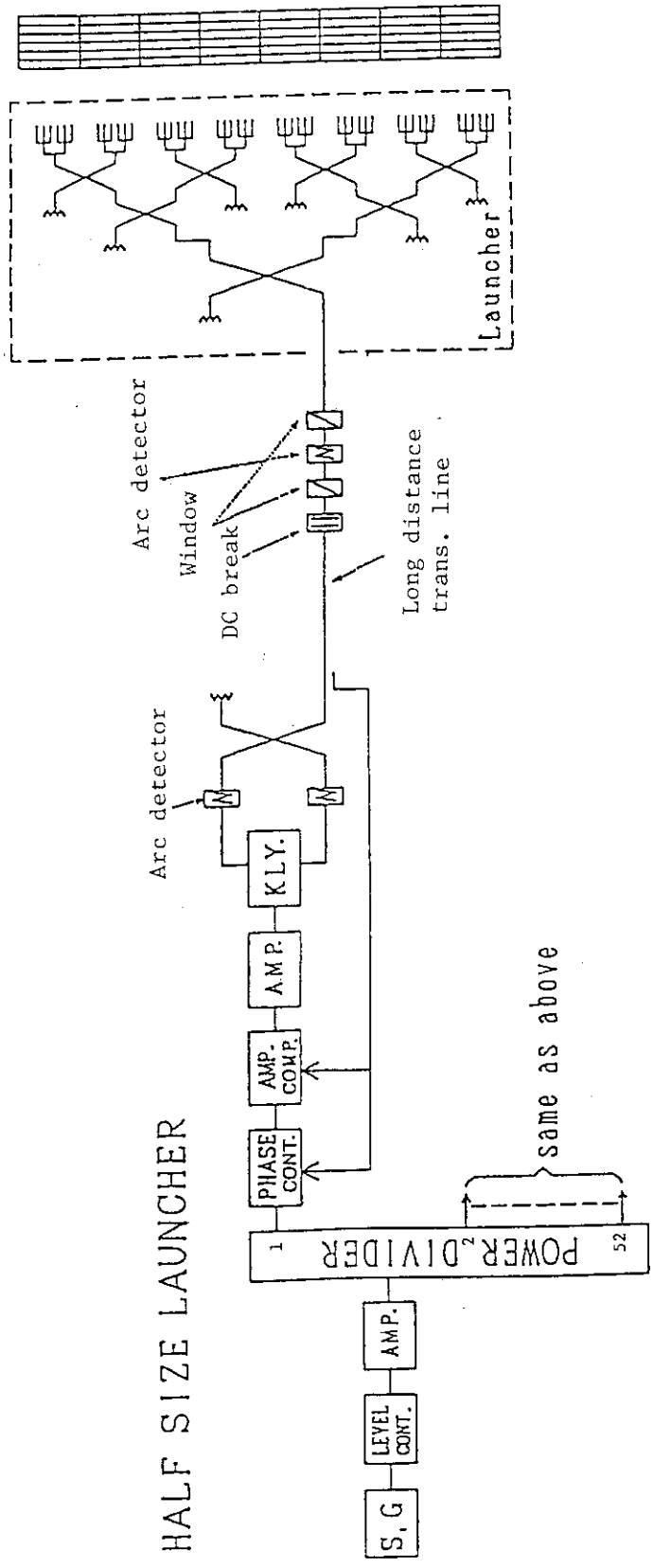

Fig. 4.25 Line-up of LHRF system for ITER

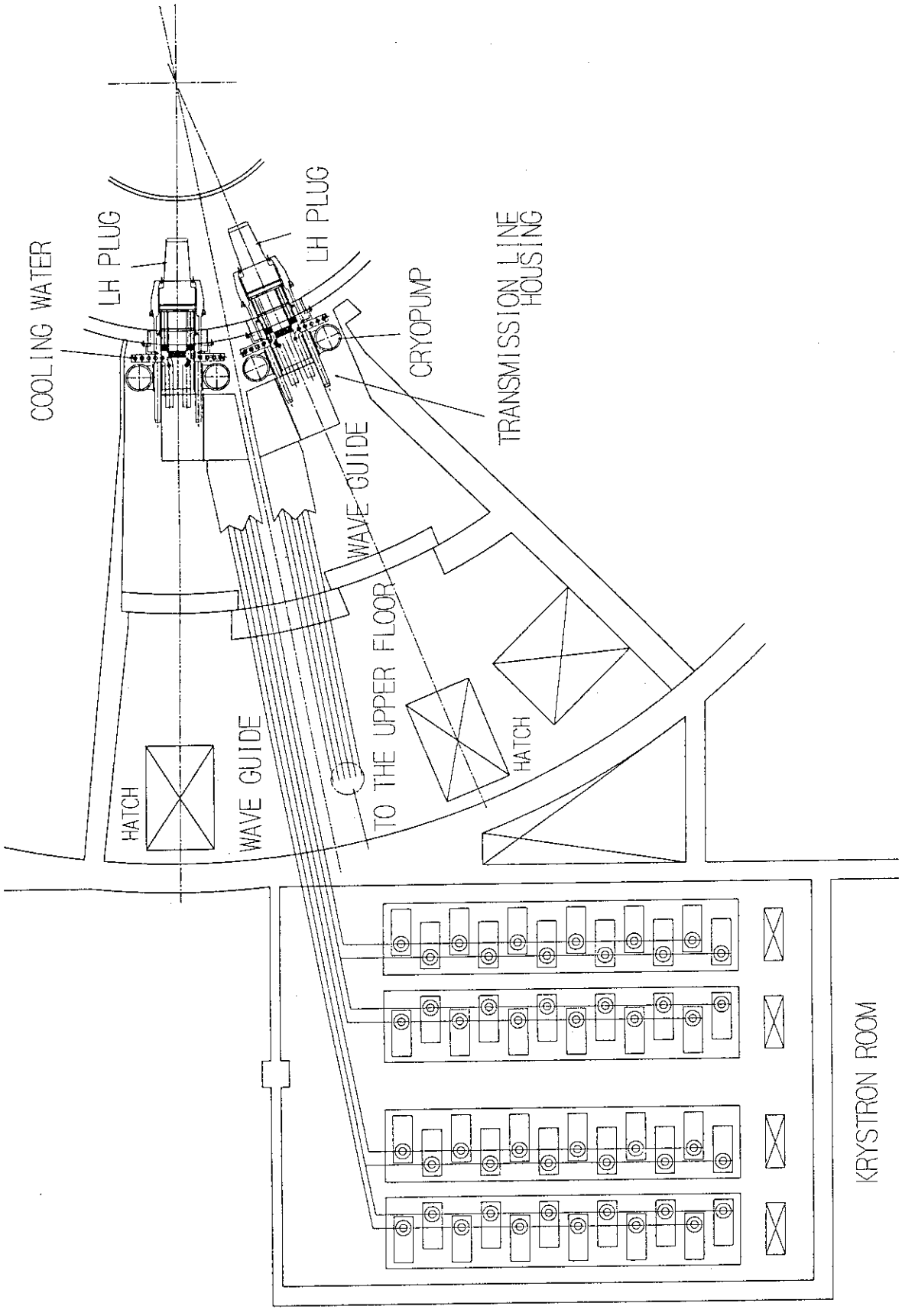

Fig. 4.26 LHRF system plane view for ITER

5. 5GHz KLYSTRON FOR ITER/FER

The 5GHz-klystron which is more than 700 kW of an RF output power and 60 % of an RF efficiency under CW operation , has been planned to be used in LHRF system for ITER/FER program. The RF output power and the RF efficiency vs the frequency in the typical klystron, which has been developed up to now, are shown in Figs.5-1 and 5-2, respectively. It is found that such a specification as ITER/FER klystron is beyond the experienced compass. In order to clarify problems so as to break through this requirement, a preliminary design for an R&D has started in cooperation with Toshiba and NEC corporations.

In first, the efficiency of klystron vs driving power are calculated using an one dimensional disk model for various parameters of the beam perveance, the dimension of cavity and the number of cavity, where the heat load at the cavity is neglected as a zero order approximation. The calculation condition are : (1) 2 mm of the beam radius (2) 3 mm of the drift-tube radius (3) 20 A of the beam current and (4) 65 kV of the beam voltage.

Figures 5-3 (a) and (b) show the efficiency of output power vs the RF driving power, where the beam perveance and the gap length at the cavity are changed when the RF output power is kept to be 700 kW and the number of cavity is 5. The calculated results show that the RF efficiency increases with the decrease of the beam perveance and the gain of the RF output power increases when the gap length is narrow. However, the design for the withstand voltage and the cooling method at the gap edge in the cavity becomes severe. In order to improve the RF efficiency, 7 cavities model using two tuning cavities for a second harmonics wave had been calculated. As shown in Fig.5-3 (c), it is found that the larger RF efficiency with 7 cavities is obtained than with 5 cavities case, which is about 65 % and is about 2.5 % larger than that of 5 cavities. As described in later, when we consider the the thermal load at the cavity due to an RF losses and the body current, the efficiency may be about 10 % lower than these calculated values.

In the second step, the thermal heat load at the cavity has been taken into account in the calculation. The incremental temperature at the cavity is beyond the permitted temperature of 100 °C to be capable for the usual water cooling system, since the size of cavity becomes as small as to be about 1.5 cm^2 for the frequency of 5 GHz. When the thermal load at the cavity is 10 kW, the incremental temperature at the gap edge must reach to 150 °C in the calculation, therefore, it is necessary to reduce the temperature increment by the improvement of the cavity design. The sectional view of a general cavity and a broad

cavity are shown in Fig.5-4. This broad cavity, whose configuration at the gap is broad so as to reduce the temperature increment, has been optimized its design by the analysis code of the electromagnetic field. In the broad cavity, however, the characteristics impedance value (R/Q) decreases from 82.7 Ω of the general type to 77.1 Ω The allowable maximum thermal powers in the general type and in the broad type are 4.7 kW and 6.7 kW, respectively. This value limits the temperature increment of 100 °C at the gap edge. Figures 5-5 (a) and (b) show the RF output power and the RF efficiency vs the output impedance within the allowable maximum thermal power, where the characteristics impedance value (R/Q) in both cases are fixed at 82.7 Ω and 77.1 Ω, and the external Q values are changed. This model is calculated for 5 cavities without tuning cavities. The maximum RF efficiency for 700 kW output power using the general type and the broad type cavity has been attained by 52.5 % and 57.0 %, respectively. The model using two tuning cavities considering the thermal load is calculating now, almost 60% of the RF efficiency may be attained in this case.

In the preliminary design, some problems have been clarified in the following;

[1] about 20 A of the beam current must be controlled within the beam radius of a few millimeters using a beam focusing ratio of 30 ~50,

[2] a new cathode having a long life time and 3~5 A/cm^2 of current density must be developed in future, or the beam focusing ratio of more than 50 must be realized,

[3] a new design of the cavity is necessary to reduce the temperature increment, or an evaporation-cooled method must be realized to be adopted instead of the water cooling method,

[4] the design using a multistage depressed collector to improve the RF efficiency, and a double cavity to reduce the withstand voltage at the gap and a low perveance about 0.7 μP to reduce the beam current, are also necessary to break through this development.

For the higher frequency amplifier it is also a candidate to use another amplifier such as gyrotron and gyroklystron. These are under the development for the availability of higher efficiency and the controllability of the phase difference.[16] In FTU tokamak at Frascati the gyrotron is used for the LHRF system for 8 GHz.[17]

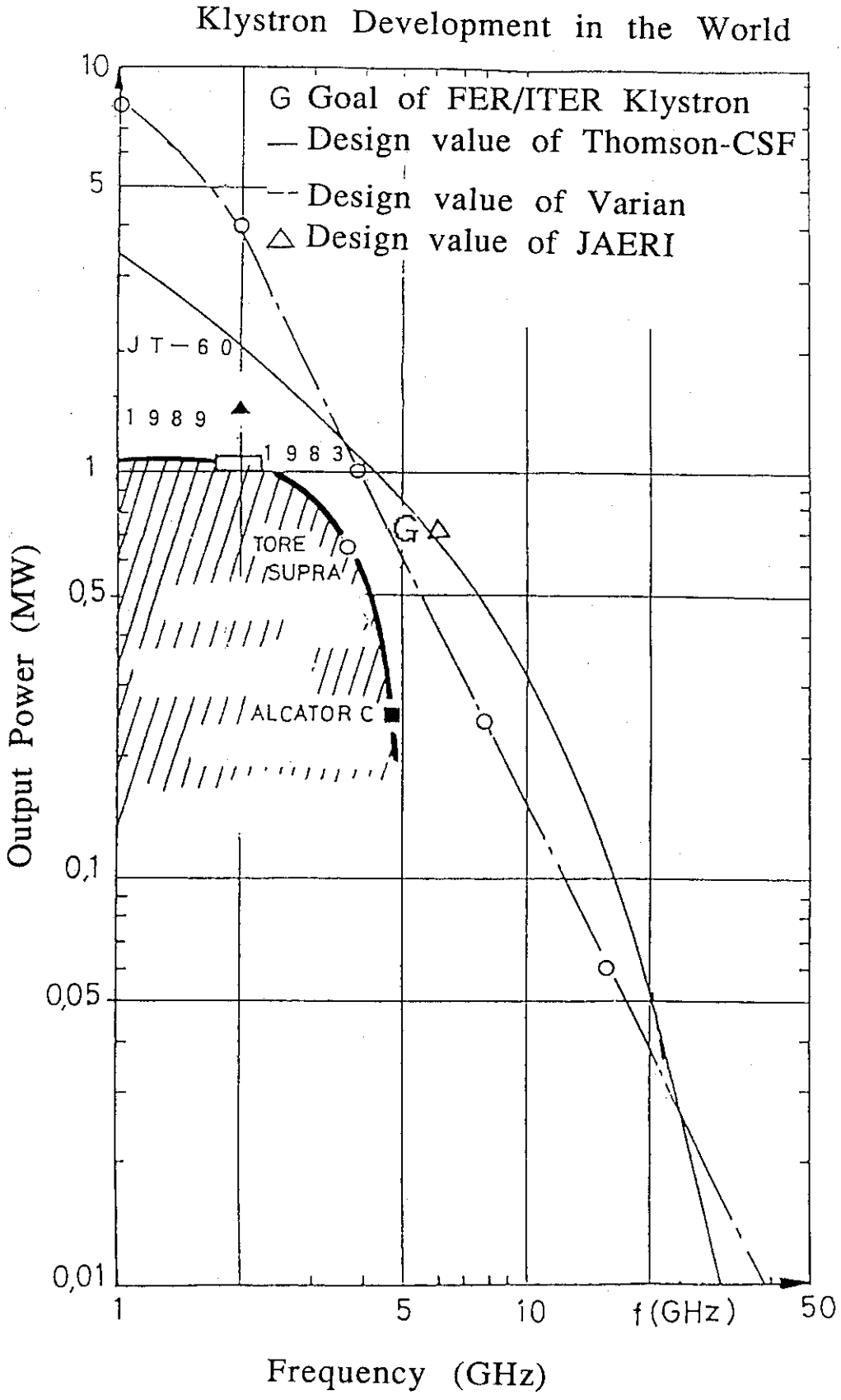

Fig. 5.1 The RF output power vs the frequency in typical klystron, which has been developed up to now

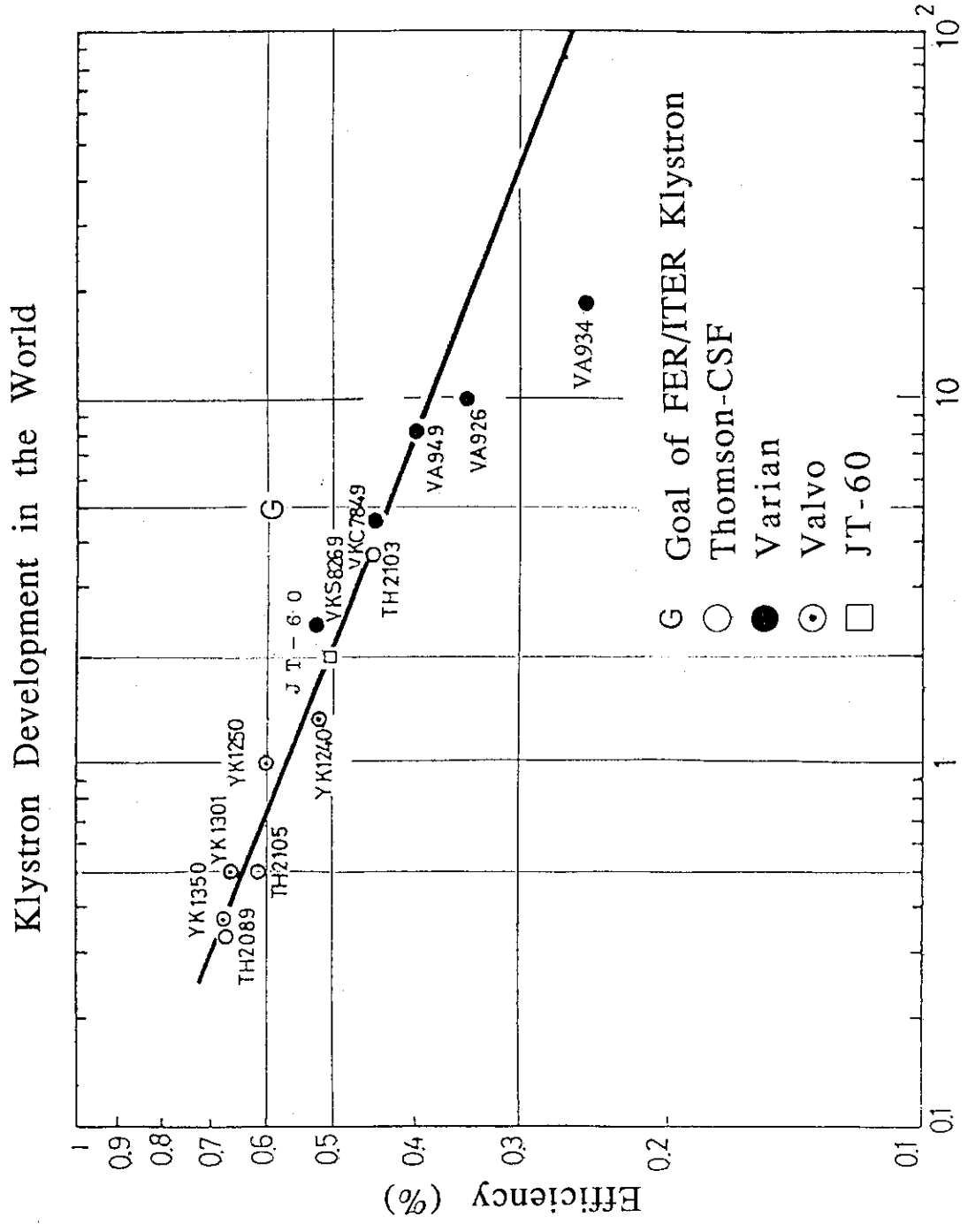

Fig. 5.2 The RF efficiency vs the frequency in the typical klystron, which has been developed up to now

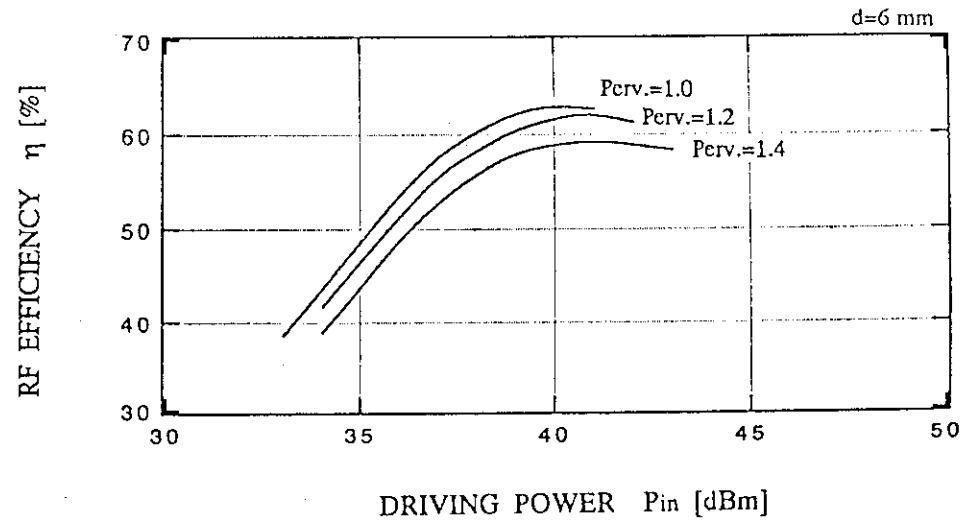

(a) The RF efficienty vs the RF driving power, where the beam perveance is changed when the RF output power is kept to be 700 kW. Here, the number of cavity is five, which could not tune for a second harmonics wave.

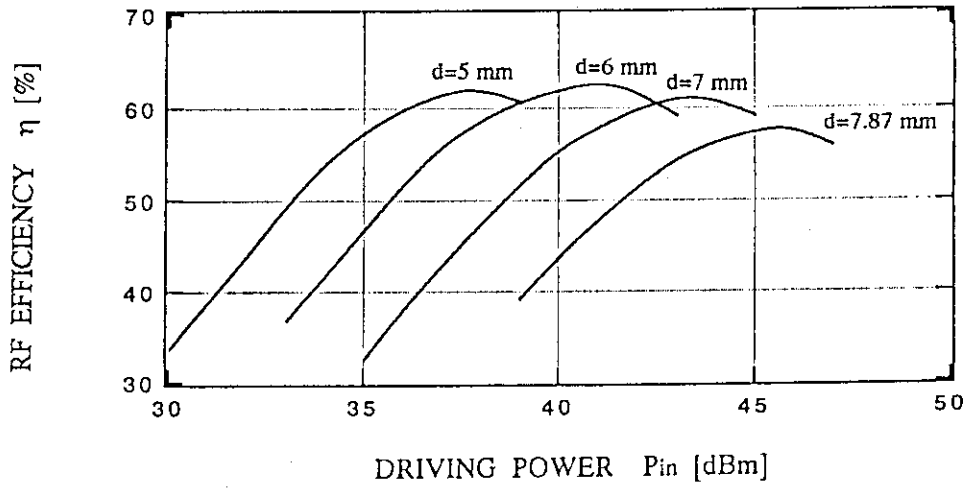

(b) The RF efficiency vs the RF driving power, where the gap length at the cavity is changed when the RF output power is kept to be 700 kW. Here, the number of cavity is five, which could not tune for a second harmonics wave.

Fig. 5.3 Calculated results of 5 GHz klystron for FER/ITER

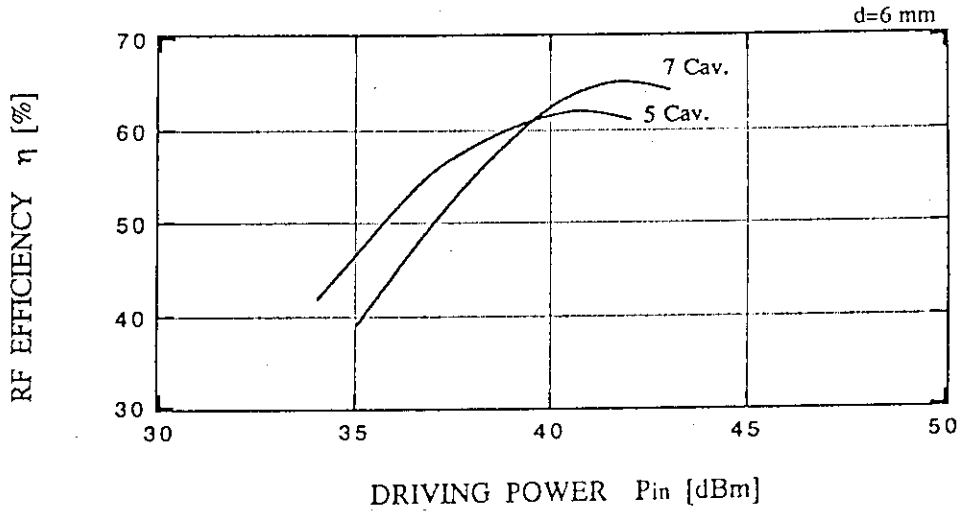

(c) The RF efficiency vs the RF driving power when the two second harmonics cavity is used to attain an enlarged RF efficiency, or not that

Fig. 5.3 Calculated results of 5 GHz klystron for FER/ITER

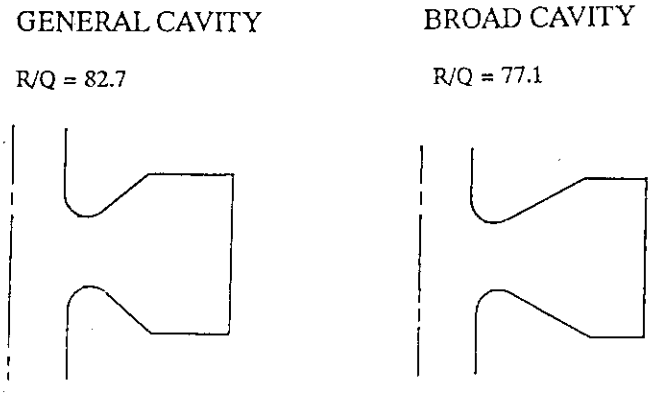

Fig. 5.4 Configuration of a general cavity and a broad cavity

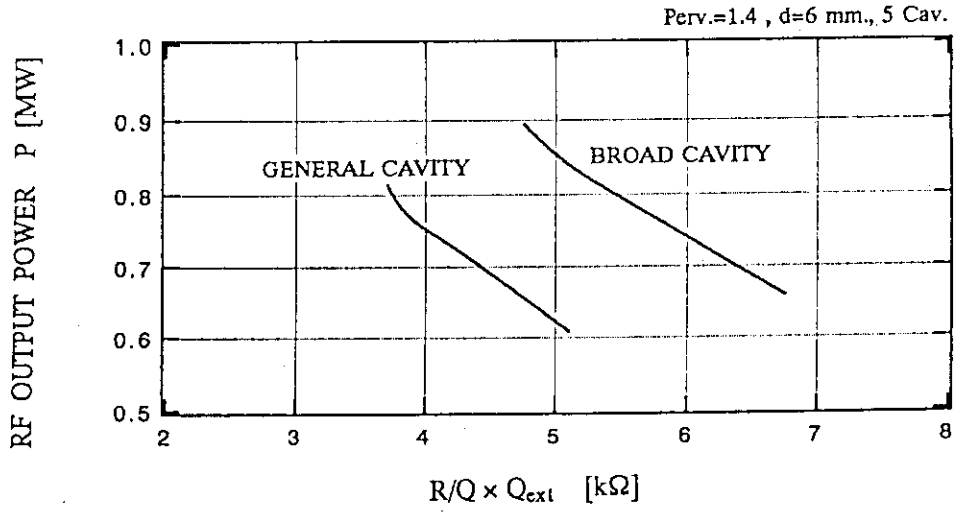

(a) The RF output power vs the output impedance when the broad cavity and the general cavity are used.

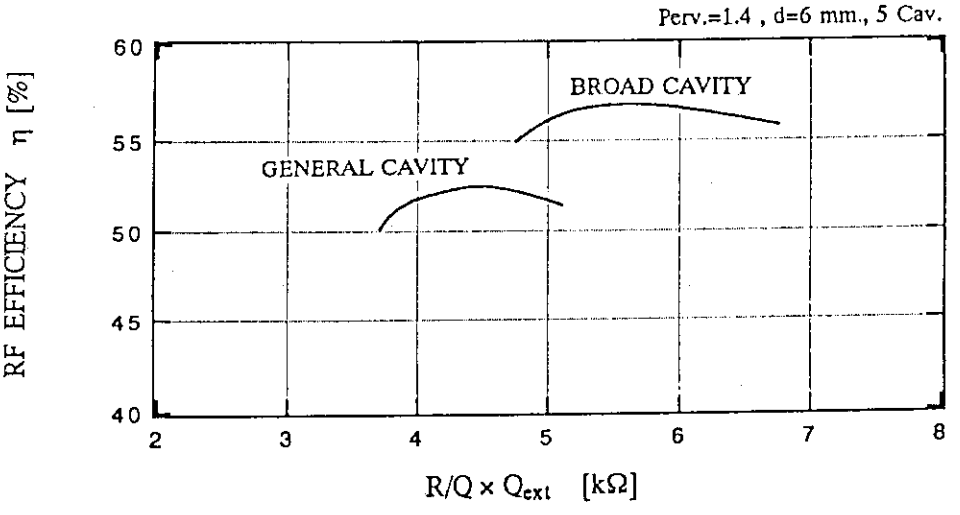

(b) The RF efficiency vs the output impedance when the broad cavity and the general cavity are used.

Fig. 5.5 Comparison of the output power and the efficiency between two cavities

6. R & D NEEDS AND CONCLUSIONS

6.1 R & D Needs

The design of CDA for ITER and FER is based mostly on technical solutions adopted in present high power LH systems for large and medium size tokamaks ; JT-60, JET, Tore-supra etc. Experience from these devices is expected to ensure the development of the conventional elements of the LH systems. Specific further developments are required and planned for ITER[16]: they include the development of a klystron meeting ITER specifications and the development and testing of the launcher mouth. A test bed will be needed to test one proto-typical channel of the complete LH system. Three main tasks in the long term R & D Programme of ITER are summarized as follows:

[1] Development of a high power ,CW, high efficiency klystron;
  (a) a frequency ; 5 GHz
  (b) power per unit ; ≥ 0.7 MW
  (c) efficiency ; 0.6

[2] Development and testing of a launcher mouth that will operate reliability in ITER

6.2 Conclusions

The conceptual design of LH wave system for FER and ITER has been carried out. The designed system satisfies the requirement of continuous injection of 30 MW for FER and 45-50 MW for ITER of Lower Hybrid Waves at 5 GHz for assist in current start-up and current drive in the boundary region. An optimization of the physics modeling is necessary as well as the experimental confirmation of theoretical models in order to justify the design study of this report.

ACKNOWLEDGEMENTS

Authors thanks all the member of ITER CDA team for the useful discussion and suggestions. They also appreciate Drs.K.Tomabechi, ITER chairman, M.Yoshikawa, T.Iijima, Y.Tanaka, S.Shimamoto and H.Shirakata for their continuous encouragement and discussions.

6. R & D NEEDS AND CONCLUSIONS

6.1 R & D Needs

The design of CDA for ITER and FER is based mostly on technical solutions adopted in present high power LH systems for large and medium size tokamaks ; JT-60, JET, Tore-supra etc. Experience from these devices is expected to ensure the development of the conventional elements of the LH systems. Specific further developments are required and planned for ITER[16]: they include the development of a klystron meeting ITER specifications and the development and testing of the launcher mouth. A test bed will be needed to test one proto-typical channel of the complete LH system. Three main tasks in the long term R & D Programme of ITER are summarized as follows:

[1] Development of a high power ,CW, high efficiency klystron;
  (a) a frequency ; 5 GHz
  (b) power per unit ; ≥ 0.7 MW
  (c) efficiency ; 0.6

[2] Development and testing of a launcher mouth that will operate reliability in ITER

6.2 Conclusions

The conceptual design of LH wave system for FER and ITER has been carried out. The designed system satisfies the requirement of continuous injection of 30 MW for FER and 45-50 MW for ITER of Lower Hybrid Waves at 5 GHz for assist in current start-up and current drive in the boundary region. An optimization of the physics modeling is necessary as well as the experimental confirmation of theoretical models in order to justify the design study of this report.

ACKNOWLEDGEMENTS

Authors thanks all the member of ITER CDA team for the useful discussion and suggestions. They also appreciate Drs.K.Tomabechi, ITER chairman, M.Yoshikawa, T.Iijima, Y.Tanaka, S.Shimamoto and H.Shirakata for their continuous encouragement and discussions.

REFERENCES

1) Matsuda S. et al. : Proc. 13th Int. Conf. on Plasma Physics and Controlled Nuclear Fusion Research, Washington (1990), IAEA-CN-53/G-2-2.

2) Tomabechi K. et al. : Proc. 13th Int. Conf. on Plasma Physics and Controlled Nuclear Fusion Research, Washington (1990), IAEA-CN-53/F-1-1.

3) Nevins W. et al. : Proc. 13th Int. Conf. on Plasma Physics and Controlled Nuclear Fusion Research, Washington (1990), IAEA-CN-53/F-3-4.

4) Zarnstorff M. et al. : Phys. Rev. Lett., 60 (1988) 1306.

5) Challis C. et al. : 14th Europe. Conf. on Contr. Fusion and Plasma Phys. (Madrid, 1987) Part III 1026.

6) Simonen T. et al., : Phys. Rev. Lett. 61 (1988) 1720.

7) JT-60 Team : 16 th Europe. Conf. on Contr. Fusion and Plasma Phys. (Venice, 1989).

8) Naito O. et al. : Nucl. Fusion 30 (1990) 1137

9) Imai T. et al., Nucl. Fusion 28 (1988) 1341

10) JT-60 team (presented by M.Nagami) Plasma Physics and Controlled Fusion 31 (1989) 1597

11) Imai T., et al., in Plasma Phys. and Controlled Nuclear Fusion Research (Proc. 13th Int. Conf. Washington, 1990) IAEA-CN-53/E-1-3, Vol.1

12) Bonoli P., Porkolab M., Nuclear Fusion **27** (1987) 1341.

13) Shibanuma K.et al., Proc. 16th Symp. on Fusion Tech. London (1990) Vol.II p.1317

14) Maki K. et al., " Japanese Contribution to ITER Shielding Neutronics Design " JAERI-M 91-046 (1991)

15) ITER DOCUMENT SERIES, No.32; Chap III, ITER CURRENT AND HEATING SYSTEM, Parail V., Fujisawa N., Hopman H., Kimura H., Wegrowe J.G. IAEA, Vienna,1991

16) Antakov I.I. et al., "International Workshop on Strong Microwaves in Plasmas", Suzdal USSR (September 1990)

17) Andreani R.et al;., Proc. 11th Symp. of Fusion Eng. Austin (1985) Vol.II p.1324